AD-A151 751 UNSTEADY NAVIER-STOKES CALCULATIONS IN AN ACCELERATED REFERENCE FRAME(U) AIR FORCE INST OF TECH WRIGHT-PATTERSON AFB OH SCHOOL OF ENGINEERING 1/1

UNCLASSIFIED T E SPEER DEC 84 AFIT/GAE/ENY/84D-26 F/G 20/4 NL

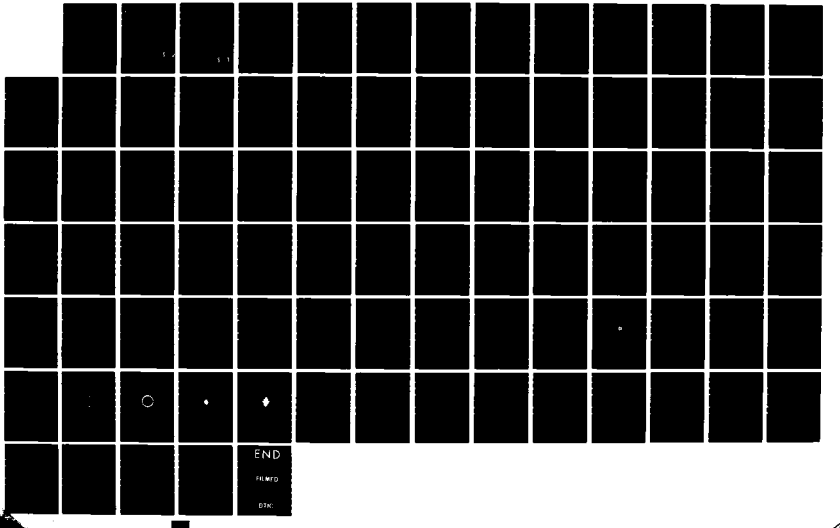

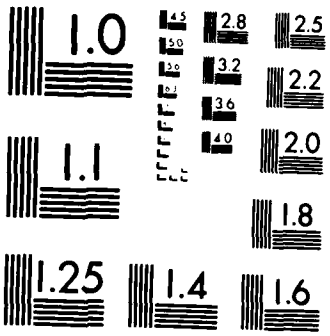

MICROCOPY RESOLUTION TEST CHART
NATIONAL BUREAU OF STANDARDS 1963 A

REPRODUCED AT GOVERNMENT EXPENSE

(1)

AD-A151 751

UNSTEADY NAVIER-STOKES CALCULATIONS IN AN ACCELERATED REFERENCE FRAME

THESIS

Thomas E. Speer
Captain, USAF

AFIT/GAE/ENY/84D-

DTIC FILE COPY

DTIC
ELECTE
MAR 28 1985
S D
D

DEPARTMENT OF THE AIR FORCE
AIR UNIVERSITY
AIR FORCE INSTITUTE OF TECHNOLOGY

Wright-Patterson Air Force Base, Ohio

85 03 13 082

AFIT/GAE/ENY/84D-26

DTIC COPY INSPECTED

Accession For
NTIS GRA&I [X]
DTIC TAB [ ]
Unannounced [ ]
Justification
By
Distribution/
Availability Codes
Dist | Avail and/or Special
A-1

UNSTEADY NAVIER-STOKES CALCULATIONS IN AN ACCELERATED REFERENCE FRAME

THESIS

Thomas E. Speer
Captain, USAF

AFIT/GAE/ENY/84D-26

DTIC ELECTE MAR 28 1985 D

Approved for public release; distribution unlimited

AFIT/GAE/ENY/84D-26

UNSTEADY NAVIER-STOKES CALCULATIONS IN AN ACCELERATED REFERENCE FRAME

THESIS

Presented to the Faculty of the School of Engineering
of the Air Force Institute of Technology
Air University
In Partial Fulfillment of the
Requirements for the Degree of
Master of Science in Aerospace Engineering

Thomas E. Speer, B.S.
Captain, USAF.

December 1984
Approved for public release; distribution unlimited

Contents

List of Figures

Preface

The purpose of this project was to develop a numerical method capable of calculating the laminar flow about a two dimensional accelerating body using the incompressible Navier–Stokes equations. This problem arises in the calculation of the dynamic stall of an airfoil and in the calculation of pitching and heaving stability derivatives for an isolated airfoil. It is also a first step toward solving the three dimensional flow about a complete wing undergoing arbitrary motion at high angles of attack, including departure, spin, and post–stall maneuvers.

The contravariant form of the momentum and continuity equations are derived and a finite difference approximation developed. The contravariant velocity formulation is based on the use of both inertial and body–axis velocities to achieve a form for the momentum equations that has the potential for improved numerical characteristics for rotating coordinate frames.

Numerical calulations to date have not been satisfactory. Test cases presented are Stoke's first problem, a circular cylinder translating at a Reynold's number of 20, and a rotating stationary circular cylinder.

I owe a great debt of gratitude to all those people that assisted me in this project. Especially my advisor, Maj James Hodge, for his many hours of help and advice, and my wife, Tamia, for her loving support throughout. Special thanks also go to Maj Dave Maunder for the use of his computer to prepare this document after mine was stricken.

INTRODUCTION

The aerodynamics of aircraft in steady flight at low to moderate angles of attack are well understood. However, the viscous flow about wings and bodies undergoing arbitrary unsteady motion is not. This is especially true for wings at high angles of attack. There is a serious need to be able to predict the performance and flying qualities of aircraft maneuvering at high angles of attack, and to be able to predict departure and spin behaviour, and to exploit post stall maneuverability. These predictions require an accurate calculation of the nonlinear forces and moments that are associated with the separated flow under such conditions. A basic requirement is to be able to calculate the flow about an isolated wing, and the analysis of a simple airfoil is the first step.

The aerodynamics of an airfoil which is pitching are influenced by the fact that the local velocity of different points on the airfoil is not the same as the velocity of the reference center. This has implications for both the flow outside the boundary layer and the resulting pressure distribution, and for the velocity profile within the boundary layer itself. Vortices that are shed into the flow are swept downstream and cause unsteady effects if their production is not continuous and constant. In addition, large separated regions exist which may vary with time. The convection of vortices and the unsteady separated regions cause time lags in the dynamic forces on the airfoil, even for incompressible flow, due to the time required for vortices to be convected away from the vicinity of the body. The flow at the body surface must follow the motion of the body in order to satisfy the no slip bounday condition. Thus, for even a steady external flow that is similar to the unsteady flow, the boundary layer will be significantly different, because the flow must transition from the external conditions to the new unsteady and spacially varying

conditions at the wall.

The complexity of these unsteady phenomena provides a strong incentive to use numerical methods to predict these flows. A full simulation of the three dimensional unsteady, viscous, and compressible effects is beyond the capability of the currently available methods and computing resources. Therefore, the scope of the problem has been reduced for this project by neglecting the effects of compressiblity and turbulence, and by restricting the analysis to two dimensional flow.

Several investigators have used numerical methods to calculate the unsteady flow about bodies. Hodge (Ref 1) considered an airfoil in steady motion at high angles of attack. The flow under these conditions (ten degrees angle of attack, a Reynolds number of 200000, and laminar flow) was unsteady, with separation bubbles forming and collapsing on the upper surface. The numerical technique used was vey similar to the present method. Primitive variables were used. The finite difference approximation used a first order backward difference in time, three point one sided upwind differences were used for first derivatives, and central differences were used for second order derivatives and pressure gradients. The equations were solved through successive–over–relaxation (SOR). The Poisson equation was used for pressure calculations. The rate of convergence of the calculations was driven by the convergence of the pressure on the wall at the sharp trailing edge. This experience provided the motivation for the present cell centered pressures.

Hegna (Ref 2) extended Hodge's work by adding a turbulence model and considered a pitching airfoil. Fictitious body forces were used to account for the accelerations due to the rotating reference frame. Constant, linearly varying, and sinusoidal pitching motions were considered.

Mehta (Ref 3), used a stream function–vorticity formulation to solve for the flow about an airfoil oscillating in pitch. The vorticity equation was based on the body–axis equations with fictitious body forces.

More recently, Taslim, et al. (Ref 4) calculated the flow about a circular cylinder and a 10% thick ellipse in pure rotation and combined rotation and translation. Their stream function–vorticity formulation was based on the inertial velocities which were convected with the body–axis velocities in the body fixed reference frame. Their calculation used an explicit method based on computing one velocity component at a given point by integrating the contributions of the vorticity in the exterior flow, on the body surface, and inside the body. The other component was obtained through continuity. Pressure gradients at the body surface were obtained from the tangential component of the momentum equation. Two point differences were used in time, upwind differences were used for convective terms, and diffusion terms were calculated from central differences.

The approach taken in this work is similar to that used by Galloway (Ref 5) in simulating the free flight of a flat plate. Galloway used the contravariant velocity formulation and the same numerical method as Hodge. This technique was used to calculate the trajectory of a flat plate in free flight. The free flight trajectory was a marked contrast to the other works above, which all used a prescribed trajectory for the body. Galloway derived the contravariant velocity relationships by starting with the equations written for an inertial control volume. He then expressed the inertial quantities in terms of the time varying transformation from the inertial to the body frame, and applied the chain rule to obtain the derivatives in the body frame. This resulted in equations that are identical to the present method, but did not provide any insight as to the physical meaning of the different terms. The Poisson equation for pressure was used, and free stream Dirichlet boundary conditions were employed to simulate the far field.

The present work differs from that of Galloway in several respects. The governing differential equations for the rotating coordinate system are derived from first principles, rather than starting with the differential equations for

the unaccelerated case.

The present numerical method differs from Galloway's by using an arbitrary grid about a thick body, and in its treatment of the viscous and pressure terms. A generalized transformation on an "O" type grid is used instead of the orthogonal "H" type grid that Galloway used to represent the flat plate. The pressure and viscous calculations are based upon a four point "X" configuration central difference operator. The exterior boundary condition is also treated differently so as to attempt to allow the disturbances in the wake region to exit the computational domain. The final difference between the present work and Galloway's is the use of cell centered pressures, rather than collocating the numerical values of the pressure at the same grid locations as the velocities. Chorin's method for solving the pressures is used throughout the domain, instead of just at the wall as was done by Hodge, Hegna, and Galloway.

The principal objective of this work was to demonstrate the use of the contravariant velocity formulation for an arbitrary body and arbitrary motion. The cell centered pressures were selected to avoid the difficulties experienced by the previous investigators in calculating the pressures at the wall. Chorin's method was selected over the Poisson equation for its simplicity in calculating the pressures at the cell centers from velocities known at the corners of the cell. The differencing scheme for the viscous terms was an outgrowth of the differencing used to calculate the pressure gradients, and was motivated by the desire to calculate the momentum equations in the strong conservation form. Subsequent results showed that the nonconservation form of the convective terms gave better results, and so the strong conservation form was used for only a minority of the cases. Finally, the inviscid boundary conditions were selected in an attempt to model the wake region more accurately than the free stream boundary conditions used by Galloway.

CONTINUUM EQUATIONS

The momentum equations used for this investigation were the contravariant, or "mixed" form of the incompressible Navier–Stokes equations. The traditional approach to computing the flow about a rotating body is to express all of the equations in terms of the velocities written in terms of the rotating, body fixed reference frame. This leads to the introduction of a number of additional terms in the momentum equations because Newton's Second Law is only valid for velocities and time derivatives taken with respect to the inertial reference frame. These additional terms are often represented as fictitious body forces (Ref 6), so that the conservation of momentum can be expressed in the same form as for the non–accelerating case. Even though represented as forces, these terms can be handled as part of the momentum flux and are treated as such in the present numerical study (c.f. below).

A purely inertial description of the momentum equations is not convenient because the position of the body is constantly changing in the inertial frame. This would preclude the use of a fixed grid in a numerical calculation. The contravariant velocity approach uses inertial velocities which are resolved in the unit vectors of the body fixed coordinate system. This affords a considerable simplification of the equations, as they are very similar to the momentum equations for the non–accelerating formulation. The fictictious forces of the traditional approach do not appear explicitly because they are implicitly contained within the inertial velocity components. Galloway derived the equations by expressing the inertial velocities in terms of the time varying transformation to the body–axis orientation, and substituted them in the conventional Navier–Stokes equations written for the inertial frame. The approach of the present investigation was to express the momentum using inertial velocities and describe the momentum transport in terms of body–axis velocities. The resulting equations are equivalent to Galloway's, and provide

considerable insight as to the physical meaning of the acceleration/rotational terms and the eigenvalues of the momentum equations.

Kinematics

This section defines the notation used to describe the position and velocities of points on the body and in the fluid. It is important to distinguish the difference between the rotating body fixed reference frame, and the unaccelerated inertial reference frame when differentiating vector quantities with respect to time. The notation and kinematic definitions are taken from Likins (Ref 2). The notation indicates the relative relationships between points and the notation for time derivatives of vector quantities explicitily indicates relative relationships between different coordinate frames. Superscripts to the left of the variable name indicate that the time derivative was computed as seen by an observer in that reference frame. Subscripts to the right of the variable name are used to indicate relative relationships.

For example, let O, P, and Q represent points, with O being fixed in inertial space, Q fixed to the body, and P located anywhere in the fluid, as shown in Figure 1. The position of P relative to Q is denoted as $r_{P/Q}$. This position vector may be resolved into components which are parallel to the instantaneous unit vectors of any frame of reference without regard to whether the unit vectors of that frame are rotating with respect to another frame . The velocity of P relative to Q relative to the inertial reference frame is the time derivative of $r_{P/Q}$:

$$\frac{{}^{I}dr_{P/Q}}{dt} = {}^{I}V_{P/Q} \qquad (1)$$

The velocity of P relative to Q relative to the rotating body reference frame

$$+ \frac{\partial}{\partial \eta}\{ {}^{I}u_{P/O}[Y_\xi ({}^{I}u_{P/O}+RY-{}^{I}u_{Q/O}) + X_\xi ({}^{I}v_{P/O}-RX-{}^{I}v_{Q/O})]\}$$

$$= \frac{\partial}{\partial \xi}\{ -\frac{Y_\eta\, \rho}{J} + \frac{\nu}{J}[\alpha \frac{\partial {}^{I}u_{P/O}}{\partial \xi} - \beta \frac{\partial {}^{I}u_{P/O}}{\partial \eta}]\}$$

$$+ \frac{\partial}{\partial \eta}\{ \frac{Y_\xi\, \rho}{J} + \frac{\nu}{J}[-\beta \frac{\partial {}^{I}u_{P/O}}{\partial \xi} + \gamma \frac{\partial {}^{I}u_{P/O}}{\partial \eta}]\} + \{R\, {}^{I}v_{P/O}\} \qquad (48)$$

$$\frac{\partial}{\partial t}\{J {}^{I}v_{P/O}\} + \frac{\partial}{\partial \xi}\{ {}^{I}v_{P/O}[Y_\eta ({}^{I}u_{P/O}+RY-{}^{I}u_{Q/O}) - X_\eta ({}^{I}v_{P/O}-RX-{}^{I}v_{Q/O})]\}$$

$$+ \frac{\partial}{\partial \eta}\{ {}^{I}v_{P/O}[Y_\xi ({}^{I}u_{P/O}+RY-{}^{I}u_{Q/O}) + X_\xi ({}^{I}v_{P/O}-RX-{}^{I}v_{Q/O})]\}$$

$$= \frac{\partial}{\partial \xi}\{ \frac{X_\eta\, \rho}{J} + \frac{\nu}{J}[\alpha \frac{\partial {}^{I}v_{P/O}}{\partial \xi} - \beta \frac{\partial {}^{I}v_{P/O}}{\partial \eta}]\}$$

$$+ \frac{\partial}{\partial \eta}\{ -\frac{X_\xi\, \rho}{J} + \frac{\nu}{J}[-\beta \frac{\partial {}^{I}v_{P/O}}{\partial \xi} + \gamma \frac{\partial {}^{I}v_{P/O}}{\partial \eta}]\} - \{R\, {}^{I}u_{P/O}\} \qquad (49)$$

Notice that these equations may be written in the form

$$\frac{\partial\{u\}}{\partial t} + \frac{\partial\{f\}}{\partial \xi} + \frac{\partial\{g\}}{\partial \eta} = \frac{\partial\{h\}}{\partial \xi} + \frac{\partial\{i\}}{\partial \eta} + \{k\} \qquad (50)$$

in which the quantities {u}, {f}, {g}, {h}, {i}, and {k} are column vectors representing each of the terms in {}, in turn, for both equations above.

These equations have substantially the same form as those written for a control volume fixed in the inertial coordinate system. The differences are the {k} vector, which results from differentiating the time derivative in the body frame, and in the mix of velocities in the convective terms. For the inertially fixed control volume ${}^{I}V_{P/Q}$ is a constant, and therefore may be taken to be zero since it will affect none of the terms in the differential

be represented as

$$J \frac{\partial C}{\partial X} = \frac{\partial}{\partial \xi}(Y_\eta C) - \frac{\partial}{\partial \eta}(Y_\xi C) \qquad (45)$$

$$J \frac{\partial C}{\partial Y} = -\frac{\partial}{\partial \xi}(X_\eta C) + \frac{\partial}{\partial \eta}(X_\xi C) \qquad (46)$$

When these relations are substituted into J times ν times the Laplacian, one obtains the result

$$J \frac{\partial}{\partial X}\left(\nu \frac{\partial C}{\partial X}\right) + J \frac{\partial}{\partial Y}\left(\nu \frac{\partial C}{\partial Y}\right)$$

$$= \frac{\partial}{\partial \xi}\left\{ \frac{\nu}{J}\left[\alpha \frac{\partial C}{\partial \xi} - \beta \frac{\partial C}{\partial \eta}\right]\right\} + \frac{\partial}{\partial \eta}\left\{ \frac{\nu}{J}\left[-\beta \frac{\partial C}{\partial \xi} + \gamma \frac{\partial C}{\partial \eta}\right]\right\} \qquad (47)$$

with:

$$\alpha = (X_\eta)^2 + (Y_\eta)^2$$

$$\beta = X_\xi X_\eta + Y_\xi Y_\eta$$

$$\gamma = (X_\xi)^2 + (Y_\xi)^2$$

$$J = |X_\xi Y_\eta - X_\eta Y_\xi|$$

Notice that no cross derivatives appear explicitly.

The final step in the derivation of the continuum equations is to apply these results to the momentum equations after multiplying them by J (which is fixed with respect to time) and dividing by ρ:

$$\frac{\partial}{\partial t}\{J\,{}^{1}u_{P/O}\} + \frac{\partial}{\partial \xi}\left\{ {}^{1}u_{P/O}\left[Y_\eta \left({}^{1}u_{P/O} + RY - {}^{1}u_{Q/O}\right) - X_\eta \left({}^{1}v_{P/O} - RX - {}^{1}v_{Q/O}\right)\right]\right\}$$

$$= -\frac{1}{\rho}\frac{\partial p}{\partial X} + \nu\left(\frac{\partial^2 {}^{i}u_{P/O}}{\partial X^2} + \frac{\partial^2 {}^{i}u_{P/O}}{\partial Y^2}\right) + R\,{}^{i}v_{P/O} \qquad (41)$$

$$\frac{\partial {}^{i}v_{P/O}}{\partial t} + \frac{\partial}{\partial X}\left[{}^{i}u_{P/O}{}^{i}v_{P/O} + {}^{i}v_{P/O}(RY - {}^{i}u_{Q/O})\right] + \frac{\partial}{\partial Y}\left[{}^{i}v_{P/O}{}^{2} + {}^{i}v_{P/O}(-RX - {}^{i}v_{Q/O})\right]$$

$$= -\frac{1}{\rho}\frac{\partial p}{\partial Y} + \nu\left(\frac{\partial^2 {}^{i}v_{P/O}}{\partial X^2} + \frac{\partial^2 {}^{i}v_{P/O}}{\partial Y^2}\right) - R\,{}^{i}u_{P/O} \qquad (42)$$

In the equations above, $\omega_{b/i}X^{b}V_{P/Q}$ has been moved to the right hand side as the source terms $R^{i}v_{P/O}$ and $R^{i}u_{P/O}$. These equations are identical to the equations derived by Galloway.

General Coordinate Transformation

The next step in the development of the continuum equations is to apply a general transformation from the physical domain to the computational domain. ξ represents the ordinate and η the abscissa in the computational domain. The continuity equation is easily transformed using the chain rule and the inverse relationships, $Y_\eta/J=\xi_X$, $X_\eta/J=\xi_Y$, $Y_\xi/J=\eta_X$, $X_\xi/J=\eta_Y$, as:

$$\frac{\partial {}^{i}u_{P/O}}{\partial \xi} Y_\eta - \frac{\partial {}^{i}u_{P/O}}{\partial \eta} Y_\xi - \frac{\partial {}^{i}v_{P/O}}{\partial \xi} X_\eta + \frac{\partial {}^{i}v_{P/O}}{\partial \eta} X_\xi = 0 \qquad (44)$$

X_ξ, X_η, Y_ξ, Y_η indicate the partial derivatives of X and Y with respect to ξ and η.

In order to put the momentum equations in conservation form, the chain rule and inverse relations above are first applied. As shown by Viviand (Ref 8), the Jacobian, J, times the derivative of some quantity, C, can be can

$$\tau_{XY} = \mu\left(\frac{\partial {}^{i}v_{P/O}}{\partial X} + \frac{\partial {}^{i}u_{P/O}}{\partial Y}\right)$$

$$\tau_{YZ} = \mu\left(\frac{\partial {}^{i}w_{P/O}}{\partial Y} + \frac{\partial {}^{i}v_{P/O}}{\partial Z}\right)$$

$$\tau_{XZ} = \mu\left(\frac{\partial {}^{i}u_{P/O}}{\partial Z} + \frac{\partial {}^{i}w_{P/O}}{\partial X}\right) \qquad (38)$$

For incompressible flow in which the viscosity is assumed constant, the right hand side of the momentum equation becomes:

$$RHS_X = \iiint_{CV} \left[-\frac{\partial p}{\partial X} + \mu\left(\frac{\partial^2 {}^{i}u_{P/O}}{\partial X^2} + \frac{\partial^2 {}^{i}u_{P/O}}{\partial Y^2} + \frac{\partial^2 {}^{i}u_{P/O}}{\partial Z^2}\right)\right] dV$$

$$RHS_Y = \iiint_{CV} \left[-\frac{\partial p}{\partial Y} + \mu\left(\frac{\partial^2 {}^{i}v_{P/O}}{\partial X^2} + \frac{\partial^2 {}^{i}v_{P/O}}{\partial Y^2} + \frac{\partial^2 {}^{i}v_{P/O}}{\partial Z^2}\right)\right] dV$$

$$RHS_Z = \iiint_{CV} \left[-\frac{\partial p}{\partial Z} + \mu\left(\frac{\partial^2 {}^{i}w_{P/O}}{\partial X^2} + \frac{\partial^2 {}^{i}w_{P/O}}{\partial Y^2} + \frac{\partial^2 {}^{i}w_{P/O}}{\partial Z^2}\right)\right] dV \qquad (39)$$

The integrands on both sides of the equations are equated for each component in turn, as with the continuity equation, to obtain the differential equations.

For two dimensional, incompressible flow, the flow will be assumed to lie in the X–Y plane. Therefore, $P = Q = {}^{i}w_{P/O} = 0$. The angle ψ will be used to represent the orientation of the body axes relative to the inertial axes, as shown in Figure 2, and its rate of change is R. Under these conditions and the continuity and momentum equations become:

$$\frac{\partial {}^{i}u_{P/O}}{\partial X} + \frac{\partial {}^{i}v_{P/O}}{\partial Y} = 0 \qquad (40)$$

$$\frac{\partial {}^{i}u_{P/O}}{\partial t} + \frac{\partial}{\partial X}\left[{}^{i}u_{P/O}{}^{2} + {}^{i}u_{P/O}(RY - {}^{i}u_{Q/O})\right] + \frac{\partial}{\partial Y}\left[{}^{i}u_{P/O}{}^{i}v_{P/O} + {}^{i}u_{P/O}(-RX - {}^{i}v_{Q/O})\right]$$

$$\iiint_{CV} \{ \frac{\partial}{\partial t}(\rho {}^{i}u_{P/O}) + \rho({}^{i}Q {}^{i}w_{P/O} - {}^{i}R {}^{i}v_{P/O}) + \nabla\cdot[\rho {}^{i}u_{P/O}({}^{i}V_{P/O} - \omega_{b/i} \times r_{P/Q} - {}^{i}V_{Q/O})] \} \, dV = RHS_X$$

$$\iiint_{CV} \{ \frac{\partial}{\partial t}(\rho {}^{i}v_{P/O}) + \rho({}^{i}R {}^{i}u_{P/O} - {}^{i}P {}^{i}w_{P/O}) + \nabla\cdot[\rho {}^{i}v_{P/O}({}^{i}V_{P/O} - \omega_{b/i} \times r_{P/Q} - {}^{i}V_{Q/O})] \} \, dV = RHS_Y$$

$$\iiint_{CV} \{ \frac{\partial}{\partial t}(\rho {}^{i}w_{P/O}) + \rho({}^{i}P {}^{i}v_{P/O} - {}^{i}Q {}^{i}u_{P/O}) + \nabla\cdot[\rho {}^{i}w_{P/O}({}^{i}V_{P/O} - \omega_{b/i} \times r_{P/Q} - {}^{i}V_{Q/O})] \} \, dV = RHS_Z \qquad (35)$$

The forces consist of pressure and viscous forces. The effect of gravity on the fluid will be neglected. These forces are typically represented as (Ref 7):

$$RHS_X = \iiint_{CV} [-\frac{\partial p}{\partial X} + (\frac{\partial \sigma'_X}{\partial X} + \frac{\partial \tau_{XY}}{\partial Y} + \frac{\partial \tau_{XZ}}{\partial Z})] \, dV$$

$$RHS_Y = \iiint_{CV} [-\frac{\partial p}{\partial Y} + (\frac{\partial \tau_{XY}}{\partial X} + \frac{\partial \sigma'_Y}{\partial Y} + \frac{\partial \tau_{YZ}}{\partial Z})] \, dV$$

$$RHS_Z = \iiint_{CV} [-\frac{\partial p}{\partial Z} + (\frac{\partial \tau_{XZ}}{\partial X} + \frac{\partial \tau_{YZ}}{\partial Y} + \frac{\partial \sigma'_Z}{\partial Z})] \, dV \qquad (36)$$

with

$$\sigma'_X = -\frac{2}{3}\mu \nabla\cdot{}^{i}V_{P/O} + 2\mu\frac{\partial {}^{i}u_{P/O}}{\partial X}$$

$$\sigma'_Y = -\frac{2}{3}\mu \nabla\cdot{}^{i}V_{P/O} + 2\mu\frac{\partial {}^{i}v_{P/O}}{\partial Y}$$

$$\sigma'_Z = -\frac{2}{3}\mu \nabla\cdot{}^{i}V_{P/O} + 2\mu\frac{\partial {}^{i}w_{P/O}}{\partial Z} \qquad (37)$$

becomes:

$$\iiint_{CV} \left| \frac{{}^b\partial(\rho\,{}^iV_{P/O})}{\partial t} + \omega_{b/i} \times (\rho\,{}^iV_{P/O}) \right| dV + \oint_{CS} \rho\,{}^iV_{P/O} \left| ({}^iV_{P/O} - \omega_{b/i} \times r_{P/Q} - {}^iV_{Q/O}) \cdot n \right| dA = RHS \qquad (33)$$

This equation can be derived from the conventional fictious body force formulation as given in Shames (Ref 6). This vector equation can be expressed in terms of its components:

$$\iiint_{CV} \left| \frac{\partial(\rho\,{}^iu_{P/O}) + \rho(Q\,{}^iw_{P/O} - R\,{}^iv_{P/O})}{\partial t} \right| dV + \oint_{CS} \rho\,{}^iu_{P/O} \left| ({}^iV_{P/O} - \omega_{b/i} \times r_{P/Q} - {}^iV_{Q/O}) \cdot n \right| dA = RHS_X$$

$$\iiint_{CV} \left| \frac{\partial(\rho\,{}^iv_{P/O}) + \rho(R\,{}^iu_{P/O} - P\,{}^iw_{P/O})}{\partial t} \right| dV + \oint_{CS} \rho\,{}^iv_{P/O} \left| ({}^iV_{P/O} - \omega_{b/i} \times r_{P/Q} - {}^iV_{Q/O}) \cdot n \right| dA = RHS_Y$$

$$\iiint_{CV} \left| \frac{\partial(\rho\,{}^iw_{P/O}) + \rho(P\,{}^iv_{P/O} - Q\,{}^iu_{P/O})}{\partial t} \right| dV + \oint_{CS} \rho\,{}^iw_{P/O} \left| ({}^iV_{P/O} - \omega_{b/i} \times r_{P/Q} - {}^iV_{Q/O}) \cdot n \right| dA = RHS_Z \qquad (34)$$

where ${}^iu_{P/O}$, ${}^iv_{P/O}$, ${}^iw_{P/O}$ are the inertial velocity components in the X, Y, and Z directions; P, Q, R are angular rates about the X, Y, and Z axes; and RHS_X, RHS_Y, RHS_Z are force components applied in the X, Y, and Z directions. When the Divergence Theorem is applied to each component, in turn, the following result is obtained:

acceleration of the body–axis reference center, Q, does not affect ${}^{i}V_{P/O}$. The other two terms represent the net momentum flux out of the control volume.

If one describes the inertial velocity vector field using the time varying position vectors of the body–axis system, the integrals for region III and region II may again be combined by recognizing that point P is being used as a dummy variable and evaluating the integrands at the same position in the body axis coordinate system. Once again, the difference divided by Δt is represented as a partial derivative, because the position in the body–axis system is held constant. The rotation of the body frame with respect to the inertial frame is still important, however. The momentum flux through the surface of the control volume is handled as with any other extensive property. Again, there is no flux for particles in the flow which appear to be moving tangential to the boundary in the body–axis system.

Applying the above relationships, as with the continuity equation, results in:

$$\iiint_{CV} \frac{{}^{i}\partial}{\partial t}(\rho\, {}^{i}V_{P/O})\, dV + \oint_{CS} \rho\, {}^{i}V_{P/O}({}^{b}V_{P/Q} \cdot n)\, dA = \oint_{CS} f_s\, dA + \iiint_{CV} f_b\, dV = RHS \qquad (32)$$

f_s is the net force per unit area acting on the surface of the control volume and f_b is the net body force per unit volume. RHS simply refers to the right hand side (force terms) of this momentum equation. The time derivative of the momentum within the control volume taken with respect to the inertial frame (which has unit vectors in the inertial frame), can be expressed in terms of a derivative taken relative to the body frame (which has unit vectors in the body frame). The body–axis velocity may also be expressed in terms of inertial velocities. After applying these changes, the momentum equation

differential element in turn.

The impulse applied to the system between t and t+Δt is:

$$I = \iiint_{III} \rho^i V_{P/O} dV - \iiint_{II} \rho^i V_{P/O} dV + \iiint_{IV} \rho^i V_{P/O} dV - \iiint_{I} \rho^i V_{P/O} dV \qquad (27)$$

The impulse is the integral from t to t+Δt, taken with respect to the inertial frame, of the forces applied to the fixed mass system:

$$I = \int F \, dt \Big|_i \qquad (28)$$

Differentiating the impulse with respect to time with respect to the inertial frame recovers the force acting on the system:

$$F = \frac{{}^i d}{dt} I \qquad (29)$$

To first order, the derivative above may be calculated as:

$$F = \frac{M(t+\Delta t) - M(t)}{\Delta t} \Big|_i \qquad (30)$$

Applying the above relationships to the integral expression for the impulse results in:

$$F = \{ [\iiint_{III} \rho^i V_{P/O} dV - \iiint_{II} \rho^i V_{P/O} dV]/\Delta t + [\iiint_{IV} \rho^i V_{P/O} dV]/\Delta t - [\iiint_{I} \rho^i V_{P/O} dV]/\Delta t \}_i \qquad (31)$$

The first bracketed expression represents the time rate of change of the momentum within the control volume, differentiated with respect to the inertial frame. The distinction that the momentum is differentiated with respect to the inertial frame accounts for the changing orientation of the unit vectors of the body frame with respect to the inertial frame. The translational

form of the continuity equation is also the same as for the non-rotating case:

$$\nabla \cdot {}^{i}V_{P/O} = 0 \qquad (21)$$

Conservation of Linear Momentum

The derivation of the expression for the conservation of linear momentum for an accelerated control volume proceeds in a parallel fashion to that for the the conservation of mass. Consider again the fixed mass system which occupies regions I and II at time t and regions III and IV at time t+Δt. The force acting on a particle at a given time is equal to the mass times its acceleration relative to the inertial frame. Thus the force acting on a particle containing a fixed amount of mass, dm, and located at point P is:

$$dF = dm \frac{{}^{i}d^2}{dt} r_{P/O} = dm \frac{{}^{i}d}{dt} {}^{i}V_{P/O} \qquad (22)$$

The linear momentum of the particle at point P is defined as the product of its mass and its inertial velocity:

$$dM = dm\ {}^{i}V_{P/O} \qquad (23)$$

The force acting on the particle is the time rate of change of the momentum of the particle, because the constant mass can be brought inside of the differentiation. The momentum of the system at time t is obtained by integrating the momentum of the particles througout regions I and II.

$$\iiint_{I} \rho\ {}^{i}V_{P/O}\, dV + \iiint_{II} \rho\ {}^{i}V_{P/O}\, dV \qquad (24)$$

The momentum at time t+Δt is given by:

$$\iiint_{III} \rho\ {}^{i}V_{P/O}\, dV + \iiint_{IV} \rho\ {}^{i}V_{P/O}\, dV \qquad (26)$$

Point P is used as a dummy variable in these integrals to indicate each

Integrating the efflux around the entire control surface and putting it into the expression for the conservation of mass for the fixed mass system yields the integral statement of the conservation of mass for the accelerated control volume:

$$\iiint_{CV} \frac{\partial}{\partial t} \rho \, dV = -\oint_{CS} \rho {}^{b}V_{P/Q} \cdot n \, dA \qquad (16)$$

Or, expressing the velocity in terms of inertial quantities:

$$\iiint_{CV} \frac{\partial}{\partial t} \rho \, dV = -\oint_{CS} \rho ({}^{i}V_{P/O} - \omega_{b/i} \times r_{P/Q} - {}^{i}V_{Q/O}) \cdot n \, dA \qquad (17)$$

Applying Gauss's Divergence Theorem yields:

$$\iiint_{CV_t} \frac{\partial}{\partial t} \rho \, dV = -\iiint_{CV} \nabla \cdot [\rho ({}^{i}V_{P/O} - \omega_{b/i} \times r_{P/Q} - {}^{i}V_{Q/O})] \, dV \qquad (18)$$

This equation must hold for all control volumes with a fixed volume, even as the control volume is shrunk to a differential size, therefore, the integrands on both sides of the equation must be the same, which leads to the differential form of the conservation of mass:

$$\frac{\partial \rho}{\partial t} = -\nabla \cdot [\rho ({}^{i}V_{P/O} - \omega_{b/i} \times r_{P/Q} - {}^{i}V_{Q/O})] \qquad (19)$$

The divergence of ${}^{i}V_{Q/O} = 0$ since it is constant throughout the entire control volume and only varies with time. The divergence of $\omega_{b/i} \times r_{P/Q}$ is zero, because $\omega_{b/i}$ is also spacially constant throughout the domain. Thus the divergence of the mass flux is the same, whether expressed in terms of the body-axis velocity or the inertial velocity, and

$$\frac{\partial \rho}{\partial t} = -\nabla \cdot (\rho {}^{i}V_{P/O}) \qquad (20)$$

which is the same as the classic result derived using a control volume fixed in inertial space. For incompressible flow, the density is constant, and the final

as Δt goes to zero, yields:

$$\lim_{\Delta t \to 0} \iiint_{CV} \frac{[\rho(t+\Delta t) - \rho(t)]}{\Delta t} dV = \iiint_{CV} \frac{\partial \rho}{\partial t} dV \qquad (13)$$

where the partial derivative has been used to represent the instantaneous time rate of change at a given point fixed in the body-axis coordinate system. This is appropriate because the density at a given point in the body fixed control volume can be written as a function of its position in the body-axis system and time, ie, $\rho(r_{S/Q},t)$. It is $r_{S/Q}$ which is being held fixed for this partial derivative.

The net mass flux out of the control volume can be obtained by integrating the efflux through each element of the control surface. The position of a particle in the system can be written using its position relative to the point on the control surface by:

$$r_{P/O} = r_{P/S} + r_{S/Q} + r_{Q/O} \qquad (14)$$

The inertial velocity of the particle then becomes:

$$\begin{aligned} {}^{i}V_{P/O} &= {}^{i}V_{P/S} + {}^{i}V_{S/Q} + {}^{i}V_{Q/O} \\ {}^{i}V_{P/O} &= {}^{b}V_{P/S} + \omega_{b/i} \times r_{P/S} + {}^{b}V_{S/Q} + \omega_{b/i} \times r_{S/Q} + {}^{i}V_{Q/O} \end{aligned} \qquad (15)$$

The efflux from the control volume at point S consists of the particles that are crossing point S at time t. The efflux though the differential element of the control surface located at point S is $\rho {}^{b}V_{P/S} \cdot n \, dA$, where n is the outward normal unit vector to the surface at S. This expression is the result of the simple observation that a particle located on the boundary at time t which does not cross the boundary must be stationary or moving tangent to the boundary, as observed from the body frame. Note that $r_{P/S} = 0$ at time t for those particles on the control volume boundary, and ${}^{b}V_{S/Q} = 0$ by the definition of the body fixed control volume. Thus, ${}^{b}V_{P/S} = {}^{b}V_{P/Q}$.

body–axis system, ie,

$$ {}^{b}V_{S/Q} = 0 \qquad (8) $$

and there is a one–to–one mapping of all points on the boundary of region II to the boundary of region III, regions II and III may be regarded as defining a body fixed control volume. Note that this also results in a one–to–one mapping of all of the points within the two regions as well as the points on the boundaries.

The mass in the system at time t is given by:

$$ \iiint_{I} \rho \, dV + \iiint_{II} \rho \, dV \qquad (9) $$

and the mass at time t+Δt is given by:

$$ \iiint_{III} \rho \, dV + \iiint_{IV} \rho \, dV \qquad (10) $$

Since the system has the same mass at both times, there can be no difference between the two expressions:

$$ \iiint_{III} \rho \, dV - \iiint_{II} \rho \, dV + \iiint_{IV} \rho \, dV - \iiint_{I} \rho \, dV = 0 \qquad (11) $$

The difference between the first two integrals above indicates the total change in the amount of mass contained within the control volume between time t and t+Δt. The second difference represents the net mass flux out of the control volume over the time interval. Because of the one–to–one relationship of the points in regions II and III, the first two integrals may be combined:

$$ \iiint_{III} \rho \, dV - \iiint_{II} \rho \, dV = \iiint_{CV} |\rho(t+\Delta t) - \rho(t)| \, dV \qquad (12) $$

provided that the difference in density at the two times is evaluated at the same point in the body fixed axis system. Dividing by Δt and taking the limit

relative to the inertial frame, will be termed the "inertial velocity" of a particle in the flow. This may be regarded as the "absolute" velocity of a particle in the fluid. ${}^{b}V_{P/Q}$, the time rate of change of the position of the particle relative to the body-axis reference point Q as seen by an observer rotating with the body frame, will be called the "body-axis velocity."

The body-axis velocity is calculated from the inertial velocity by:

$$ {}^{b}V_{P/Q} = {}^{i}V_{P/O} - \omega_{b/i} \times r_{P/Q} - {}^{i}V_{Q/O} \qquad (6) $$

This quantity is seen to vary with the translational velocity of point Q relative to O, with the angular rate of the body frame relative to the inertial frame, and with the position of point P in the body-axis system. The inertial velocity, ${}^{i}V_{P/O}$ is utterly independent of any motion of Q or rate of rotation of the body frame.

The only quantities which will be referred to as forces in this paper are those forces for which Newton's second law, $F = m\,a$, holds in an inertial reference frame. Thus, the sum of the forces acting on a particle of fixed mass m at point P is

$$ F = m \frac{{}^{i}d^2}{dt^2} r_{P/O} = m \frac{{}^{i}d}{dt} {}^{i}V_{P/O} \qquad (7) $$

Conservation of Mass

The derivation of the relationship defining the conservation of mass for an accelerating control volume begins by examining a fixed mass system of particles, as shown in Figure 2. The fixed mass system at time t consists of the particles in region I and region II (regions I and II are mutually exclusive, as are regions III and IV). At a later time, $t+\Delta t$, the fixed mass system occupies regions III and IV. Let point S represent any arbitrary point on the boundary of region II. If, at $t+\Delta t$ point S maintains its position in the

is expressed as:

$$\frac{{}^{b}dr_{P/Q}}{dt} = {}^{b}V_{P/Q} \qquad (2)$$

The rate of rotation of the unit vectors which define the orientation of the body frame relative to the inertial frame is denoted by $\omega_{b/i}$, and the velocities relative to the inertial and body frames are related by:

$${}^{i}V_{P/Q} = \frac{{}^{i}dr_{P/Q}}{dt} = \frac{{}^{b}dr_{P/Q}}{dt} + \omega_{b/i} \times r_{P/Q} = {}^{b}V_{P/Q} + \omega_{b/i} \times r_{P/Q} \qquad (4)$$

Note that the unit vectors which define the orientation of a reference frame are not bound to any point. Thus the only time rate of change of the unit vectors is their angular rate, ω. Translational velocitites are handled by explicitly noting the points at the head and tail of the position vectors. Thus, the inertial velocity of P relative to O is related to the velocity of P relative to Q by:

$${}^{i}V_{P/O} = {}^{i}V_{P/Q} + {}^{i}V_{Q/O} \qquad (5)$$

For the rest of the paper, the points P, Q, and O will have a special significance. Point O will be taken to be a point which has no acceleration when viewed from an inertial reference frame. Thus, there exists some Galilean transformation for which the point O may be considered to be "fixed." Point Q will refer to the reference center of the body fixed axis system. Positions in the body-axis system will be measured relative to point Q. Point P will be used to designate the location of a particular particle, having a fixed mass, in the fluid. $r_{P/O}$ is the position of point P measured from the unaccelerated point O, and $r_{P/Q}$ is the position of the particle relative to the accelerating body-axis reference point.

${}^{i}V_{P/O}$, the time rate of change of the position of the particle relative to the unaccelerated reference point as viewed by an observer who is not rotating

equation. With ${}^{I}V_{P/Q} = 0$, ${}^{I}V_{P/O} = {}^{I}V_{P/Q} = {}^{b}V_{P/Q}$. The terms in parentheses then become equal to ${}^{I}V_{P/Q}$, {k} goes to zero, and ${}^{I}V_{P/Q}$ can also be substituted for ${}^{I}V_{P/O}$, thus eliminating the mixed use of velocities from different reference framse. The advantage of describing the flow in terms of the inertial velocities results from the simplicity of the terms arising from the time derivatives. The source term, {k}, is half the magnitude of the typical Coriolis acceleration. The centripetal acceleration and the angular acceleration do not appear explicity. This is an advantage numerically, as these terms depend upon the magnitude of $r_{P/Q}$, which approaches infinity at the exterior of the computational domain. The acceleration of the body is also not required. The disadvantage in using the inertial velocity is a loss in the intuitive interpretation of the flow about the body. The body-axis velocity is easily calculated from the inertial velocity, however, and so this disadvantage is not great.

Convective Term Eigenvalues

The numerical approximation to the fluxes will depend on eigenvalues of the isolated convective terms. These are most conveniently found by considering the equations in linearized form. By applying the chain rule, Equation 31 becomes:

$$\frac{\partial\{U\}}{\partial t} + F\frac{\partial\{U\}}{\partial \xi} + G\frac{\partial\{U\}}{\partial \eta} = \frac{\partial\{h\}}{\partial \xi} + \frac{\partial\{i\}}{\partial \eta} + \{k\} \qquad (51)$$

where:

$$\{U\} = J\,{}^{I}V_{P/O}$$

$$F = \frac{\partial\{f\}}{\partial\{U\}}$$

$$G = \frac{\partial\{g\}}{\partial\{U\}}$$

The matrices F and G are

$$F = \begin{bmatrix} \frac{Y_\eta}{J}({}^bu_{P/Q}+{}^iu_{P/O}) - \frac{X_\eta}{J}{}^bv_{P/Q} & -\frac{X_\eta}{J}{}^iu_{P/O} \\ \frac{Y_\eta}{J}{}^iv_{P/O} & \frac{Y_\eta}{J}{}^bu_{P/Q} - \frac{X_\eta}{J}({}^bv_{P/Q}+{}^iv_{P/O}) \end{bmatrix} \quad (52)$$

$$G = \begin{bmatrix} -\frac{Y_\xi}{J}({}^bu_{P/Q}+{}^iu_{P/O}) + \frac{X_\xi}{J}{}^bv_{P/Q} & \frac{X_\xi}{J}{}^iu_{P/O} \\ -\frac{Y_\xi}{J}{}^iv_{P/O} & -\frac{Y_\xi}{J}{}^bu_{P/Q} + \frac{X_\xi}{J}({}^bv_{P/Q}+{}^iv_{P/O}) \end{bmatrix} \quad (53)$$

with

$${}^bu_{P/Q} = {}^iu_{P/O}+RY-{}^iu_{Q/O}$$

$${}^bv_{P/Q} = {}^iv_{P/O}-RX-{}^iv_{Q/O}$$

If continuity is exactly satisfied, then the nonconservative form is equally valid, and the matrices F and G become:

$$F = \begin{bmatrix} \frac{Y_\eta}{J}{}^bu_{P/Q} - \frac{X_\eta}{J}{}^bv_{P/Q} & 0 \\ 0 & \frac{Y_\eta}{J}{}^bu_{P/Q} - \frac{X_\eta}{J}{}^bv_{P/Q} \end{bmatrix} \quad (54)$$

$$G = \begin{bmatrix} -\frac{Y_\xi}{J}{}^bu_{P/Q} + \frac{X_\xi}{J}{}^bv_{P/Q} & 0 \\ 0 & -\frac{Y_\xi}{J}{}^bu_{P/Q} + \frac{X_\xi}{J}{}^bv_{P/Q} \end{bmatrix} \quad (55)$$

These matrices are also the same as would be obtained by quasi-linearising the equations, assuming that the body-axis velocity is locally

constant. This assumption is better for regions of the flow which are some distance from the body, so that the body's disturbances are small compared with the magnitude of the "freestream" flow. Since the body-axis velocity is the negative of the inertial velocity of the grid plus the inertial velocity of the flow, the inertial velocities may be viewed as perturbations to the grid velocity.

The eigenvalues of F and G (assuming continuity is satisfied) are:

$$\lambda_F = \frac{Y_\eta}{J}{}^b u_{P/Q} - \frac{X_\eta}{J}{}^b v_{P/Q}$$

$$\lambda_G = -\frac{Y_\xi}{J}{}^b u_{P/Q} + \frac{X_\xi}{J}{}^b v_{P/Q} \qquad (56)$$

The eigenvalues are seen to depend upon the body-axis velocity, not the inertial velocity. This is a direct consequence of the use of the body-axis velocity to describe the transport of momentum through the control volume. The sign of these eigenvalues indicates the flow of information due to these terms. The numerical algorithm depends upon the sign of these eigenvalues to determine in which direction the upwind finite differences will be made.

This result indicates an important rule for understanding the role of the body axis and inertial velocities. Whenever one is using a velocity in a context which regards the convective transport of any quantity, the appropriate velocity to use is the body-axis velocity. If the context regards the linear momentum contained within the flow, inertial velocity is the appropriate one. For example, if one is calculating the stream function by integrating along a line in the computational grid, the body-axis velocity should be used. This is because the stream function represents the mass flux accross the line used in the integration. Only in this manner will the stream function have a constant value at the body surface.

Near the body, the body-axis velocities are dominated by the inertial

velocity, since at the body surface the inertial velocity is identical to the velocity of the grid and the body-axis velocity is zero (no slip boundary condition). Ideally, continuity should be satisfied at all times, but this may not be true numerically as the solution is iterated to convergence at a given time step. If this is the case, then the additional terms of the conservative form may be a source of error in the momentum equations. Therefore, it is useful to examine the continuity terms as they appear in the the momentum equations. The differences between the conservation and nonconservation forms of F and G are:

$$F' = \begin{bmatrix} \frac{Y_\eta}{J}{}^i u_{P/O} & -\frac{X_\eta}{J}{}^i u_{P/O} \\ \frac{Y_\eta}{J}{}^i v_{P/O} & -\frac{X_\eta}{J}{}^i v_{P/O} \end{bmatrix} \qquad (58)$$

$$G' = \begin{bmatrix} -\frac{Y_\xi}{J}{}^i u_{P/O} & \frac{X_\xi}{J}{}^i u_{P/O} \\ -\frac{Y_\xi}{J}{}^i v_{P/O} & \frac{X_\xi}{J}{}^i v_{P/O} \end{bmatrix} \qquad (59)$$

If F' and G' are combined along with their associated velocity derivatives, the result is $\{u\}(\nabla \cdot {}^i V_{P/O})$. The eigenvalues for F' and G' are:

$$\lambda_{F'1} = \frac{Y_\eta}{J}{}^i u_{P/O} - \frac{X_\eta}{J}{}^i v_{P/O}$$

$$\lambda_{F'2} = 0$$

$$\lambda_{G'1} = -\frac{Y_\xi}{J}{}^i u_{P/O} + \frac{X_\xi}{J}{}^i v_{P/O}$$

$$\lambda_{G'2} = 0 \qquad (60)$$

The associated eigenvectors for the non-zero eigenvalues are {U} for both

matrices. If continuity is not satisfied due to incomplete numerical convergence, the upwind differencing of these terms must be considered, especially if conservative differencing is used. For any area of the flow in which the body–axis velocities are decelerated, the eigenvalues of F and F' or of G and G' may be of opposite sign. This happens close to the body, in separated regions, and near the stagnation streamline. These error terms will then be downwind differenced and may be unstable.

FINITE DIFFERENCE EQUATIONS

The continuum equations are approximated numerically with finite difference equations. The finite difference equations are then solved using a block successive over relaxation (SOR) method. Each column vector in Equation 31 is differenced so as to model the physical dynamics which it represents. Second order spacial differences are used throughout. For the remainder of this paper, U and V will be understood to be ${}^{i}u_{P/O}$ and ${}^{i}v_{P/O}$ (the inertial velocities).

A curvilinear, body fitted grid is used to define the mapping to the computational domain. This is shown in Figure 2. The computational domain is a rectangular area, in which the grid lines are straight, orthogonal, and spaced one unit apart ($\Delta\xi$=1, $\Delta\eta$=1). The geometry of the body and grid, and the velocities are defined at the mesh node points, and indexed by i in the ξ direction and by j in the η direction. The metric quantities X_ξ, Y_ξ, X_η, Y_η, and J are defined at the center of the quadrilateral cells bounded by the mesh points. In addition to the metrics, the pressure (P), viscosity, and velocity gradients are also defined at the cell centers. The cell centers are defined in the transformed plane rather than the physical plane, and the geometrical coordinates of the centers are not explicity calculated. The center points are indexed similarly to the mesh points, ie., the point (i+1/2,j+1/2) lies within the cell bounded by (i,j), (i+1,j), (i, j+1), (i+1,j+1). These indices will be indicated using subscripts, and the time level of the variables will be indicated using superscripts. The index n will indicate the present time, and n−1 will indicate one time step (Δt) in the past.

Upwind Differencing

The velocity components are differenced in time using a first order backward difference.

$$\frac{\partial\{U\}}{\partial t} \cong \left(\{U\}^{n}_{i,j} - \{U\}^{n-1}_{i,j} \right)/\Delta t = \left(\{u\}^{n}_{i,j} - \{u\}^{n-1}_{i,j} \right)J/\Delta t \qquad (61)$$

This results in an implicit method with no stability limitations. The time step, Δt, is therefore, only constrained by the accuracy required to adequately model the unsteady flow dynamics.

The convective terms are differenced using three point one sided differences which are differenced in the upwind direction. The upwind direction is determined by the sign of the eigenvalue, as calculated by Equation 36. The upwind differences are, for positive eigenvalues:

$$\frac{\partial\{f\}}{\partial\xi} \cong 3/2\ \{f\}^{n}_{i,j} - 2\ \{f\}^{n}_{i-1,j} + 1/2\ \{f\}^{n}_{i-2,j}$$

$$\frac{\partial\{g\}}{\partial\eta} \cong 3/2\ \{g\}^{n}_{i,j} - 2\ \{g\}^{n}_{i,j-1} + 1/2\ \{g\}^{n}_{i,j-2} \qquad (62)$$

and for negative eigenvalues:

$$\frac{\partial\{f\}}{\partial\xi} \cong -3/2\ \{f\}^{n}_{i,j} + 2\ \{f\}^{n}_{i+1,j} - 1/2\ \{f\}^{n}_{i+2,j}$$

$$\frac{\partial\{g\}}{\partial\eta} \cong -3/2\ \{g\}^{n}_{i,j} + 2\ \{g\}^{n}_{i,j+1} - 1/2\ \{g\}^{n}_{i,j+2} \qquad (63)$$

One sided differences were selected for these terms because they correctly modelled the flow of information represented by the fluid, and because they have dissipative truncation error characteristics that enhance the stability of the calculation. Metric terms appearing within the flux vectors were calculated using conventional central differences.

A nonlinear consistency analysis was performed for these terms differenced in both conservative and nonconservative linearized form. The

nonconservative form is obtained by evaluating the diagonal F and G matrices at the i,j location for all terms. This is in contrast to differencing them at each point in the mesh molecule, as is done implicitly when differencing the {f} and {g} vectors in the conservative manner above. For simplicity, the analysis assumed a uniform rectangular grid and differencing such that $\Delta X = \Delta\xi$ and $\Delta Y = \Delta\eta$. For the conservative differencing, this results in:

$$\begin{aligned}
&\frac{\partial}{\partial\xi}\left({}^{l}u_{P/O}\,{}^{b}u_{P/Q}\right) + \frac{\partial}{\partial\eta}\left({}^{l}u_{P/O}\,{}^{b}v_{P/Q}\right) \\
&= {}^{b}u_{P/Q}u_{\xi} + u(u_{\xi}+v_{\eta}) + {}^{b}v_{P/Q}u_{\eta} \\
&\quad - [(2u_{\xi}+R)u_{\xi\xi} + 1/3(u+{}^{b}u_{P/Q})u_{\xi\xi\xi}](\Delta\xi)^2 \\
&\quad - [(v_{\eta}-R)u_{\eta\eta}) + u_{\eta}v_{\eta\eta} \\
&\quad + 1/3\,{}^{b}v_{P/Q}u_{\eta\eta\eta} + 1/3uv_{\eta\eta\eta}](\Delta\eta)^2 \\
&\quad + O[(\Delta\xi)^3,(\Delta\eta)^3] \qquad (64)
\end{aligned}$$

$$\begin{aligned}
&\frac{\partial}{\partial\xi}\left({}^{l}v_{P/O}\,{}^{b}u_{P/Q}\right) + \frac{\partial}{\partial\eta}\left({}^{l}v_{P/O}\,{}^{b}v_{P/Q}\right) \\
&= {}^{b}u_{P/Q}v_{\xi} + v(u_{\xi}+v_{\eta}) + {}^{b}v_{P/Q}v_{\eta} \\
&\quad - [(v_{\xi}u_{\xi\xi} + (u_{\xi}+R)v_{\xi\xi} + 1/3vu_{\xi\xi\xi} \\
&\quad + 1/3\,{}^{b}u_{P/Q}v_{\xi\xi\xi}](\Delta\xi)^2 \\
&\quad - [(2v_{\eta}-R)v_{\eta\eta} + 1/3(v+{}^{b}v_{P/Q})v_{\eta\eta\eta}](\Delta\eta)^2 \\
&\quad + O[(\Delta\xi)^3,(\Delta\eta)^3] \qquad (65)
\end{aligned}$$

The unadorned velocities and their derivatives are inertial velocities at the i,j

grid point. Using nonconservative differencing for the same case results in:

$$
\begin{aligned}
&{}^{b}u_{P/Q}\underset{\partial\xi}{\partial}{}^{i}u_{P/O} + {}^{b}v_{P/Q}\underset{\eta}{\partial}{}^{i}u_{P/O} \\
&= {}^{b}u_{P/Q}u_{\xi} + {}^{b}v_{P/Q}u_{\eta} \\
&\quad - [1/3{}^{b}u_{P/Q}u_{\xi\xi\xi}](\Delta\xi)^2 - [1/3{}^{b}v_{P/Q}u_{\eta\eta\eta}](\Delta\eta)^2 \\
&\quad + O[(\Delta\xi)^3,(\Delta\eta)^3]
\end{aligned}
\qquad (66)
$$

$$
\begin{aligned}
&{}^{b}u_{P/Q}\underset{\partial\xi}{\partial}{}^{i}v_{P/O} + {}^{b}v_{P/Q}\underset{\eta}{\partial}{}^{i}v_{P/O} \\
&= {}^{b}u_{P/Q}v_{\xi} + {}^{b}v_{P/Q}v_{\eta} \\
&\quad - [1/3{}^{b}u_{P/Q}v_{\xi\xi\xi}](\Delta\xi)^2 - [1/3{}^{b}v_{P/Q})v_{\eta\eta\eta}](\Delta\eta)^2 \\
&\quad + O[(\Delta\xi)^3,(\Delta\eta)^3]
\end{aligned}
\qquad (67)
$$

Both methods are second order accurate. When compared with nonconservative differencing, conservative differencing is subject to a diffusion truncation error whose sign depends on the sign of the rotation and the first order velocity derivatives, and thus may be stabilizing or destabilizing in different parts of the flow.. It also includes the velocity divergence terms, as expected. These latter terms are identically zero in the ideal case. Numerically, however, these terms may not be identically zero due to many reasons. These include not solving directly for all of the points in the domain, but updating them in a point wise or row wise manner; errors in the pressure calculation; and incomplete convergence of the equations in general. Nonconservative differencing may be expected to be more robust under these conditions because of the fewer truncation error terms.

Four Point Central Difference Operator

The pressure gradient and viscous terms were differenced using a four point central difference scheme. This scheme results from a continuous linear interpolation operator, which was based upon the ideas of Walitt (Ref 5). The linear interpolator for some quantitiy, X, with $i \leq \xi \leq i+1$, $j \leq \eta \leq j+1$, is given by:

$$\begin{aligned} X^n(\xi,\eta) \cong\ & X^n_{i,j}(i+1-\xi)(j+1-\eta) + X^n_{i+1,j}(\xi-i)(j+1-\eta) \\ & + X^n_{i,j+1}(i+1-\xi)(\eta-j) + X^n_{i+1,j+1}(\xi-i)(\eta-j) \end{aligned} \qquad (68)$$

This function reduces to linear interpolation at the boundaries, and at the center, it becomes the average of the corner points. If the derivatives with respect to ξ and η are also evaluated at the center, they too become the simple average of the central differences at the edges:

$$X^n_\xi\ (\xi=i+1/2,\eta=j+1/2) \cong (-X^n_{i,j} + X^n_{i+1,j} - X^n_{i,j+1} + X^n_{i+1,j+1})/4$$

$$X^n_\eta\ (\xi=i+1/2,\eta=j+1/2) \cong (-X^n_{i,j} - X^n_{i+1,j} + X^n_{i,j+1} + X^n_{i+1,j+1})/4 \qquad (69)$$

The operator is second order accurate, as seen from the modified equations for the ξ and η derivatives:

$$\begin{aligned} X_\xi\ (\xi=i+1/2,\eta=j+1/2) =\ & X_\xi + X_{\xi\xi\xi}(\Delta\xi)^2/24 \\ & + X_{\xi\eta\eta}(\Delta\eta)^2/8 + O[(\Delta\xi)^4, (\Delta\eta)^4] \end{aligned}$$

$$\begin{aligned} X_\eta\ (\xi=i+1/2,\eta=j+1/2) =\ & X_\eta + X_{\eta\eta\eta}(\Delta\eta)^2/24 \\ & + X_{\xi\xi\eta}(\Delta\xi)^2/8 + O[(\Delta\xi)^4, (\Delta\eta)^4] \end{aligned} \qquad (71)$$

This central difference operator is used repeatedly to calculate the {h} and {i} vectors at the cell centers by calculating the metrics and velocity gradient terms from the surrounding mesh nodes, as in

$$u^n_{\xi i+1/2,j+1/2} = (-u^n_{i,j} + u^n_{i+1,j} - u^n_{i,j+1} + u^n_{i+1,j+1})/4$$

$$u^n_{\eta i+1/2,j+1/2} = (-u^n_{i,j} - u^n_{i+1,j} + u^n_{i,j+1} + u^n_{i+1,j+1})/4$$

$$v^n_{\xi i+1/2,j+1/2} = (-v^n_{i,j} + v^n_{i+1,j} - v^n_{i,j+1} + v^n_{i+1,j+1})/4$$

$$v^n_{\eta i+1/2,j+1/2} = (-v^n_{i,j} - v^n_{i+1,j} + v^n_{i,j+1} + v^n_{i+1,j+1})/4 \qquad (72)$$

in order to form the {h} and {i} vectors. Once the {h} and {i} vectors are calculated at the cell centers, the four point central difference operator is again applied to calculate their derivatives at the mesh node point of interest. The pressure gradient at the node point is also calculated from the cell centered pressures in the same manner.

Discrete Momentum Equations

When the finite difference approximations above are substituted into the momentum equations (28–29) the convective portion becomes (for positive eigenvalues):

$$\begin{aligned}
&\{J/\Delta t + 3/2[(Y_{\eta i,j} - Y_{\xi i,j})\ {}^b u^n_{i,j} + (X_{\xi i,j} - X_{\eta i,j})\ {}^b v^n_{i,j}]\}\ u^n_{i,j} - R\ v^n_{i,j} \\
&= 2[(Y^n_{\eta i-1,j}\ {}^b u^n_{i-1,j} - X^n_{\eta i-1,j}\ {}^b v^n_{i-1,j})\ u^n_{i-1,j} \\
&\quad + (Y^n_{\xi i,j-1}\ {}^b u^n_{i,j-1} + X^n_{\xi i,j-1}\ {}^b v^n_{i,j-1})\ u^n_{i,j-1}] \\
&\quad - 1/2[(Y^n_{\eta i-2,j}\ {}^b u^n_{i-2,j} - X^n_{\eta i-2,j}\ {}^b v^n_{i-2,j})\ u^n_{i-2,j} \\
&\quad + (-Y^n_{\xi i,j-2}\ {}^b u^n_{i,j-2} + X^n_{\xi i,j-2}\ {}^b v^n_{i,j-2})\ u^n_{i,j-2}] \\
&\quad + (J/\Delta t)\ u^{n-1}_{i,j} + RHS_X
\end{aligned}$$

$$\begin{aligned}
&\{J/\Delta t + 3/2[(Y_{\eta i,j} - Y_{\xi i,j})\ {}^b u^n_{i,j} + (X_{\xi i,j} - X_{\eta i,j})\ {}^b v^n_{i,j}]\}\ v^n_{i,j} + R\ u^n_{i,j} \\
&= 2[(Y^n_{\eta i-1,j}\ {}^b u^n_{i-1,j} - X^n_{\eta i-1,j}\ {}^b v^n_{i-1,j})\ v^n_{i-1,j} \\
&\quad + (Y^n_{\xi i,j-1}\ {}^b u^n_{i,j-1} + X^n_{\xi i,j-1}\ {}^b v^n_{i,j-1})\ v^n_{i,j-1}] \\
&\quad - 1/2[(Y^n_{\eta i-2,j}\ {}^b u^n_{i-2,j} - X^n_{\eta i-2,j}\ {}^b v^n_{i-2,j})\ v^n_{i-2,j} \\
&\quad + (-Y^n_{\xi i,j-2}\ {}^b u^n_{i,j-2} + X^n_{\xi i,j-2}\ {}^b v^n_{i,j-2})\ v^n_{i,j-2}] \\
&\quad + (J/\Delta t)\ v^{n-1}_{i,j} + RHS_Y
\end{aligned} \qquad (73)$$

with

$$
\begin{aligned}
{}^{b}u^{n}_{i,j} &= u^{n}_{i,j} + R\,Y_{ij} - {}^{i}u_{Q/Oi,j}{}^{n} \\
{}^{b}v^{n}_{i,j} &= v^{n}_{i,j} - R\,X_{ij} - {}^{i}v_{Q/Oi,j}{}^{n}
\end{aligned}
$$

The rotational source terms have been brought back to the left hand side above, in preparation for the block SOR calculation. In contrast to the {h} and {i} vectors, the metric terms in the {f} and {g} vectors are calculated using conventional central differences about the node points:

$$
\begin{aligned}
X_{\xi ij} &= (X_{i+1,j} - X_{i-1,j})/2 \\
X_{\eta ij} &= (X_{i,j+1} - X_{i,j-1})/2 \\
Y_{\xi ij} &= (Y_{i+1,j} - Y_{i-1,j})/2 \\
Y_{\eta ij} &= (Y_{i,j+1} - Y_{i,j-1})/2
\end{aligned}
\qquad (74)
$$

Calculating the metrics at each i,j location and differencing them with the fluxes allows an intuitive interpretation of these terms. The centrally differenced metrics may be considered to represent the face areas of a cell which is centered about the grid line. Multiplying this area by the velocity at the line is an approximation to the total momentum flux moving through that face. These fluxes are then differenced to calculate the net flux moving through the cell. This is analogous to a finite volume approach.

The force terms become:

$$
\begin{aligned}
RHS_X \;=\; & 1/2\{\, [P/\rho(Y_\xi - Y_\eta)]^n_{i+1/2,j+1/2} - [P/\rho(Y_\eta + Y_\xi)]^n_{i+1/2,j-1/2} \\
& \quad + [P/\rho(Y_\eta - Y_\xi)]^n_{i-1/2,j-1/2} + [P/\rho(Y_\eta + Y_\xi)]^n_{i-1/2,j+1/2} \,\} \\
& + 1/4\{\, u^n_{i,j} \,[\, - a^n_{i+1/2,j+1/2} - a^n_{i-1/2,j+1/2} - a^n_{i-1/2,j-1/2} - a^n_{i+1/2,j-1/2} \\
& \qquad + 2(b^n_{i+1/2,j+1/2} - b^n_{i-1/2,j+1/2} - b^n_{i+1/2,j-1/2} + b^n_{i-1/2,j-1/2}) \\
& \qquad - g^n_{i+1/2,j-1/2} - g^n_{i+1/2,j-1/2} - g^n_{i-1/2,j+1/2} - g^n_{i-1/2,j-1/2}] \\
& + u^n_{i+1,j+1}\,[a^n_{i+1/2,j+1/2} - 2b^n_{i+1/2,j+1/2} + g^n_{i+1/2,j+1/2}] \\
& + u^n_{i+1,j-1}\,[a^n_{i+1/2,j-1/2} + 2b^n_{i+1/2,j-1/2} + g^n_{i+1/2,j-1/2}] \\
& + u^n_{i-1,j+1}\,[a^n_{i-1/2,j+1/2} + 2b^n_{i-1/2,j+1/2} + g^n_{i-1/2,j+1/2}] \\
& + u^n_{i-1,j-1}\,[a^n_{i-1/2,j-1/2} - 2b^n_{i+1/2,j+1/2} + g^n_{i-1/2,j-1/2}] \\
& + u^n_{i+1,j}\,[a^n_{i+1/2,j+1/2} + a^n_{i+1/2,j-1/2} - g^n_{i+1/2,j+1/2} - g^n_{i+1/2,j-1/2}] \\
& + u^n_{i,j+1}\,[g^n_{i+1/2,j+1/2} + g^n_{i-1/2,j+1/2} - a^n_{i+1/2,j+1/2} - a^n_{i-1/2,j+1/2}] \\
& + u^n_{i-1,j}\,[a^n_{i-1/2,j+1/2} + a^n_{i-1/2,j-1/2} - g^n_{i-1/2,j+1/2} - g^n_{i-1/2,j-1/2}] \\
& + u^n_{i,j-1}\,[g^n_{i-1/2,j-1/2} + g^n_{i+1/2,j-1/2} - a^n_{i-1/2,j-1/2} - a^n_{i+1/2,j-1/2}] \,\}
\end{aligned}
$$

$$
\begin{aligned}
RHS_Y \;=\; & 1/2\{\, [P/\rho(X_\eta - X_\xi)]^n_{i+1/2,j+1/2} - [P/\rho(X_\eta + X_\xi)]^n_{i-1/2,j+1/2} \\
& \quad + [P/\rho(X_\xi - X_\eta)]^n_{i-1/2,j-1/2} + [P/\rho(X_\eta + X_\xi)]^n_{i+1/2,j-1/2} \,\} \\
& + 1/4\{\, v^n_{i,j} \,[\, - a^n_{i+1/2,j+1/2} - a^n_{i-1/2,j+1/2} - a^n_{i-1/2,j-1/2} - a^n_{i+1/2,j-1/2} \\
& \qquad + 2(b^n_{i+1/2,j+1/2} - b^n_{i-1/2,j+1/2} - b^n_{i+1/2,j-1/2} + b^n_{i-1/2,j-1/2}) \\
& \qquad - g^n_{i+1/2,j-1/2} - g^n_{i+1/2,j-1/2} - g^n_{i-1/2,j+1/2} - g^n_{i-1/2,j-1/2}] \\
& + v^n_{i-1,j+1}\,[a^n_{i-1/2,j+1/2} + 2b^n_{i-1/2,j+1/2} + g^n_{i-1/2,j+1/2}] \\
& + v^n_{i-1,j-1}\,[a^n_{i-1/2,j-1/2} - 2b^n_{i+1/2,j+1/2} + g^n_{i-1/2,j-1/2}] \\
& + v^n_{i+1,j+1}\,[a^n_{i+1/2,j+1/2} - 2b^n_{i+1/2,j+1/2} + g^n_{i+1/2,j+1/2}] \\
& + v^n_{i+1,j-1}\,[a^n_{i+1/2,j-1/2} + 2b^n_{i+1/2,j-1/2} + g^n_{i+1/2,j-1/2}] \\
& + v^n_{i+1,j}\,[a^n_{i+1/2,j+1/2} + a^n_{i+1/2,j-1/2} - g^n_{i+1/2,j+1/2} - g^n_{i+1/2,j-1/2}] \\
& + v^n_{i,j+1}\,[g^n_{i+1/2,j+1/2} + g^n_{i-1/2,j+1/2} - a^n_{i+1/2,j+1/2} - a^n_{i-1/2,j+1/2}] \\
& + v^n_{i-1,j}\,[a^n_{i-1/2,j+1/2} + a^n_{i-1/2,j-1/2} - g^n_{i-1/2,j+1/2} - g^n_{i-1/2,j-1/2}] \\
& + v^n_{i,j-1}\,[g^n_{i-1/2,j-1/2} + g^n_{i+1/2,j-1/2} - a^n_{i-1/2,j-1/2} - a^n_{i+1/2,j-1/2}] \,\}
\end{aligned}
\qquad (75)
$$

where:

$$a = \nu\alpha/J$$

$$b = \nu\beta/J$$

$$g = \nu\gamma/J$$

Again, the quantities at i±1/2, j±1/2 are defined at the centers of the cells surrounding the i,j node point.

The nine point combination of velocities representing the viscous contribution is still second order accurate. As an example, consider a straight, uniform, but not necessarily orthogonal grid in which α, γ, and β are constant. For this case, the viscous terms (RHS_{Visc}) become:

$$\begin{aligned} RHS_{ViscX} = {} & (-a - g)\, u^n_{i,j} + (a - g)\, u^n_{i+1,j}/2 + (a - g)\, u^n_{i-1,j}/2 \\ & + (-a + g)\, u^n_{i,j+1}/2 + (-a + g)\, u^n_{i,j-1}/2 \\ & + (a - 2b + g)\, u^n_{i+1,j+1}/4 + (a + 2b + g)\, u^n_{i-1,j+1}/4 \\ & + (a + 2b + g)\, u^n_{i+1,j-1}/4 + (a - 2b + g)\, u^n_{i-1,j-1}/4 \end{aligned} \quad (76)$$

The other component has the same form. When Taylor series are substituted into the equation above, the modified equation is obtained:

$$\begin{aligned} RHS_{ViscX} = {} & a\, u_{\xi\xi} - 2\, b\, u_{\xi\eta} + g\, u_{\eta\eta} + a(\Delta\xi)^2\, u_{\xi\xi\xi\xi}/12 \\ & - b(\Delta\xi)^2\, u_{\xi\xi\xi\eta}/3 + [g(\Delta\xi)^2 + a(\Delta\eta)^2]\, u_{\xi\xi\eta\eta}/4 \\ & - b(\Delta\eta)^2\, u_{\xi\eta\eta\eta}/3 + g(\Delta\eta)^2\, u_{\eta\eta\eta\eta}/12 + O[(\Delta\xi)^4, (\Delta\eta)^4] \end{aligned} \quad (77)$$

The cross derivative term has appeared implicitly even though it was not expicitly written into the original difference equation.

Next, these equations are solved for $u^n_{i,j}$ and $v^n_{i,j}$. This requires the solving for them simultaneously, since the rotation terms couple the two components together. The equations may be put into the form $[A]\{u\}=\{B\}$, where $[A]$ is a two by two matrix and $\{B\}$ is a column vector containing all of the terms except for the ones containing $u^n_{i,j}$ and $v^n_{i,j}$. The elements of $[A]$ and $B\}$ are (for positive eigenvalues):

$$\begin{aligned} A_{11} = A_{22} = {} & J/\Delta t + 3/2[(Y_\eta - Y_\xi)_{i,j}\, {}^b u^n_{i,j} + (X_\xi - X_\eta)_{i,j}\, {}^b v^n_{i,j}] \\ & + 1/4[a^n_{i+1/2,j+1/2} + a^n_{i-1/2,j+1/2} + a^n_{i+1/2,j-1/2} + a^n_{i-1/2,j-1/2} \\ & - 2(b^n_{i+1/2,j+1/2} - b^n_{i-1/2,j+1/2} - b^n_{i+1/2,j-1/2} + b^n_{i-1/2,j-1/2}) \\ & + g^n_{i+1/2,j+1/2} + g^n_{i-1/2,j+1/2} + g^n_{i+1/2,j-1/2} + g^n_{i-1/2,j-1/2}] \end{aligned}$$

$$\begin{aligned} A_{12} &= -R \\ A_{21} &= R \end{aligned} \quad (78)$$

CONCLUSIONS AND RECOMMENDATIONS

The objective of developing a method to calculate the laminar incompressible Navier Stokes equations about arbitrary bodies undergoing arbitrary motion was not completely achieved.

The derivation of the Navier Stokes equations for an accelerating control volume was accomplished. The nonconservative and strong conservation form for these equations, including viscous terms in conservation form, was derived. The use of inviscid boundary conditions allowing disturbances to exit the domain was also investigated, but not conclusively demonstrated.

The numerical solutions have been characterized by slow convergence and difficulties in conserving mass throughout the domain. There is some evidence to suggest that there are long period periodic error components which are not being eliminated by the relaxation method used to solve the equations.

It is recommended that further investigations be conducted to resolve these problems. Approaches which might be profitable include:

1. Abandoning the cell centered pressures and artificial compressiblity method in favor of the more traditional Poisson equation for pressures evaluated at the nodal points.

2. Using a different method to solve the discrete equations. Possible candidates would include using a conjugate gradient algorithm to minimize some measure of the residuals, and multigrid methods.

3. Investigating different boundary conditions, particularly for the cell centered pressures.

The pressure contours highlight the asymmetric nature of the solution. They also indicate that there may be some difficulty in the forward stagnation region. The change in slope crossing the periodic boundary is an indication that a similar error to that seen in Stokes first problem may be occuring.

The remaining two frames show the global domain. Once again, the major effects of the solution are confined to the immediate vicinity of the body, indicting a lack of convergence in the flowfield.

free stream condition for this case. This is also shown by the streamlines, pressure contours, and vorticity contours.

The remaining plots show the same information, but for the entire domain. Some pressure influence has propagated throughout the domain in a symmetric fashion. The looping shape of the pressure contours suggests that there may be a periodic error which has a period of one half the width of the computational domain.

The third test case is the same circular cylinder which has been impulsively accelerated from rest to a constant speed at a Reynolds number of 20. . At the time of the results shown in Figure 8, the cylinder has moved a distance of 0.4 diameters. Ten time steps have been used with 20 SOR iterations at each time step. The inviscid boundary conditions have been used at the far field.

The inertial velocity vectors of Figure 8a indicate that very little acceleration of the flow is taking place at the midpoints of the cylinder and the wake region shows little deceleration of the flow except in the immediate vicinity of the cylinder. The flow is also not symmetric. These observations are also indicated by the body-axis velocity vectors of the next plot. This plot also indicates that the flow is attached all the way to the aft stagnation point.

The third view shows the streamlines. The stream function was calculated by integrating

$$\Psi = \int \rho^b u_{P/Q}\, dy \; - \; \int \rho^b v_{P/Q}\, dx \qquad (93)$$

along the radial grid lines extending from the surface out to the exterior boundary. The streamlines are lines of constant Ψ. The trapezoidal rule was used for integration. A careful comparison of the body-axis velocity vectors and the stream function contours shows that the velocity vectors are not parallel to the contours, particularly in the region above the cylinder. This indicates that mass is not being conserved in this region.

program is having difficulty in eliminating errors in this area. During the initial stages of the calculation, the magnitude of the velocity was seen to decrease across the entire domain except at the very last point. Here the velocity was set equal to the velocity at the other side of the domain because of the periodic boundary condition. The error in the velocity thus had a sawtooth pattern. As the calculation was iterated, the mean value of the velocity at a given height increased, and the magnitude of the sawtooth decreased. The pressure contours are reflecting this error in the velocity calculation.

The final plot from Stoke's first problem shows contours of constant vorticity. As expected, they are parallel to the surface. Since the ideal pressure gradient is zero, boundary layer theory indicates that the velocity profile next to the wall should be linear. Thus the normal derivative of the vorticity should be zero. The wider spacing of the vorticity contours next to the wall indicate that this condition is being approximately satisfied.

The next case to be considered is a circular cylinder in pure rotation. Figure 6 shows the grid used for this case. It consists of 46 points in the circumferential direction and 41 points in the radial direction. The radial distribution is geometrically stretched so as to maintain a constant aspect ratio for each cell. The outer boundary is at 25 radii. The rate of rotation was chosen to give a Reynolds number (based on the diameter) of 100 at the cylinder wall. Dirichlet free stream boundary conditions were used again for this case. 100 time steps have elapsed, with five SOR iterations being performed at each time step.

The inertial velocity vectors are shown in Figure 7a. It can be seen that the solution has hardly progressed from the region in the immediate vicinity of the cylinder. This is also shown by the body-axis velocities shown in the next plot. The no-slip boundary condition is enforced and the flow rapidly transitions to the apparent solid-body rotation which represents the

Two time steps were used, with 100 SOR iterations at each time step. A single iteration consisted of relaxing each point along a line of ξ=constant starting from the wall and proceeding outward to the outer boundary. This sweep was applied to each vertical grid line, moving from left to right across the entire domain. It was then repeated while moving the line sweeps from right to left, also sweeping from the wall to the outside along each line. A relaxation parameter of 1 was used. The elapsed time was chosen so that the top of the domain at the final time corresponds to η = 2, where η is Schlichting's nondimensional height, $\eta = Y/(2\sqrt{\nu t})$. The plate is moving from left to right.

The inertial velocity vectors shown in Figure 5a indicate the unknowns for which the equations are solved. Plotted for comparison is the exact solution. It can be seen that the qualitative agreement is good. The flow is parallel to the plate and the profiles at each location are the same. There is some numerical disagreement. This may be due to the small number of large time steps and the attendant lag caused by the truncation error. It may also be due to a lack of complete convergence in the calculation. The velocity profile was still evolving slowly when the program was terminated after 100 iterations.

The next view in Figure 5 shows the body-axis velocity vectors. These show the boundary layer profile and illustrate the no-slip boundary condition at the wall. The streamlines presented in the next view are also consistent with the velocity vectors, indicating parallel flow.

Figure 5d presents lines of equal pressure. The spacing between the lines corresponds to a change in c_p of 1.6×10^{-7}. This verifies that for the outer boundary conditions chosen, the pressures are essentially constant. Over most of the domain, the pressure gradient is also zero. However, near the corners of the domain the large relative changes in the pressure indicate that the

COMPUTATIONAL RESULTS

The numerical experiments which have been performed indicate that the method is promising, but not yet fully developed. Test cases which have been tried include Stoke's first problem, a circular cylinder in pure rotation, a circular cylinder in pure translation, an elliptical cylinder in pure translation, and an elliptical cylinder in pure rotation. The results from the first three test cases will be presented to illustrate some of the problems that have been encountered.

Stokes first problem consists of a quiet fluid bounded by a flat plate which is infinite in extent in both directions. The plate is instantaneously set in motion at a constant speed. This results in a shear layer next to the plate which diffuses upward as time progresses. The exact solution for this case is presented in Schlichting (Ref 7). The pressure should be zero throughout the domain, and the flow is parallel to the plate. In addition, the velocity profiles at each location at a given time are identical. This case was selected as a benchmark because it has an exact solution for comparison. It is sensitive to the pressure calculation and the flow is parallel to the outer boundary, which provides a difficult test of the exterior boundary conditions.

The computational grid for this example is shown in Figure 4. It is a uniform rectangular mesh with 16 points in the ξ direction and 41 points in the η direction. Periodic boundary conditions are applied to the ends of the domain (ξ=1 and ξ=16). Since this is a simply connected physical domain, rather than the doubly connected physical domain surrounding a closed body, the periodic boundary conditions can be regarded as simulating an inifinite series of domains stretching to the right and left of the domain under consideration at a given iteration. For the results shown in Figure 5, free stream Dirichlet boundary conditions were applied to the top of the domain. Thus this calculation is equivalent to non-steady Couette flow.

along the entire boundary. Note that this is similar to applying Dirichlet boundary conditions at phantom grid locations just outside of the boundary. This had a negligible effect for translating cases, since the eigenvalues on the downstream side of the grid resulted in differencing into the domain.

Pressures were assumed to be zero outside of the domain. This was modelled after the common experimental observation that the static pressure rapidly returns to the free stream value as one moves away from the body. Since the outer boundary was typically more than ten chords away from the body surface, this was judged to be a reasonable assumption. It also has the effect of fixing the value of the pressure, since the absolute value of the pressure is arbitrary, and only its gradient affects the fluid dynamics. The effect of the assumed pressures outside the domain on the pressures inside is felt in an indirect way. The outside pressures only affect the velocities on the boundary. These velocities are then used to compute the pressures at the centers of the cell just inside the boundary.

No means were explicitly employed to ensure that the net mass flux through the entire boundary was conserved. It was assumed that the pressure calculation would enforce the conservation of mass throughout the domain. This is the principal deficiency in these boundary conditions. It is especially apparent for symmetric cases involving flow parallel to the boundary, such as the case of the circular cylinder in spinning motion. Here there is no constraint to ensure that the velocities at the boundary are directed in a strictly tangential direction.

terms. Viscous terms were neglected at the boundary since mathematically they are elliptic in nature and require values outside of the domain. This is in keeping with the observed fact that the Euler equations are a good approximation to the flow outside of the boundary layer. If the fluid was flowing into the domain, the upwind difference formula required inertial velocity values outside. These were assumed to be zero, corresponding to undisturbed fluid. If fluid was exiting the domain, the upwind differencing only required values inside and at the boundary itself, and no boundary condition was required for these terms. The determination as to whether fluid was entering or leaving the domain was made by examining the sign of the eigenvalues of the convective terms.

Two variations were tried for the outer boundary conditions. In the first, the eigenvalues were computed in the same manner as in the rest of the domain, that is, based upon the body-axis velocities at the boundary points. The second method was similar to the first, except that the inertial velocities were ignored. That is, ${}^{b}V_{P/Q}$ was assumed to be approximately $-{}^{i}V_{Q/O}$ for the purpose of determining the direction of the upwind differencing. This is generally a good approximation, since the exterior boundary should be far enough from the body that the inertial velocities will be small. For most cases, there was a negligible difference between the two methods. The second method was somewhat better in the event that the exterior flow is essentially parallel to the entire outer boundary. An example of such a situation is the flow about a circular cylinder in pure rotation using a polar grid. If the flow had a slight outward component, the undisturbed condition existing outside the domain had no influence at all on the flow inside the domain when the first method was used. There was nothing to fix the value of the flow at the boundary. With the second method, the algorithm was biased slightly by differencing outward when the eigenvalue was exactly zero. Thus, for cases such as the rotating cylinder, the differences were in the outward direction

BOUNDARY CONDITIONS

Three types of boundary conditions are required for this problem. The computational domain is bounded at the bottom by the solid body, at the top by the fluid outside the computational domain, and on each side by the opposite side of the domain.

At the surface of the body, the no slip condition is applied. This requires that

$$^{b}V_{P/Q} = 0 \qquad (91)$$

When applied to the inertial velocities, this requires that $^{i}V_{P/O} = {}^{i}V_{Q/O}$, where point Q is taken to be the point on the body at which the boundary condition is being applied. In other words, the velocity of the fluid must follow the velocity of the wall.

The periodic boundary conditon at the sides of the domain results from making a branch cut from the ouside of the physical domain to the body in order to map the doubly connected physical domain to a singly connected computational domain. This boundary condition was enforced by taking points from the opposite side of the domain when the difference formula would have required points outside. The points at $\xi = 1$ and $\xi = i_{MAX}$ were at the same location, and represented opposite sides of the branch cut. For example, values at i−1 in the finite difference stencil evaluated at i=1 were obtained from i_{MAX}−1. In addition, the values at $i = i_{MAX}$ were set equal to those at i = 1 as soon as they were computed.

The boundary conditions at the outer boundary were designed to allow undisturbed fluid ($^{i}V_{P/O}$=0) to enter the domain where the edge of the domain is advancing, and to allow disturbances, particularly the momentum defect in the wake, to exit the domain where the edge is retreating.

This was handled through the upwind differencing of the convective

boundary conditions.

An alternate pressure calculation to the formula above was also investigated. For an inertial control volume, consider the case in which the velocity divergence is locally constant over an entire cell in the computational grid. For this case $\rho J \nabla \cdot V$ represents the net mass flux out of the cell. The equation above can then be interpreted as relating the pressure within a cell to the net production of mass within that cell. The net mass flux may also be calculated by integrating around the boundary of the cell. This suggests:

$$\Delta P = -2\ \Omega\ \{J/\ [\Delta t(\alpha + \gamma)]\}\ \Delta\Psi \qquad (88)$$

with:

$$\Delta\Psi = \oint \rho^b u_{P/Q}\, dy \ - \ \oint \rho^b v_{P/Q}\, dx \qquad (89)$$

If trapezoidal integration is used on each side of the cell, the discrete approximation is obtained:

$$\begin{aligned}\Delta P^n_{i+1/2,j+1/2} = -\Omega\ \rho\ J_{i+1/2,j+1/2}\ /\ |\Delta t(\alpha_{i+1/2,j+1/2} + \gamma_{i+1/2,j+1/2})| \\ * |({}^b u^n_{i+1,j+1} - {}^b u^n_{i,j})(Y_{i,j+1} - Y_{i+1,j}) \\ + ({}^b u^n_{i+1,j} - {}^b u^n_{i,j+1})(Y_{i+1,j+1} - Y_{i,j}) \\ + ({}^b v^n_{i+1,j+1} - {}^b v^n_{i,j})(X_{i+1,j} - X_{i,j+1}) \\ + ({}^b v^n_{i,j+1} - {}^b v^n_{i+1,j})(X_{i+1,j+1} - X_{i,j})\ |\end{aligned} \qquad (90)$$

This method converged faster than the first. It was also possible to use the conservation form for the momentum equations for this method, whereas the original one led to instablities unless the nonconservation form was used.

calculated (as in Gauss–Seidel iteration), and so storage at both iteration levels is not required. The calculations above are iterated at the same time step until sufficiently converged.

Pressure Calculation

The velocity calculations above depend upon the use of the pressures to enforce the conservation of mass while iterating to convergence. The artificial compressiblity approach was selected for the pressure calculation. In this method, the change in pressure between iterations is proportional to the velocity divergence (Ref 6). This approach has been shown by Hodge (Ref 7) to be equivalent to the SOR solution for the Poisson equation for pressure for inertial control volumes. Hodge also presents the optimum acceleration parameter, Φ, for this calculation as:

$$\Phi = \Omega J^2 / |\Delta t (\alpha + \gamma)| \qquad (85)$$

$$\Delta P = - \rho \Phi \nabla \cdot {}^{I}V_{P/O} \qquad (86)$$

When applied to the pressure calculation, this results in:

$$\begin{aligned}\Delta P^{n}_{i+1/2,j+1/2} = & -\Omega J_{i+1/2,j+1/2} / |\Delta t (\alpha_{i+1/2,j+1/2} + \gamma_{i+1/2,j+1/2})| \\ & * |(Y_{\eta i+1/2,j+1/2} + Y_{\xi i+1/2,j+1/2}) u^{n}_{i,j} + (Y_{\xi i+1/2,j+1/2} - Y_{\eta i+1/2,j+1/2}) u^{n}_{i+1,j} \\ & + (Y_{\eta i+1/2,j+1/2} - Y_{\xi i+1/2,j+1/2}) u^{n}_{i,j+1} - (Y_{\eta i+1/2,j+1/2} + Y_{\xi i+1/2,j+1/2}) u^{n}_{i+1,j+1} \\ & + (X_{\eta i+1/2,j+1/2} + X_{\xi i+1/2,j+1/2}) v^{n}_{i,j} + (X_{\xi i+1/2,j+1/2} - X_{\eta i+1/2,j+1/2}) v^{n}_{i+1,j} \\ & + (X_{\eta i+1/2,j+1/2} - X_{\xi i+1/2,j+1/2}) v^{n}_{i,j+1} - (X_{\eta i+1/2,j+1/2} + X_{\xi i+1/2,j+1/2}) v^{n}_{i+1,j+1} |\end{aligned} \qquad (87)$$

at the cell center. One advantage of this approach is that the pressure calculation itself requires no boundary conditions, since the pressure is only calculated at the cell centers which are wholly within the control volume. Pressure boundary conditions are still required for the momentum equations, but these may be be easily implemented for both Dirichlet and Von Neuman

$$
\begin{aligned}
B_2 \;=\; & 1/4\{a^n_{i-1/2,j+1/2} + a^n_{i-1/2,j-1/2} - g^n_{i-1/2,j+1/2} - g^n_{i-1/2,j-1/2}\}\, v^n_{i-1,j} \\
& + 1/4\{-a^n_{i-1/2,j-1/2} - a^n_{i+1/2,j-1/2} + g^n_{i-1/2,j-1/2} + g^n_{i+1/2,j-1/2}\}\, v^n_{i,j-1} \\
& + 1/2\{Y_{\eta i+2,j}\, {}^b u^n_{i+2,j} - X_{\eta i+2,j}\, {}^b v^n_{i+2,j}\}\, v^n_{i+2,j} \\
& + 1/2\{Y_{\eta i,j+2}\, {}^b u^n_{i,j+2} - X_{\eta i,j+2}\, {}^b v^n_{i,j+2}\}\, v^n_{i,j+2} \\
& + [-2(Y_{\eta i+1,j}\, {}^b u^n_{i+1,j} - X_{\eta i+1,j}\, {}^b v^n_{i+1,j}) \\
& + 1/4\{a^n_{i+1/2,j+1/2} + a^n_{i+1/2,j-1/2} - g^n_{i+1/2,j+1/2} - g^n_{i+1/2,j-1/2}\}]\, v^n_{i+1,j} \\
& + [2(-Y_{\xi i,j+1}\, {}^b u^n_{i,j+1} + X_{\xi i,j+1}\, {}^b v^n_{i,j+1}) \\
& + 1/4\{-a^n_{i+1/2,j+1/2} - a^n_{i-1/2,j+1/2} + g^n_{i+1/2,j+1/2} + g^n_{i-1/2,j+1/2}\}]\, v^n_{i,j+1} \\
& + 1/4\{a^n_{i+1/2,j+1/2} - 2b^n_{i+1/2,j+1/2} + g^n_{i+1/2,j+1/2}\}\, v^n_{i+1,j+1} \\
& + 1/4\{a^n_{i-1/2,j+1/2} + 2b^n_{i-1/2,j+1/2} + g^n_{i-1/2,j+1/2}\}\, v^n_{i-1,j+1} \\
& + 1/4\{a^n_{i+1/2,j-1/2} + 2b^n_{i+1/2,j-1/2} + g^n_{i+1/2,j-1/2}\}\, v^n_{i+1,j-1} \\
& + 1/4\{a^n_{i-1/2,j-1/2} - 2b^n_{i-1/2,j-1/2} + g^n_{i-1/2,j-1/2}\}\, v^n_{i-1,j-1} \\
& + 1/2\{\,[P/\rho(X_\eta - X_\xi)]^n_{i+1/2,j+1/2} - [P/\rho(X_\eta + X_\xi)]^n_{i-1/2,j+1/2} \\
& + [P/\rho(X_\xi - X_\eta)]^n_{i-1/2,j-1/2} + [P/\rho(X_\eta + X_\xi)]^n_{i+1/2,j-1/2}\,\} \\
& + (J/\Delta t)\, v^{n-1}_{i,j} \qquad (82)
\end{aligned}
$$

The equations above have been grouped so that if sufficient storage exists, the metric quantities in brackets may be calculated once during grid generation and stored for use during the flowfield calculation.

Solving for $u^n_{i,j}$ and $v^n_{i,j}$:

$$
\begin{aligned}
u^{*n}_{i,j} &= (B_1\, A_{22} - A_{12}\, B_2) \,/\, (A_{11}\, A_{22} - A_{12}\, A_{21}) \\
v^{*n}_{i,j} &= (B_2\, A_{11} - A_{21}\, B_1) \,/\, (A_{11}\, A_{22} - A_{12}\, A_{21}) \qquad (83)
\end{aligned}
$$

The block successive over relaxation algorithm (SOR) first calculates the velocities at a point, as above. It then over relaxes the velocities using the relaxation parameter, Ω, as:

$$
\begin{aligned}
u^{n(s)}_{i,j} &= \Omega\, u^{*n}_{i,j} + (1 - \Omega)\, u^{n(s-1)}_{i,j} \\
v^{n(s)}_{i,j} &= \Omega\, v^{*n}_{i,j} + (1 - \Omega)\, v^{n(s-1)}_{i,j} \qquad (84)
\end{aligned}
$$

where the superscript (s) indicates the present iteration level, and (s-1) indicates values at the previous iteration level. Ω must be less than 2 for stability. The computer algorithm replaces the values at i,j as they are

For negative eigenvalues, the equations become:

$$
\begin{aligned}
A_{11} = A_{22} = {} & J/\Delta t - 3/2\{(Y_\eta - Y_\xi)_{ij}\, {}^b u^n_{i,j} + (X_\xi - X_\eta)_{ij}\, {}^b v^n_{i,j}\} \\
& + 1/4\{a^n_{i+1/2,j+1/2} + a^n_{i-1/2,j+1/2} + a^n_{i+1/2,j-1/2} + a^n_{i-1/2,j-1/2} \\
& - 2(b^n_{i+1/2,j+1/2} - b^n_{i-1/2,j+1/2} - b^n_{i+1/2,j-1/2} + b^n_{i-1/2,j-1/2}) \\
& + g^n_{i+1/2,j+1/2} + g^n_{i-1/2,j+1/2} + g^n_{i+1/2,j-1/2} + g^n_{i-1/2,j-1/2}\} \\
A_{12} = {} & -R \\
A_{21} = {} & R
\end{aligned}
\qquad (80)
$$

$$
\begin{aligned}
B_i = {} & 1/4\{a^n_{i-1/2,j+1/2} + a^n_{i-1/2,j-1/2} - g^n_{i-1/2,j+1/2} - g^n_{i-1/2,j-1/2}\}\, u^n_{i-1,j} \\
& + 1/4\{-a^n_{i-1/2,j-1/2} - a^n_{i+1/2,j-1/2} + g^n_{i-1/2,j-1/2} + g^n_{i+1/2,j-1/2}\}\, u^n_{i,j-1} \\
& + 1/2\{Y_{\eta i+2,j}\, {}^b u^n_{i+2,j} - X_{\eta i+2,j}\, {}^b v^n_{i+2,j}\}\, u^n_{i+2,j} \\
& + 1/2\{Y_{\eta i,j+2}\, {}^b u^n_{i,j+2} - X_{\eta i,j+2}\, {}^b v^n_{i,j+2}\}\, u^n_{i,j+2} \\
& + \{-2(Y_{\eta i+1,j}\, {}^b u^n_{i+1,j} - X_{\eta i+1,j}\, {}^b v^n_{i+1,j}) \\
& + 1/4\{a^n_{i+1/2,j+1/2} + a^n_{i+1/2,j-1/2} - g^n_{i+1/2,j+1/2} - g^n_{i+1/2,j-1/2}\}\}\, u^n_{i+1,j} \\
& + [2\{-Y_{\xi i,j+1}\, {}^b u^n_{i,j+1} + X_{\xi i,j+1}\, {}^b v^n_{i,j+1}) \\
& + 1/4\{-a^n_{i+1/2,j+1/2} - a^n_{i-1/2,j+1/2} + g^n_{i+1/2,j+1/2} + g^n_{i-1/2,j+1/2}\}]\, u^n_{i,j+1} \\
& + 1/4\{a^n_{i+1/2,j+1/2} - 2b^n_{i+1/2,j+1/2} + g^n_{i+1/2,j+1/2}\}\, u^n_{i+1,j+1} \\
& + 1/4\{a^n_{i-1/2,j+1/2} + 2b^n_{i-1/2,j+1/2} + g^n_{i-1/2,j+1/2}\}\, u^n_{i-1,j+1} \\
& + 1/4\{a^n_{i+1/2,j-1/2} + 2b^n_{i+1/2,j-1/2} + g^n_{i+1/2,j-1/2}\}\, u^n_{i+1,j-1} \\
& + 1/4\{a^n_{i-1/2,j-1/2} - 2b^n_{i-1/2,j-1/2} + g^n_{i-1/2,j-1/2}\}\, u^n_{i-1,j-1} \\
& + 1/2\{ [P/\rho(Y_\xi - Y_\eta)]^n_{i+1/2,j+1/2} - [P/\rho(Y_\eta + Y_\xi)]^n_{i+1/2,j-1/2} \\
& + [P/\rho(Y_\eta - Y_\xi)]^n_{i-1/2,j-1/2} + [P/\rho(Y_\eta + Y_\xi)]^n_{i-1/2,j+1/2}\} \\
& + (J/\Delta t)\, u^{n-1}_{i,j}
\end{aligned}
$$

$$
\begin{aligned}
B_1 \;=\; & \big[\, 2\big(Y_{\eta i-1,j}{}^{b}u^{n}_{i-1,j} - X_{\eta i-1,j}{}^{b}v^{n}_{i-1,j}\big) \\
& + 1/4\big(a^{n}_{i-1/2,j+1/2} + a^{n}_{i-1/2,j-1/2} - g^{n}_{i-1/2,j+1/2} - g^{n}_{i-1/2,j-1/2}\big)\big]\, u^{n}_{i-1,j} \\
& + \big[\, 2\big(-Y_{\xi i,j-1}{}^{b}u^{n}_{i,j-1} + X_{\xi i,j-1}{}^{b}v^{n}_{i,j-1}\big) \\
& + 1/4\big(-a^{n}_{i-1/2,j-1/2} - a^{n}_{i+1/2,j-1/2} + g^{n}_{i-1/2,j-1/2} + g^{n}_{i+1/2,j-1/2}\big)\big]\, u^{n}_{i,j-1} \\
& - 1/2\big[Y_{\eta i-2,j}{}^{b}u^{n}_{i-2,j} - X_{\eta i-2,j}{}^{b}v^{n}_{i-2,j}\big]\, u^{n}_{i-2,j} \\
& - 1/2\big[Y_{\eta i,j-2}{}^{b}u^{n}_{i,j-2} - X_{\eta i,j-2}{}^{b}v^{n}_{i,j-2}\big]\, u^{n}_{i,j-2} \\
& + 1/4\big[-a^{n}_{i+1/2,j+1/2} - a^{n}_{i+1/2,j-1/2} + g^{n}_{i+1/2,j+1/2} + g^{n}_{i+1/2,j-1/2}\big]\, u^{n}_{i+1,j} \\
& + 1/4\big[a^{n}_{i+1/2,j+1/2} + a^{n}_{i-1/2,j+1/2} - g^{n}_{i+1/2,j+1/2} - g^{n}_{i-1/2,j+1/2}\big]\, u^{n}_{i,j+1} \\
& + 1/4\big[a^{n}_{i+1/2,j+1/2} - 2b^{n}_{i+1/2,j+1/2} + g^{n}_{i+1/2,j+1/2}\big]\, u^{n}_{i+1,j+1} \\
& + 1/4\big[a^{n}_{i-1/2,j+1/2} + 2b^{n}_{i-1/2,j+1/2} + g^{n}_{i-1/2,j+1/2}\big]\, u^{n}_{i-1,j+1} \\
& + 1/4\big[a^{n}_{i+1/2,j-1/2} + 2b^{n}_{i+1/2,j-1/2} + g^{n}_{i+1/2,j-1/2}\big]\, u^{n}_{i+1,j-1} \\
& + 1/4\big[a^{n}_{i-1/2,j-1/2} - 2b^{n}_{i-1/2,j-1/2} + g^{n}_{i-1/2,j-1/2}\big]\, u^{n}_{i-1,j-1} \\
& + 1/2\big\{\, [P/\rho(Y_\xi - Y_\eta)]^{n}_{i+1/2,j+1/2} - [P/\rho(Y_\eta + Y_\xi)]^{n}_{i+1/2,j-1/2} \\
& + [P/\rho(Y_\eta - Y_\xi)]^{n}_{i-1/2,j-1/2} + [P/\rho(Y_\eta + Y_\xi)]^{n}_{i-1/2,j+1/2}\,\big\} \\
& + (J/\Delta t)\, u^{n-1}_{i,j}
\end{aligned}
$$

$$
\begin{aligned}
B_2 \;=\; & \big[2\big(Y_{\eta i-1,j}{}^{b}u^{n}_{i-1,j} - X_{\eta i-1,j}{}^{b}v^{n}_{i-1,j}\big) \\
& + 1/4\big(a^{n}_{i-1/2,j+1/2} + a^{n}_{i-1/2,j-1/2} - g^{n}_{i-1/2,j+1/2} - g^{n}_{i-1/2,j-1/2}\big)\big]\, v^{n}_{i-1,j} \\
& + \big[2\big(-Y_{\xi i,j-1}{}^{b}u^{n}_{i,j-1} + X_{\xi i,j-1}{}^{b}v^{n}_{i,j-1}\big) \\
& + 1/4\big(-a^{n}_{i-1/2,j-1/2} - a^{n}_{i+1/2,j-1/2} + g^{n}_{i-1/2,j-1/2} + g^{n}_{i+1/2,j-1/2}\big)\big]\, v^{n}_{i,j-1} \\
& - 1/2\big[Y_{\eta i-2,j}{}^{b}u^{n}_{i-2,j} - X_{\eta i-2,j}{}^{b}v^{n}_{i-2,j}\big]\, v^{n}_{i-2,j} \\
& - 1/2\big[Y_{\eta i,j-2}{}^{b}u^{n}_{i,j-2} - X_{\eta i,j-2}{}^{b}v^{n}_{i,j-2}\big]\, v^{n}_{i,j-2} \\
& + 1/4\big[a^{n}_{i+1/2,j+1/2} + a^{n}_{i+1/2,j-1/2} - g^{n}_{i+1/2,j+1/2} - g^{n}_{i+1/2,j-1/2}\big]\, v^{n}_{i+1,j} \\
& + 1/4\big[-a^{n}_{i+1/2,j+1/2} - a^{n}_{i-1/2,j+1/2} + g^{n}_{i+1/2,j+1/2} + g^{n}_{i-1/2,j+1/2}\big]\, v^{n}_{i,j+1} \\
& + 1/4\big[a^{n}_{i+1/2,j+1/2} - 2b^{n}_{i+1/2,j+1/2} + g^{n}_{i+1/2,j+1/2}\big]\, v^{n}_{i+1,j+1} \\
& + 1/4\big[a^{n}_{i-1/2,j+1/2} + 2b^{n}_{i-1/2,j+1/2} + g^{n}_{i-1/2,j+1/2}\big]\, v^{n}_{i-1,j+1} \\
& + 1/4\big[a^{n}_{i+1/2,j-1/2} + 2b^{n}_{i+1/2,j-1/2} + g^{n}_{i+1/2,j-1/2}\big]\, v^{n}_{i+1,j-1} \\
& + 1/4\big[a^{n}_{i-1/2,j-1/2} - 2b^{n}_{i-1/2,j-1/2} + g^{n}_{i-1/2,j-1/2}\big]\, v^{n}_{i-1,j-1} \\
& + 1/2\big\{\, [P/\rho(X_\eta - X_\xi)]^{n}_{i+1/2,j+1/2} - [P/\rho(X_\eta + X_\xi)]^{n}_{i-1/2,j+1/2} \\
& + [P/\rho(X_\xi - X_\eta)]^{n}_{i-1/2,j-1/2} + [P/\rho(X_\eta + X_\xi)]^{n}_{i+1/2,j-1/2}\,\big\} \\
& + (J/\Delta t)\, v^{n-1}_{i,j}
\end{aligned}
\qquad (79)
$$

Bibliography

1. Hodge, James H., et al. "Numerical Solution for Airfoils near Stall in Optimized Boundary-Fitted Curvilinear Coordinates". AIAA Journal, 17: 458-464 (May 1975).

2. Hegna, Harwood A. Numerical Prediction of Dynamic Forces on Arbitrarily Pitched Airfoils in Turbulent Flow. AIAA-82-0092, January, 1982.

3. Mehta, Unmeel B. "Dynamic Stall of an Oscillating Airfoil." Proceedings of the AGARD Fluid Dynamics Panel Symposium on Unsteady Aerodynamics. Ottawa, Canada. September, 1977.

4. Taslim, Mohamed E. eta al. "Analysis of Two-Dimensional Viscous Flow over Cylinders in Unsteady Motion," AIAA Journal, 22(5): 586-594 (May 1984).

5. Galloway, Charles R. Numerical Analysis of a Free Falling Autorotating Plate. PhD disertation (AA/83-1). School of Engineering, Air Force Institute of Technology (AU), Wright-Patterson AFB OH, 1983.

6. Shames, Irving H. Mechanics of Fluids. New York: Mc Graw Hill, 1962.

7. Likins, Peter W. Elements of Engineering Mechanics. New York: Mc Graw Hill, 1973.

8. Schlichting, Hermann. Boundary Layer Theory. New York: Mc Graw Hill, 1979.

9. Viviand, H. "Conservative Forms of the Gas Dynamic Equations. La Recherche Aerospatiale, No. 1974-1. 1974.

10. Walitt, Leonard. Development of a Locally Mass Flux Conservative Computer Code for Calculating 3-D Viscous flow in Turbomachines. NASA Contractor Report 3539, April 1982.

11. Peret and Taylor. Computational Methods for Fluid Flow. New York: Springer-Verlag, 1983.

12. Galloway, C. R. and Hankey W. L. Free-Falling Autorotating Plate - A Coupled Fluid and Flight Mechanics Problem. AIAA 84-2079. 1984.

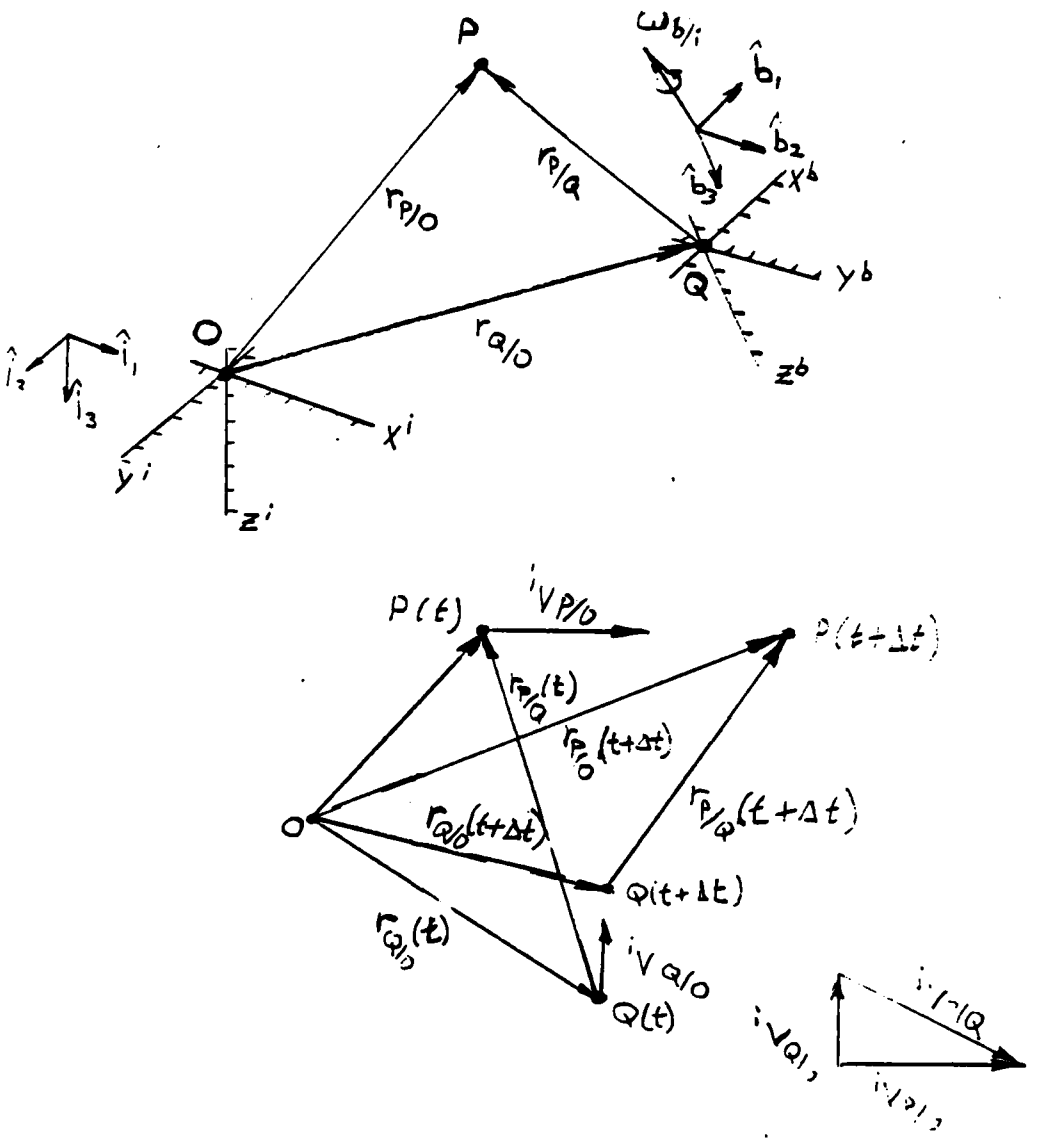

Figure 1. Positions and Velocities

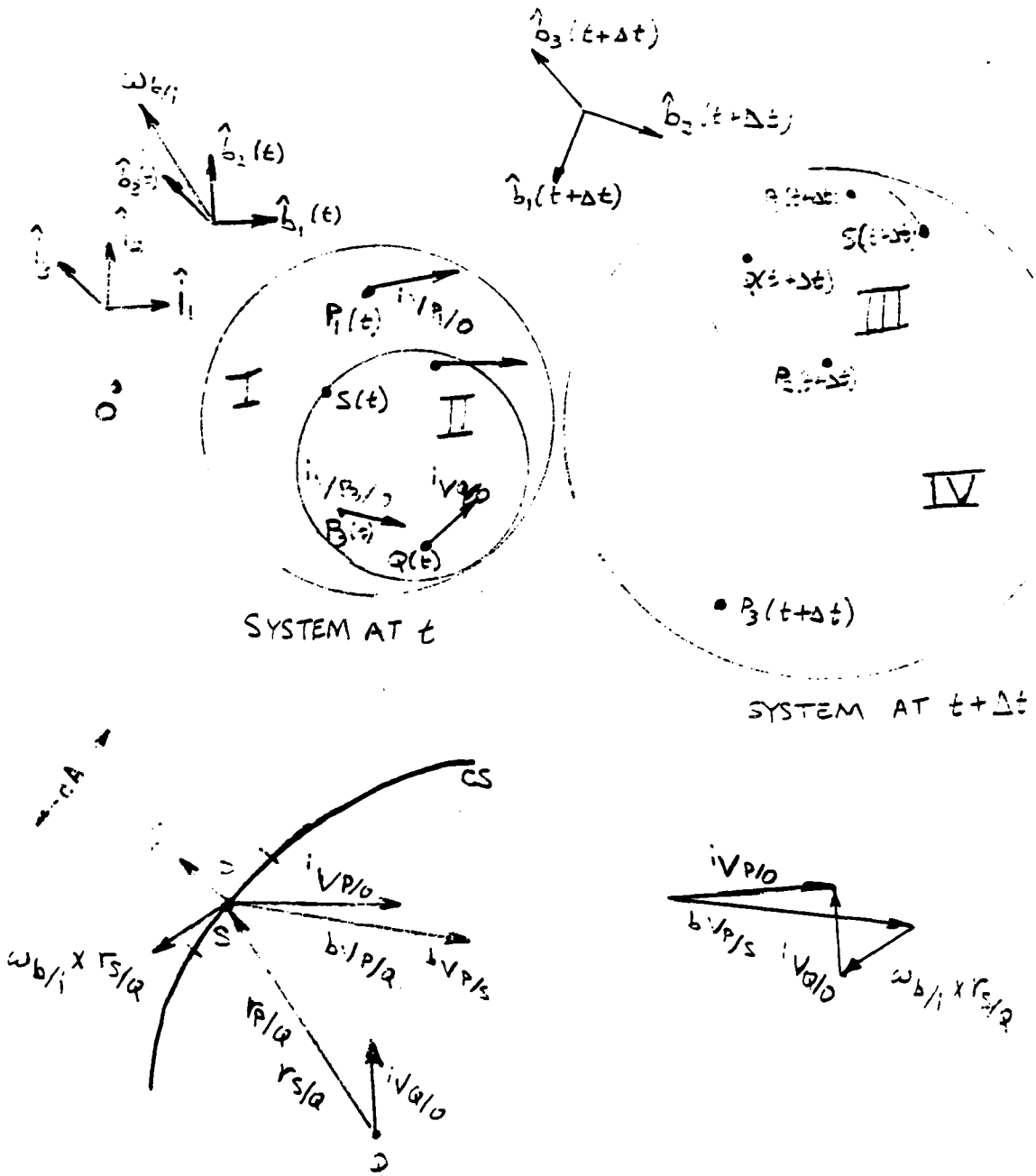

Figure 2. Control Volume/Control Surface Relationships

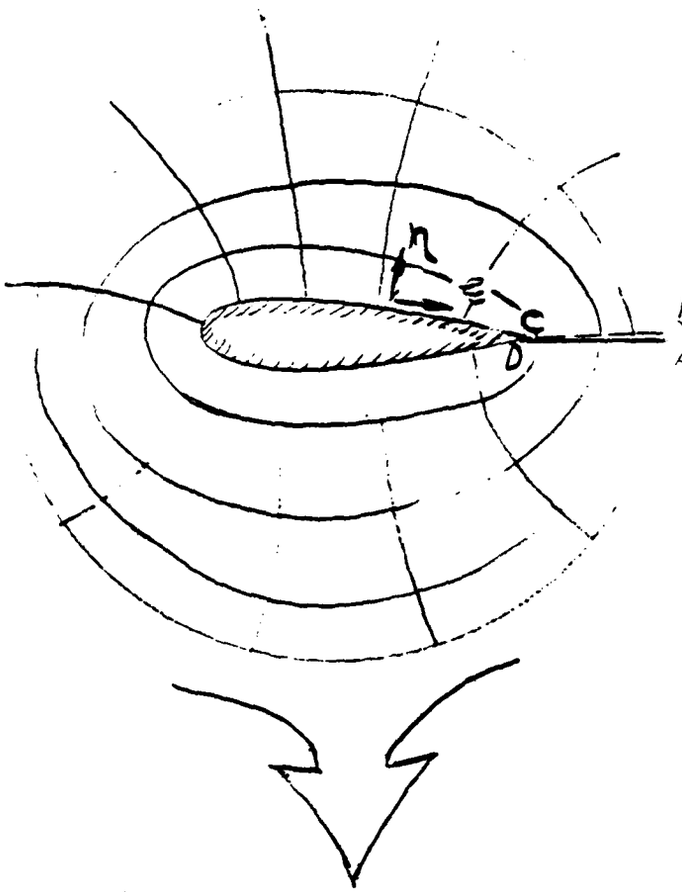

Physical Domain

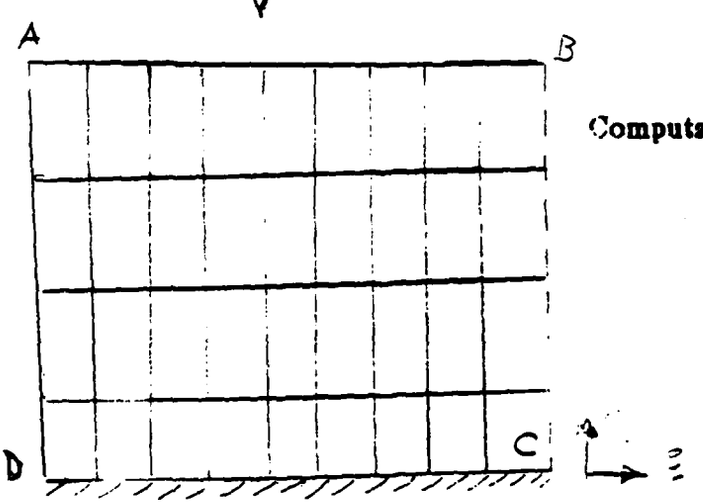

Computational Domain

Global View

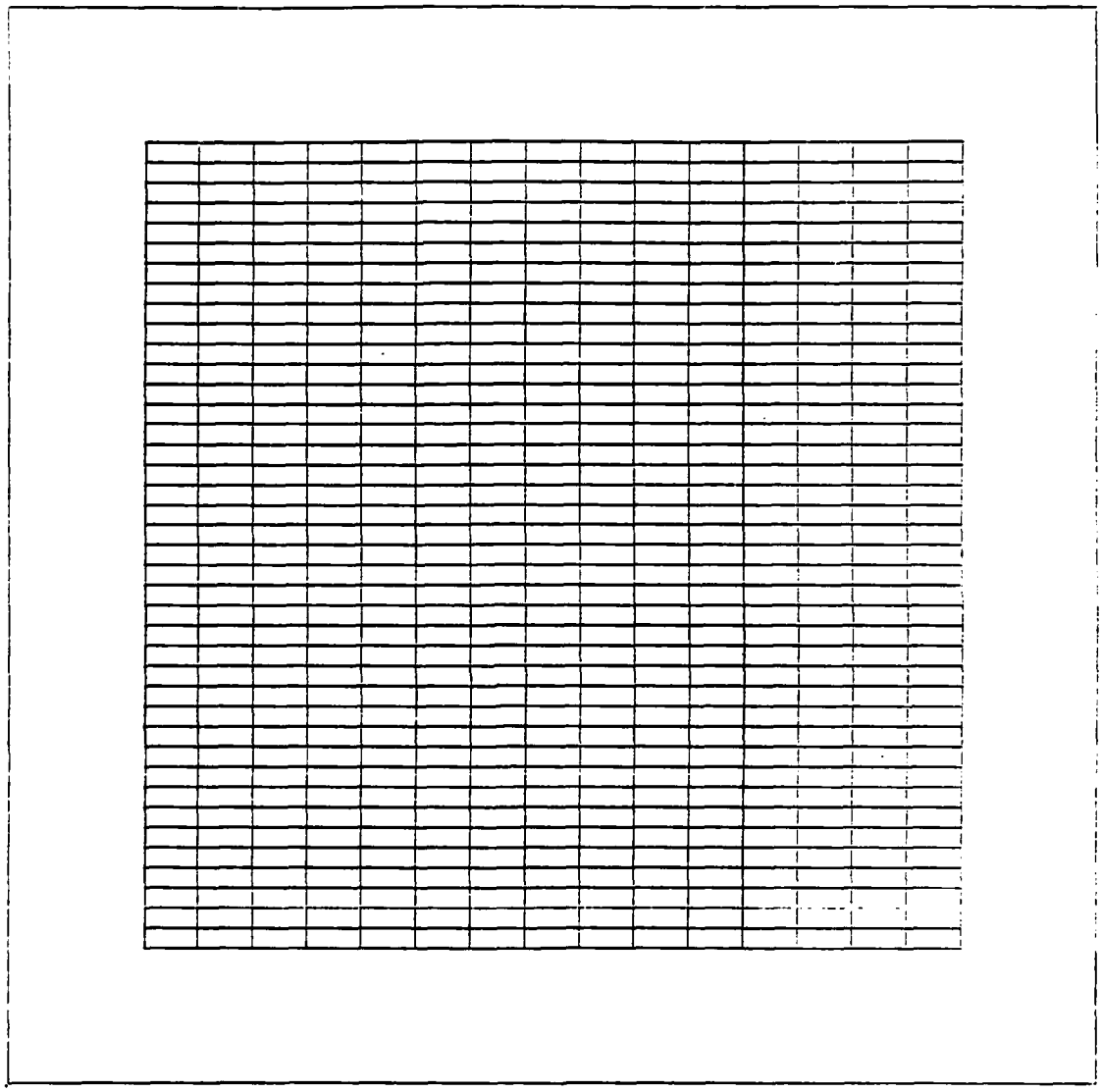

Figure 4a. Computational Grid– Stoke's First Problem

Inertial Velocity Vectors

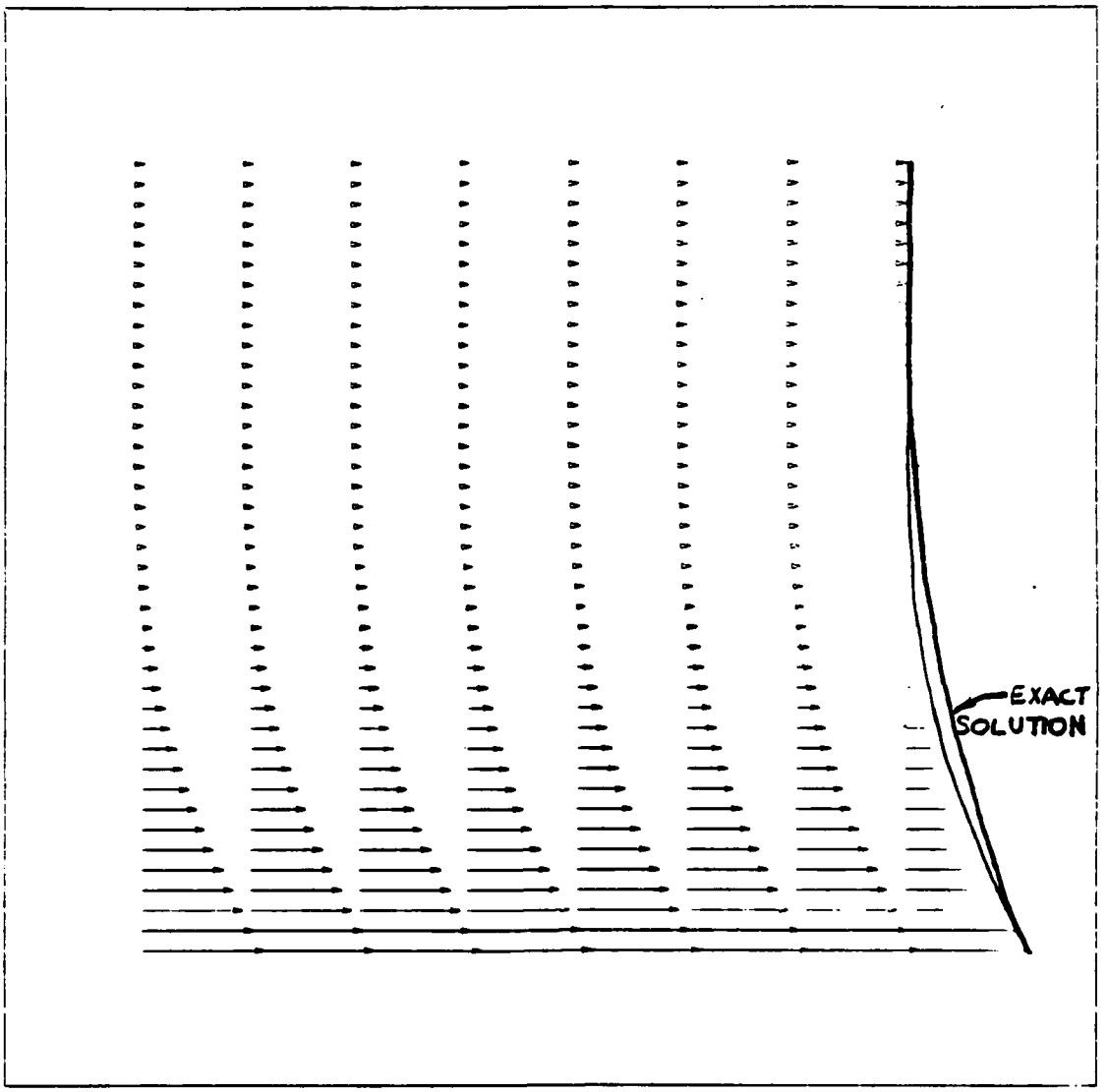

Figure 5a. Stoke's First Problem

Body-Axis Velocity Vectors

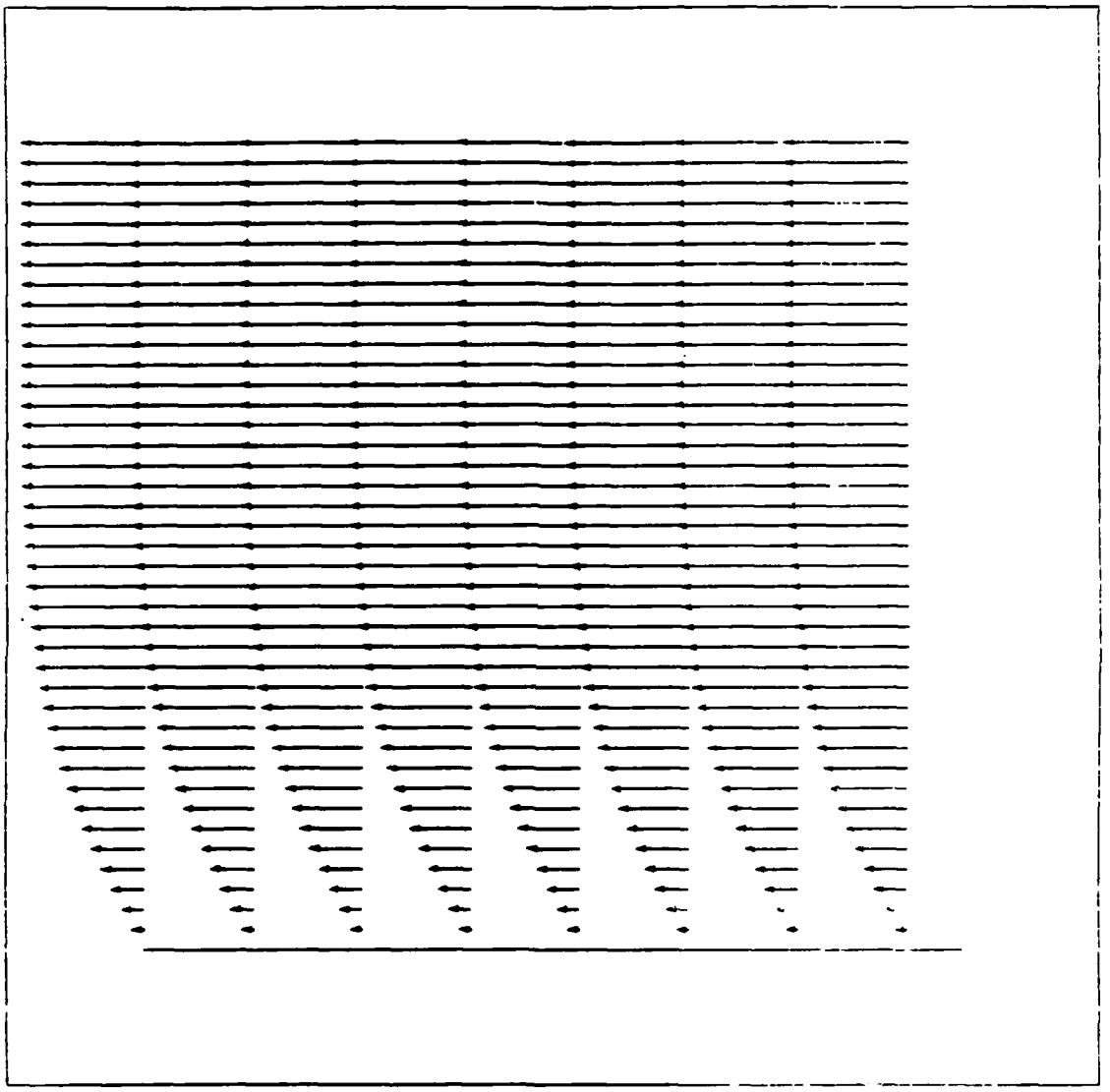

Figure 5b. Stoke's First Problem

Streamlines

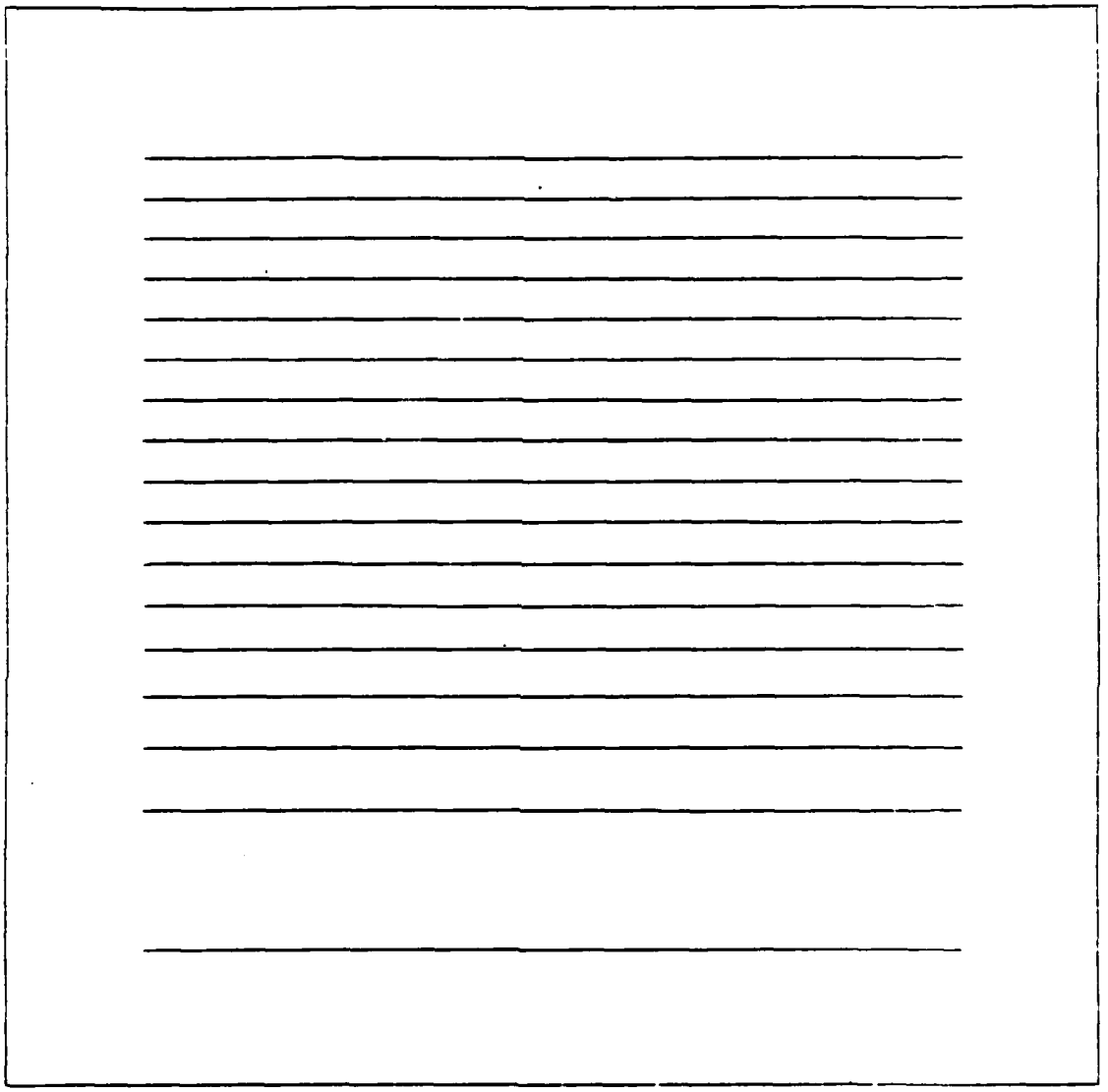

Figure 5c. Stoke's First Problem

Pressure Isobars

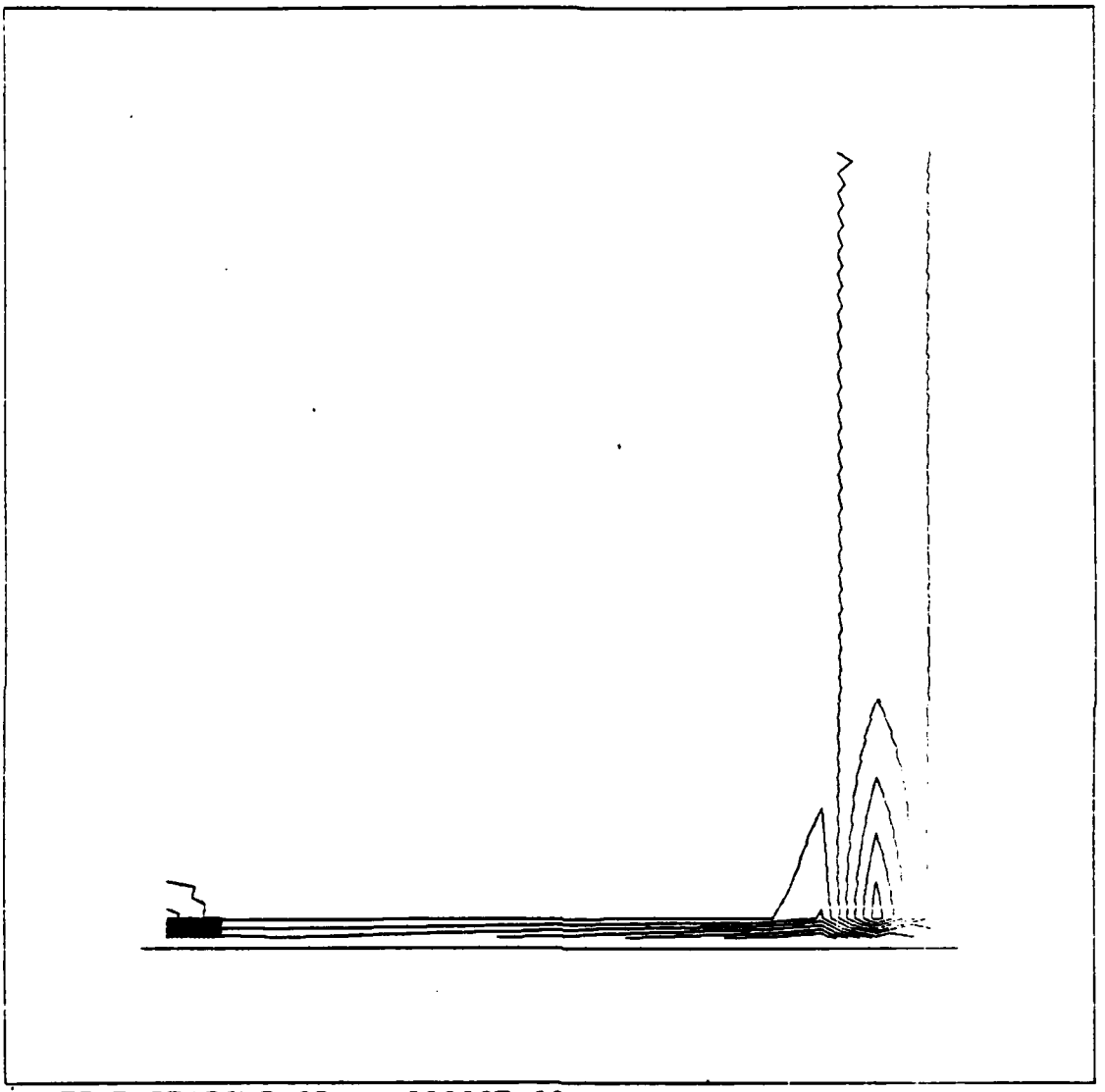

Figure 5d. Stoke's First Problem

Vorticity Contours

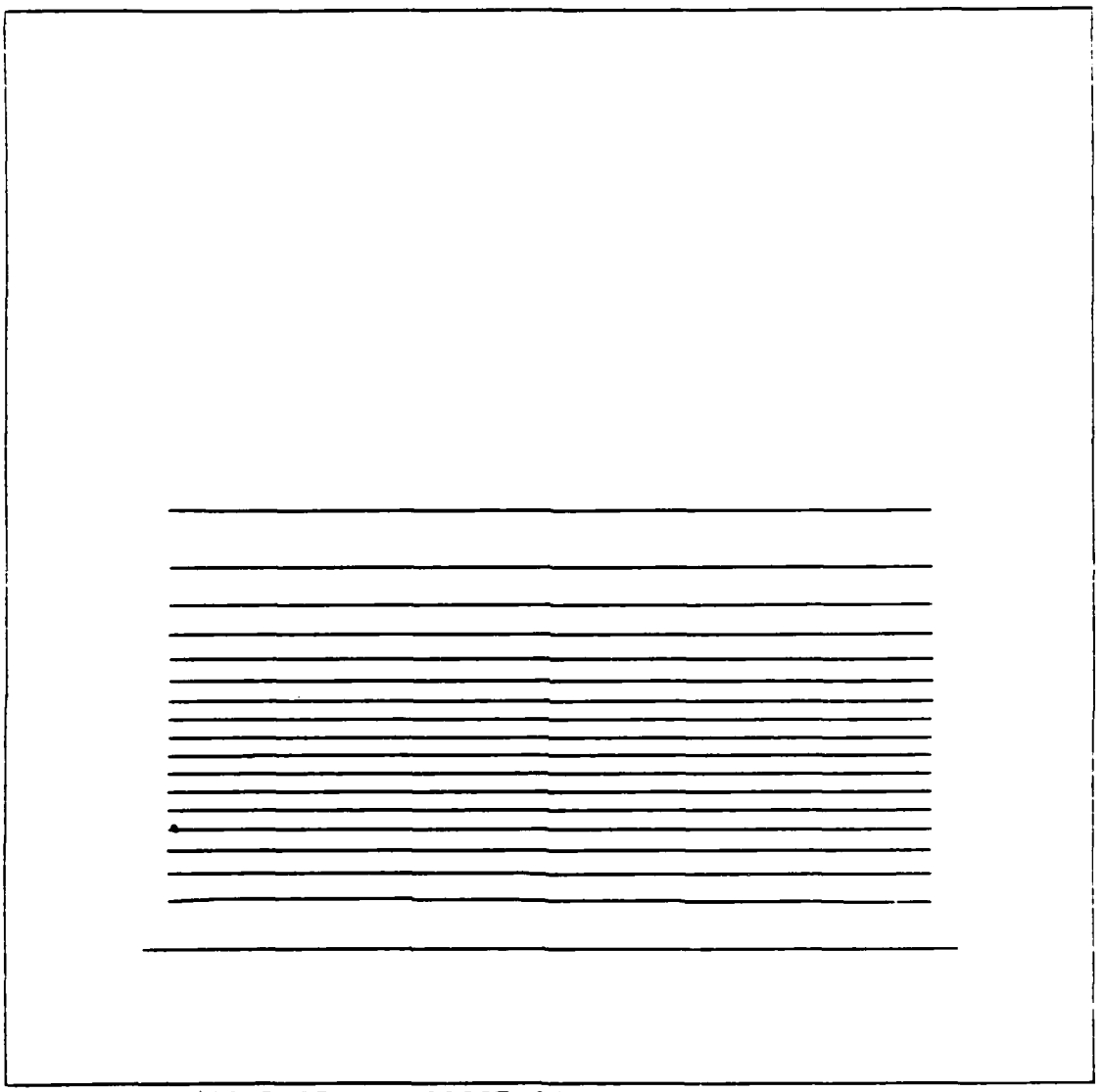

Figure 5e. Stoke's First Problem

Global View

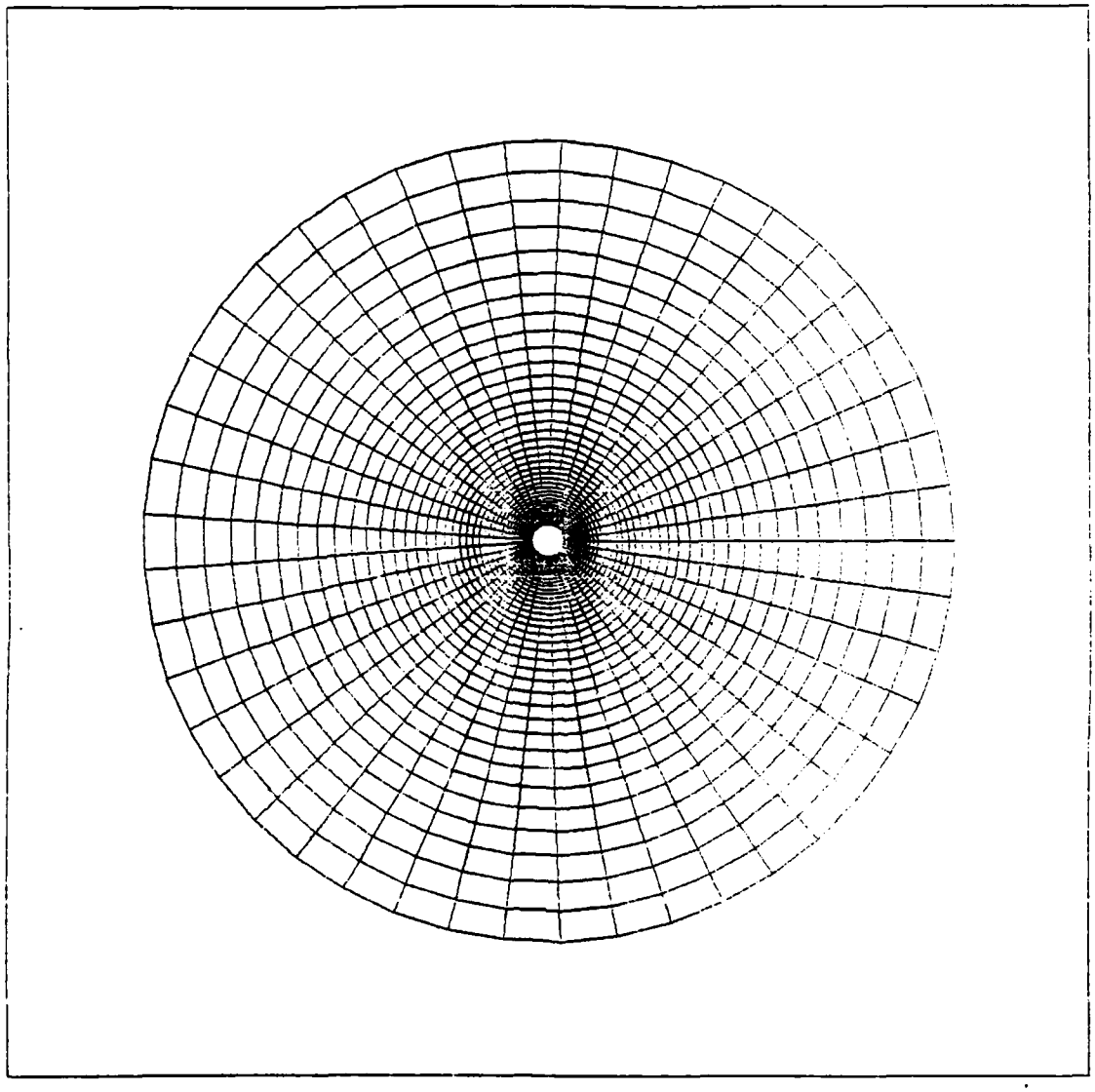

Figure 6a. Computational Grid– Circular Cylinder

Expanded View

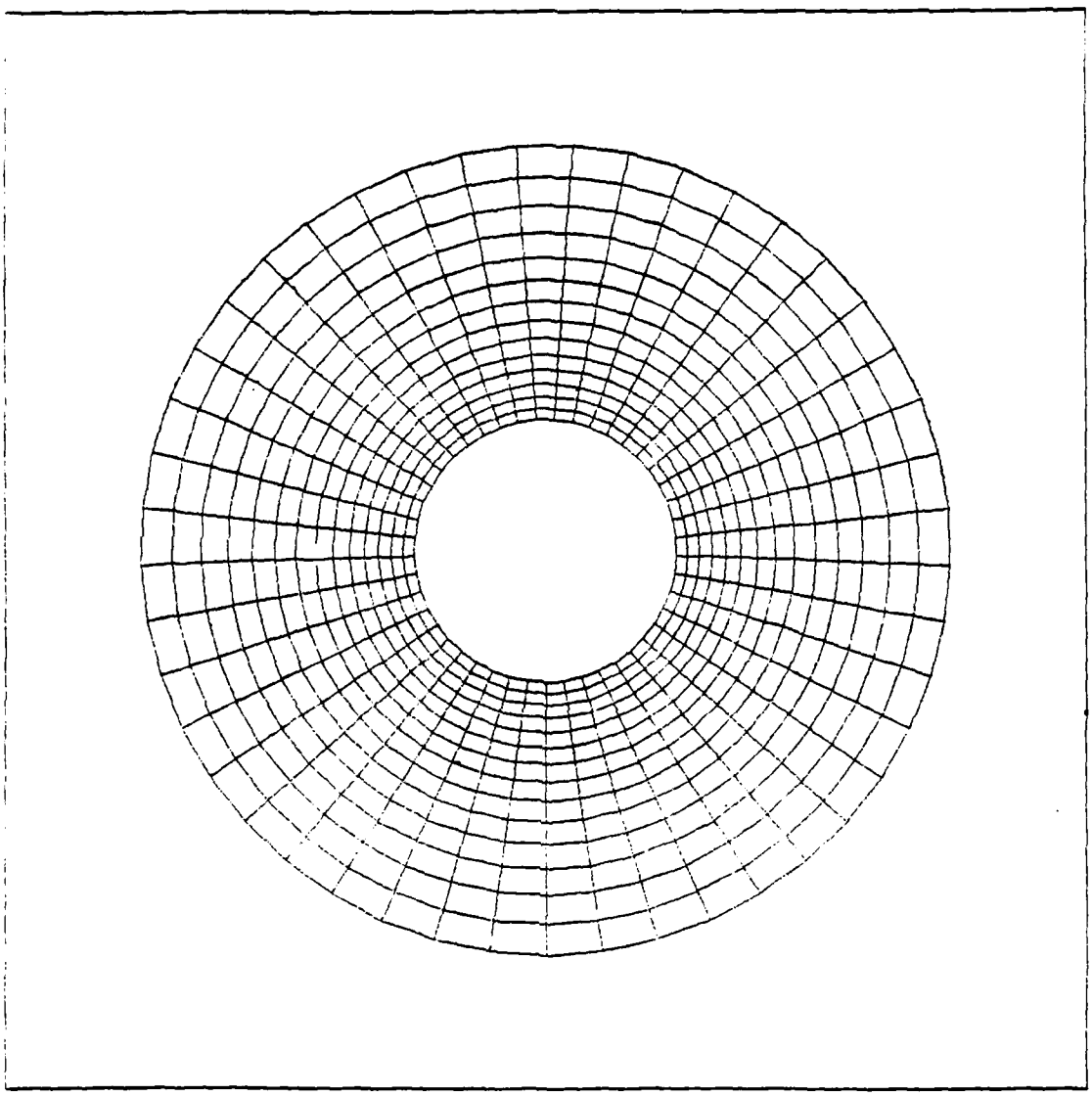

Figure 6b. Computational Grid– Circular Cylinder

Inertial Velocity Vectors

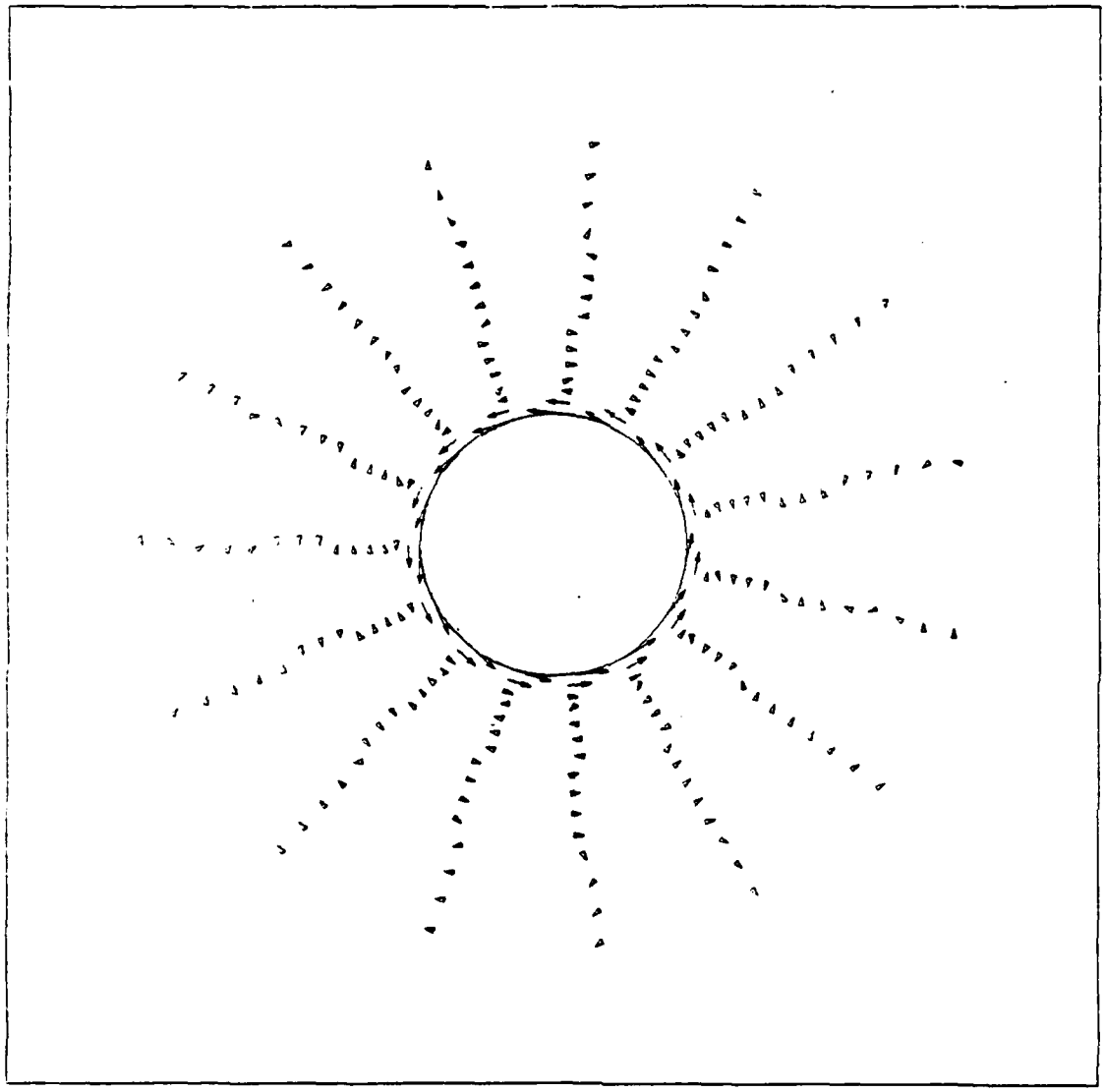

Figure 7a. Circular Cylinder– Pure Rotation

Body–Axis Velocity Vectors

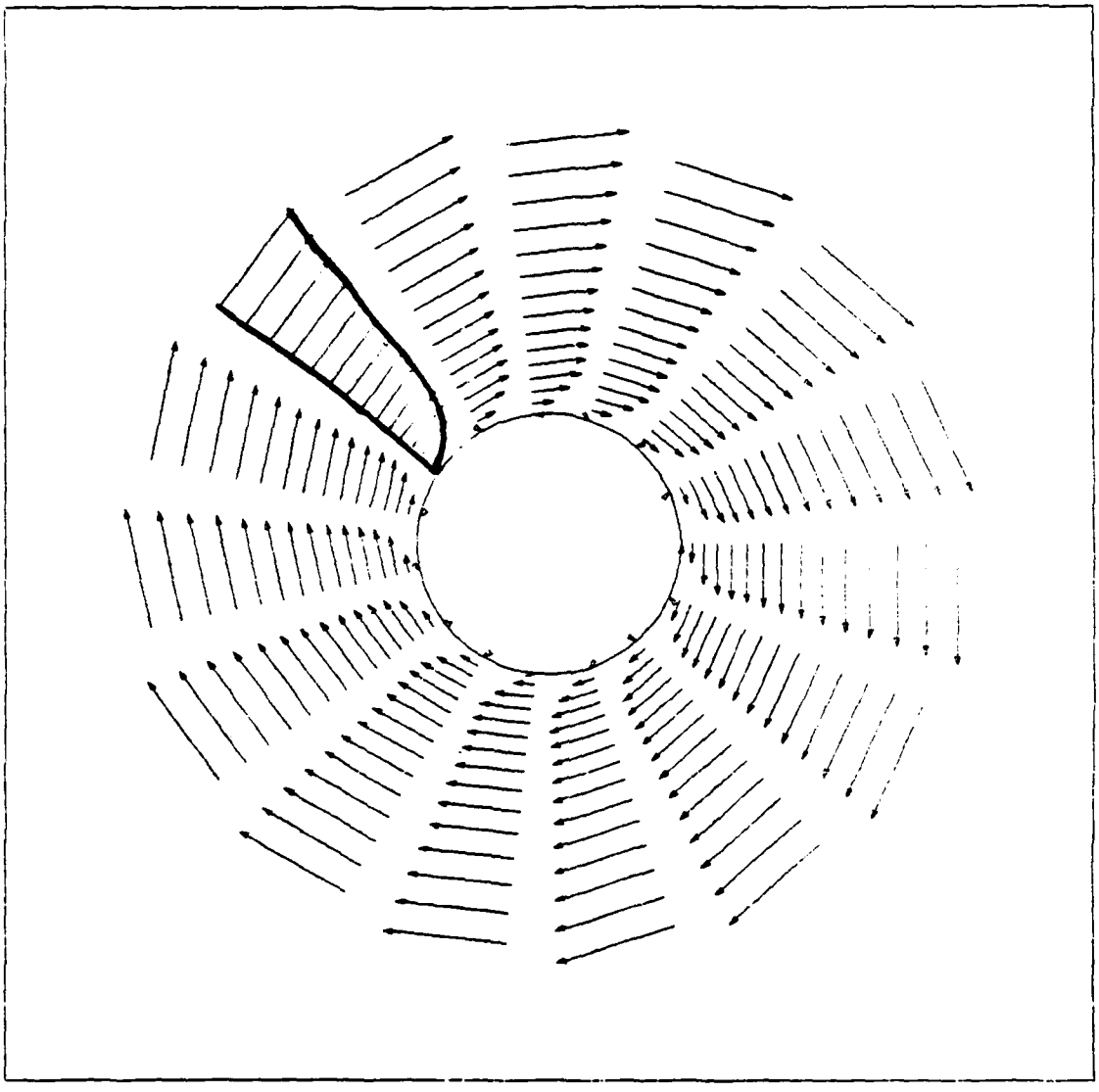

Figure 7b. Circular Cylinder– Pure Rotation

Pressure Isobars

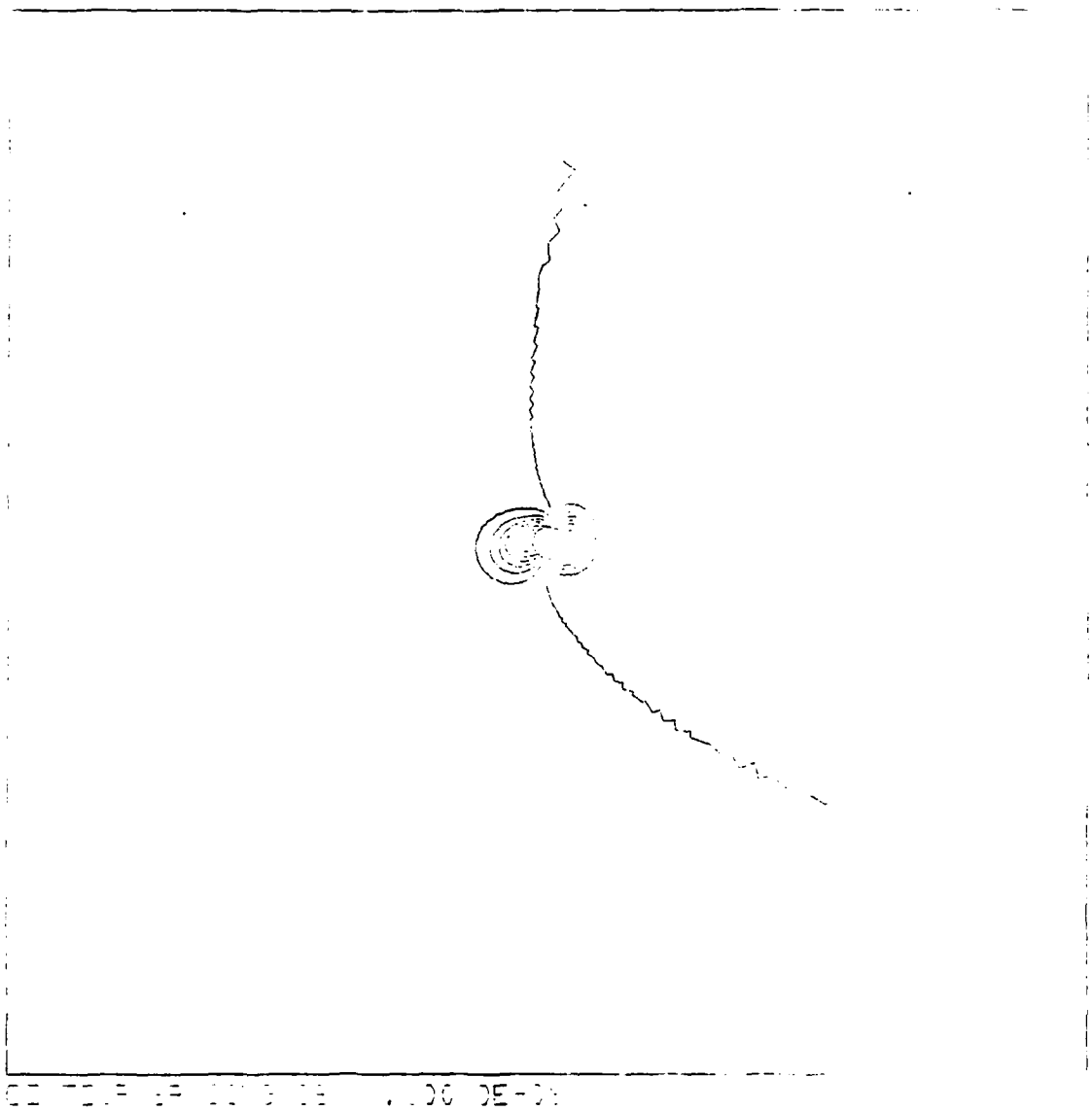

Figure 8f. Circular Cylinder– Pure Translation

Vorticity Contours

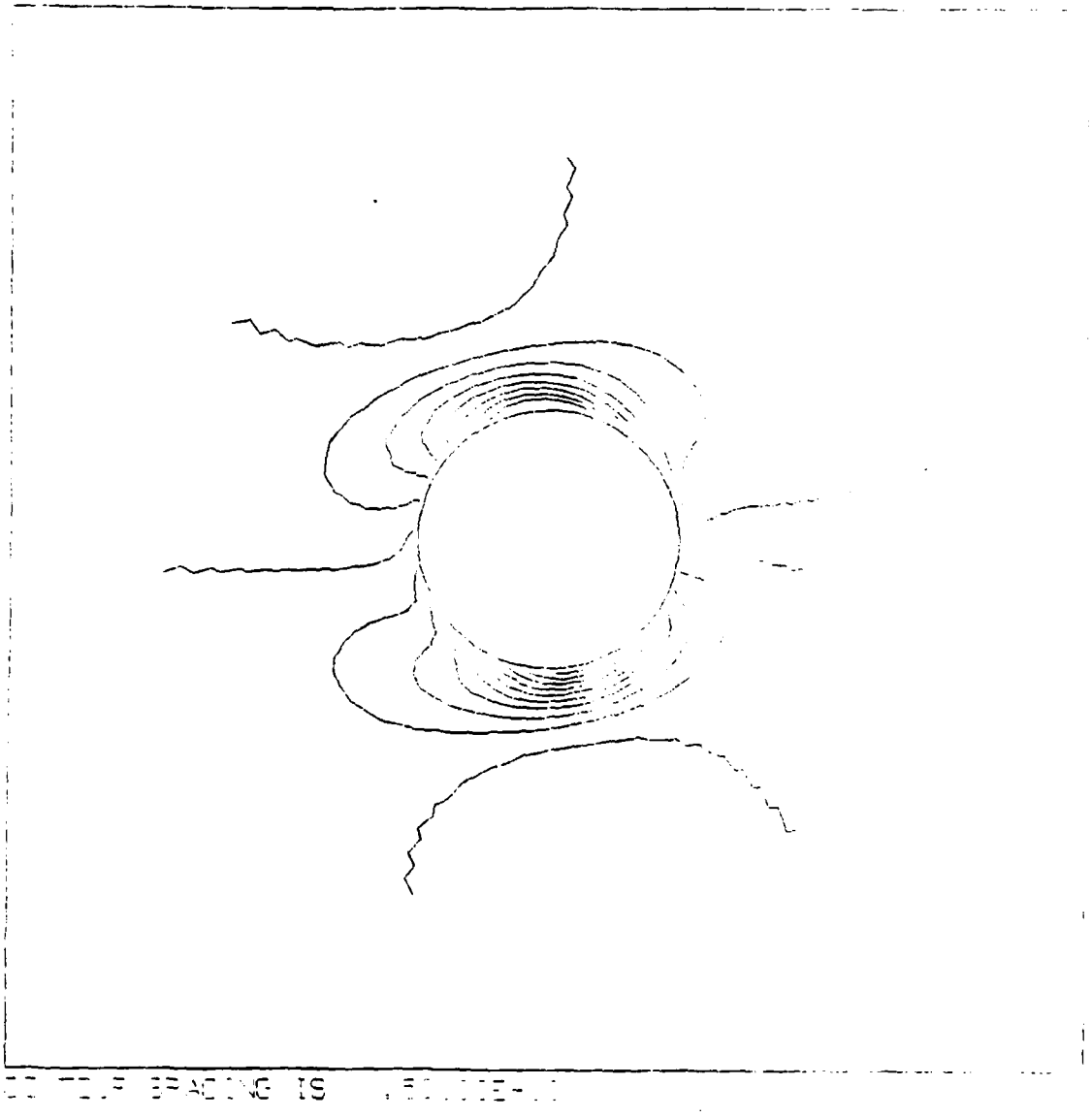

Figure 8e. Circular Cylinder– Pure Translation

Pressure Isobars

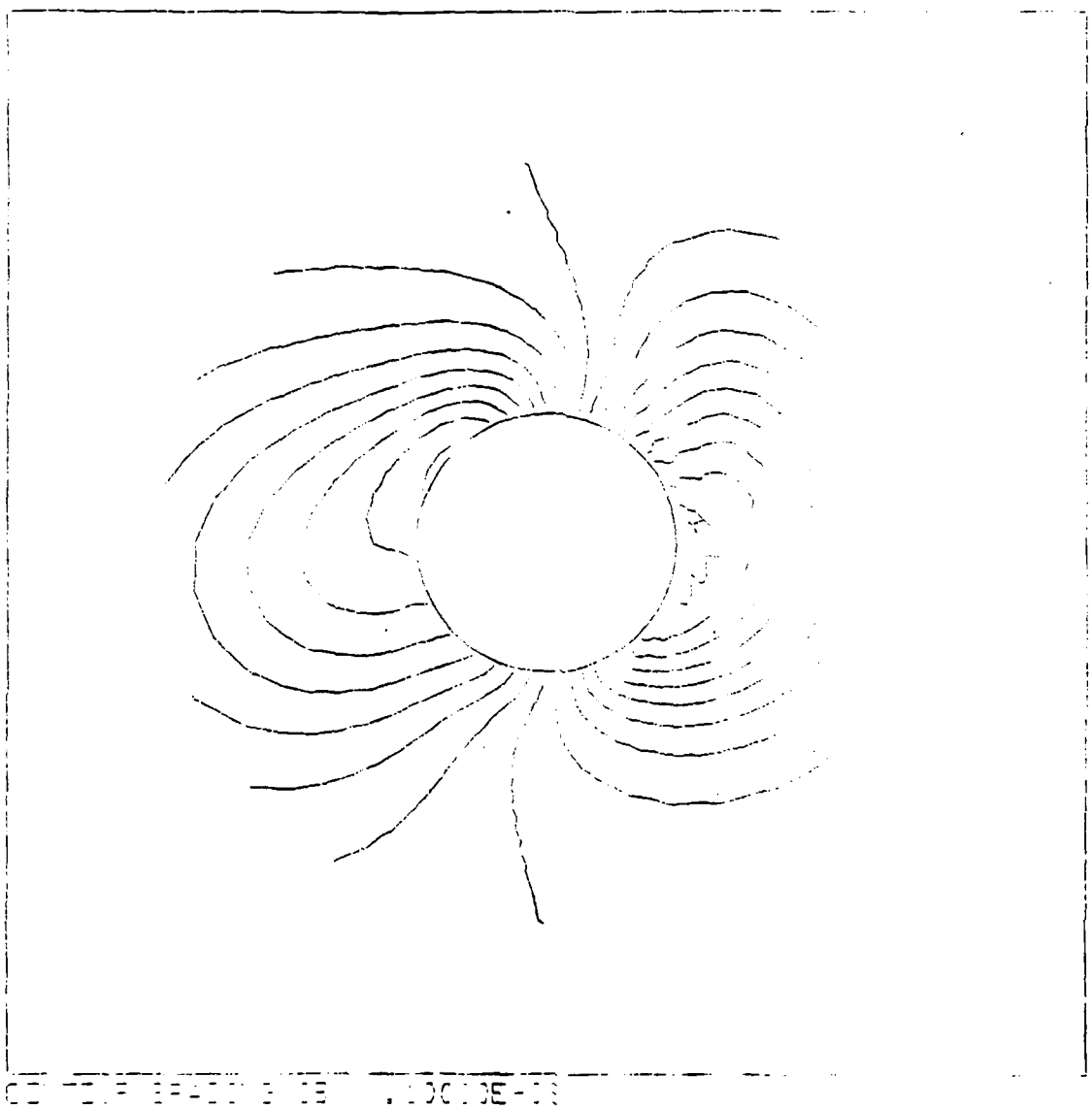

Figure 8d. Circular Cylinder– Pure Translation

Streamlines

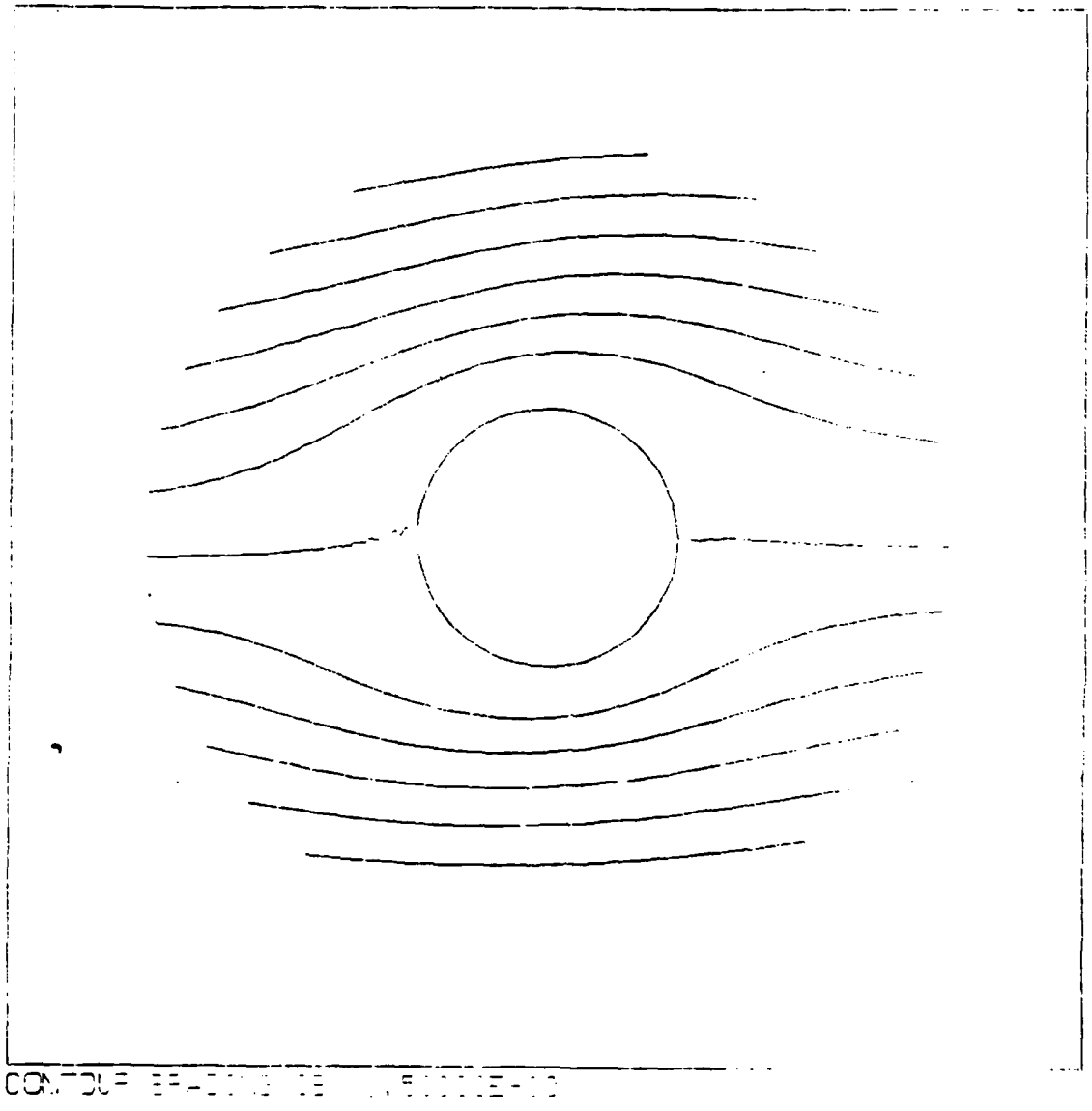

Figure 8c. Circular Cylinder– Pure Translation

Body-Axis Velocity Vectors

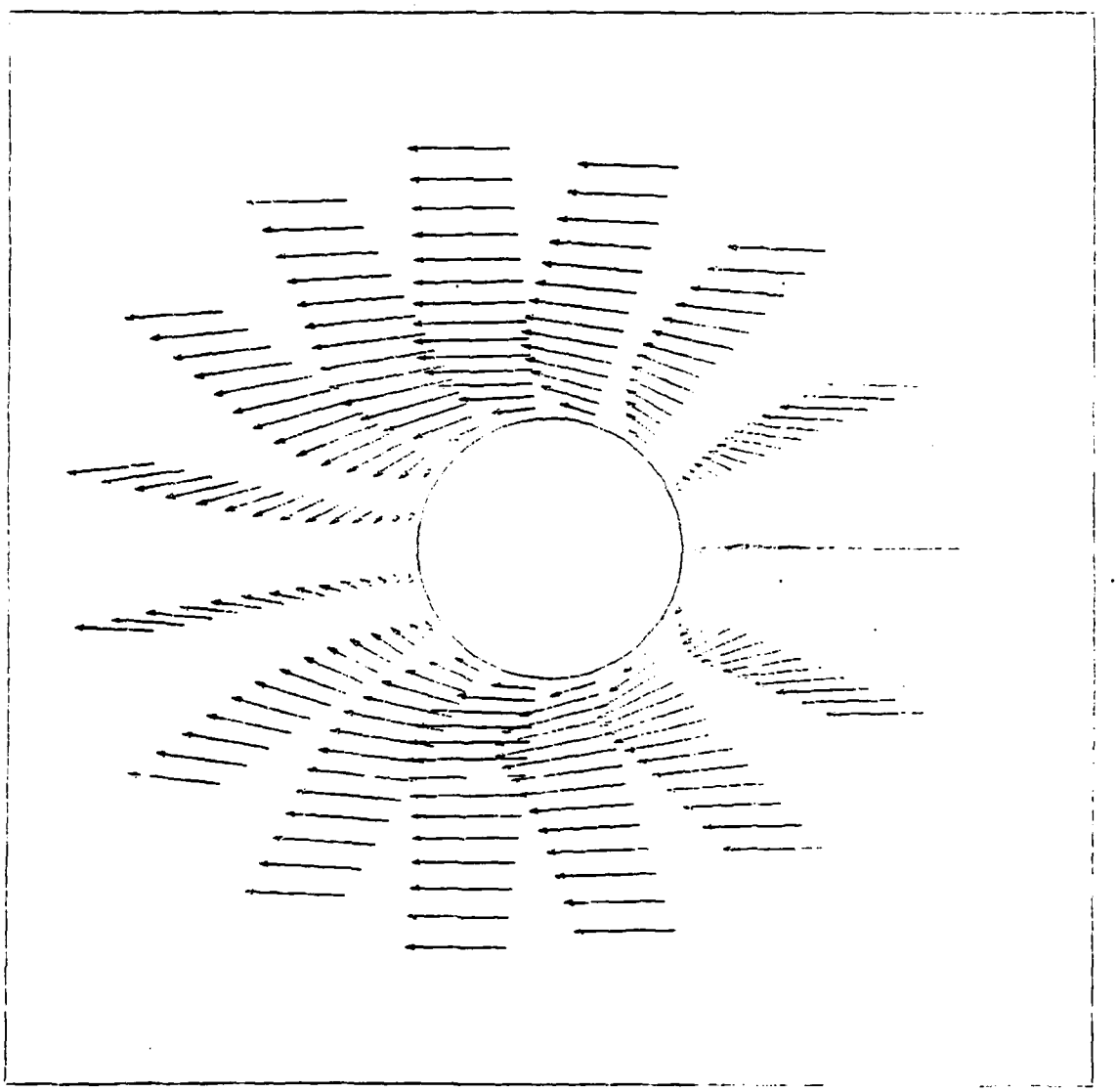

Figure 8b. Circular Cylinder- Pure Translation

Inertial Velocity Vectors

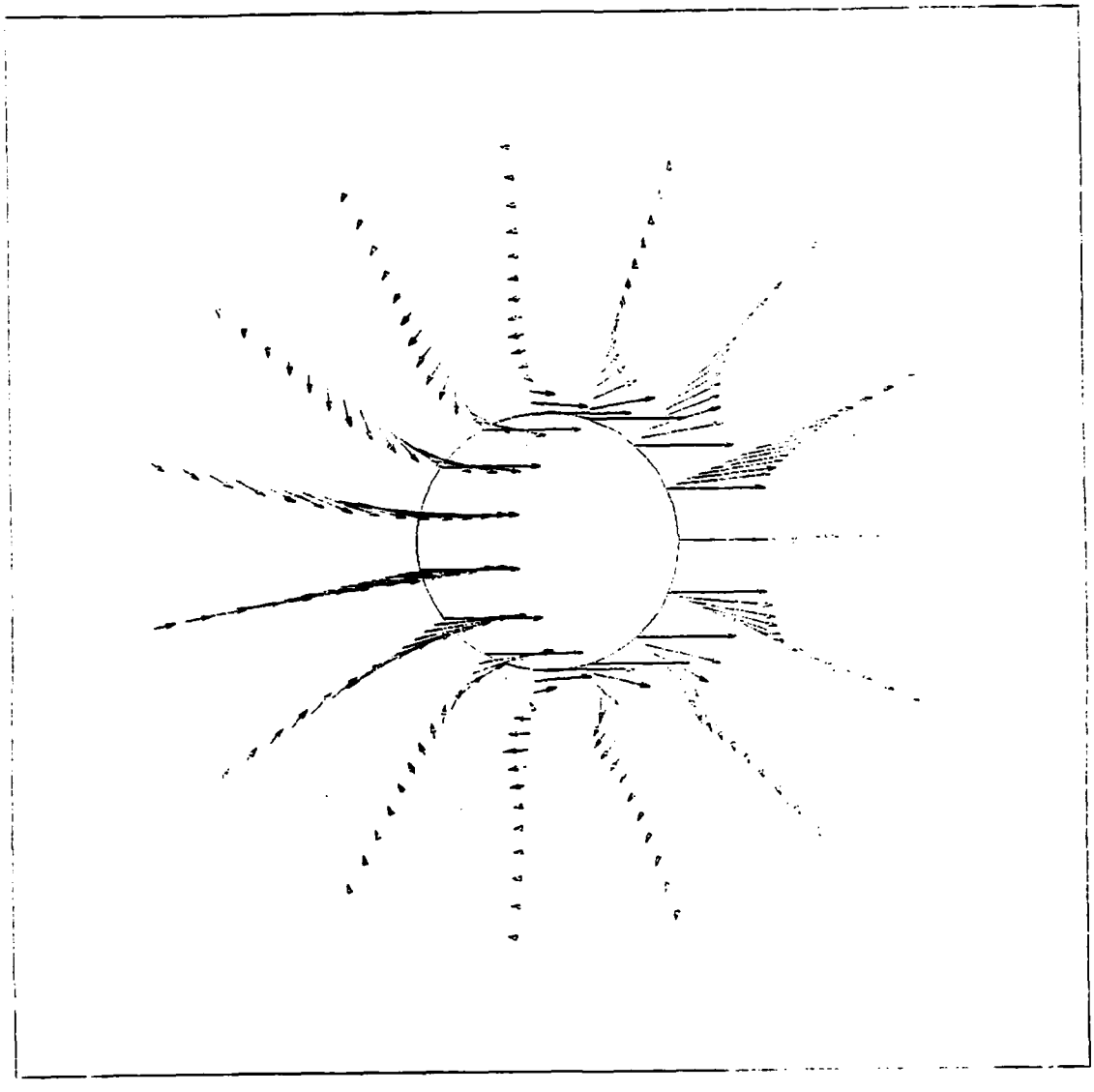

Figure 8a. Circular Cylinder– Pure Translation

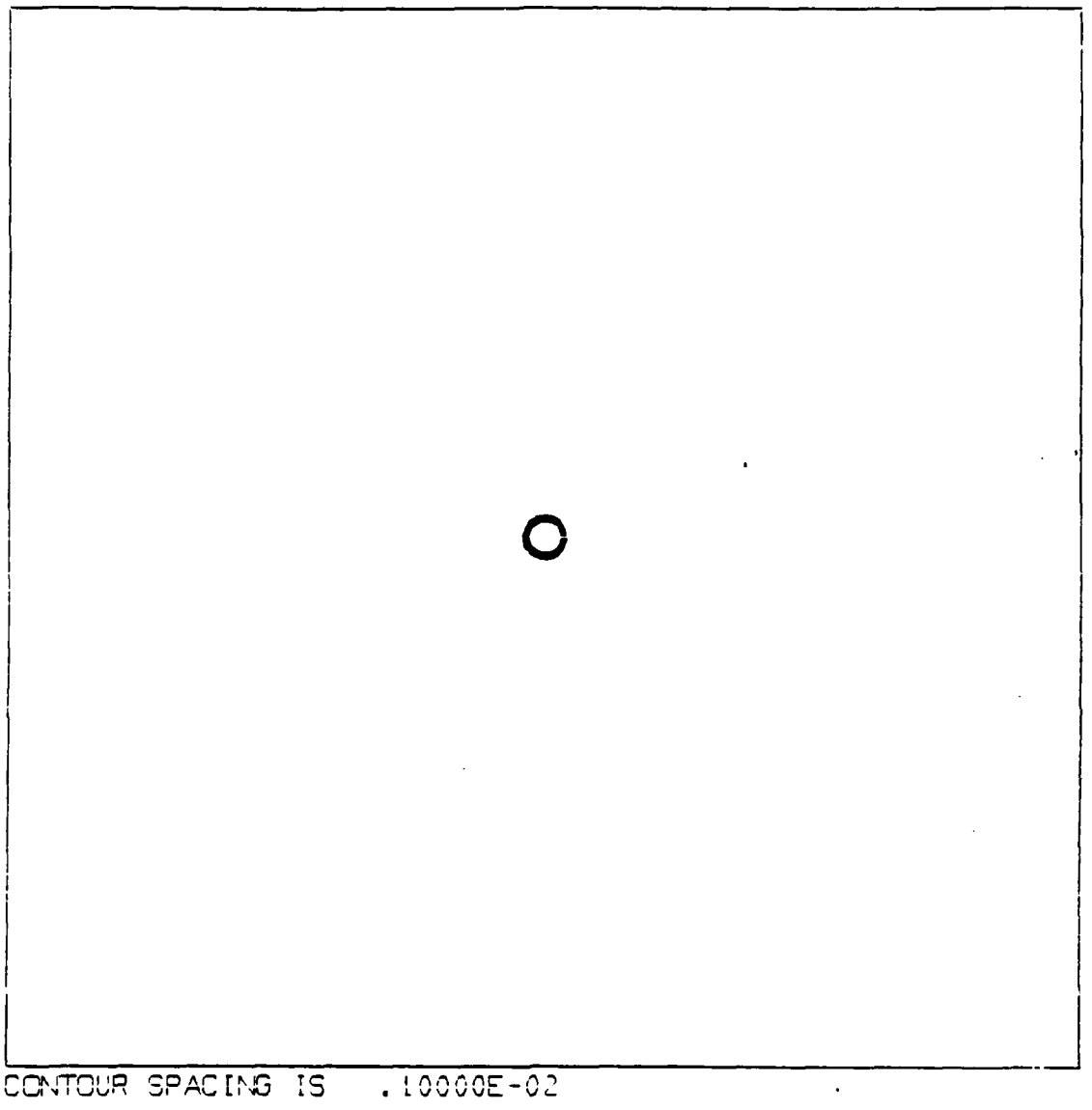

Figure 7j. Circular Cylinder– Pure Rotation

Pressure Isobars

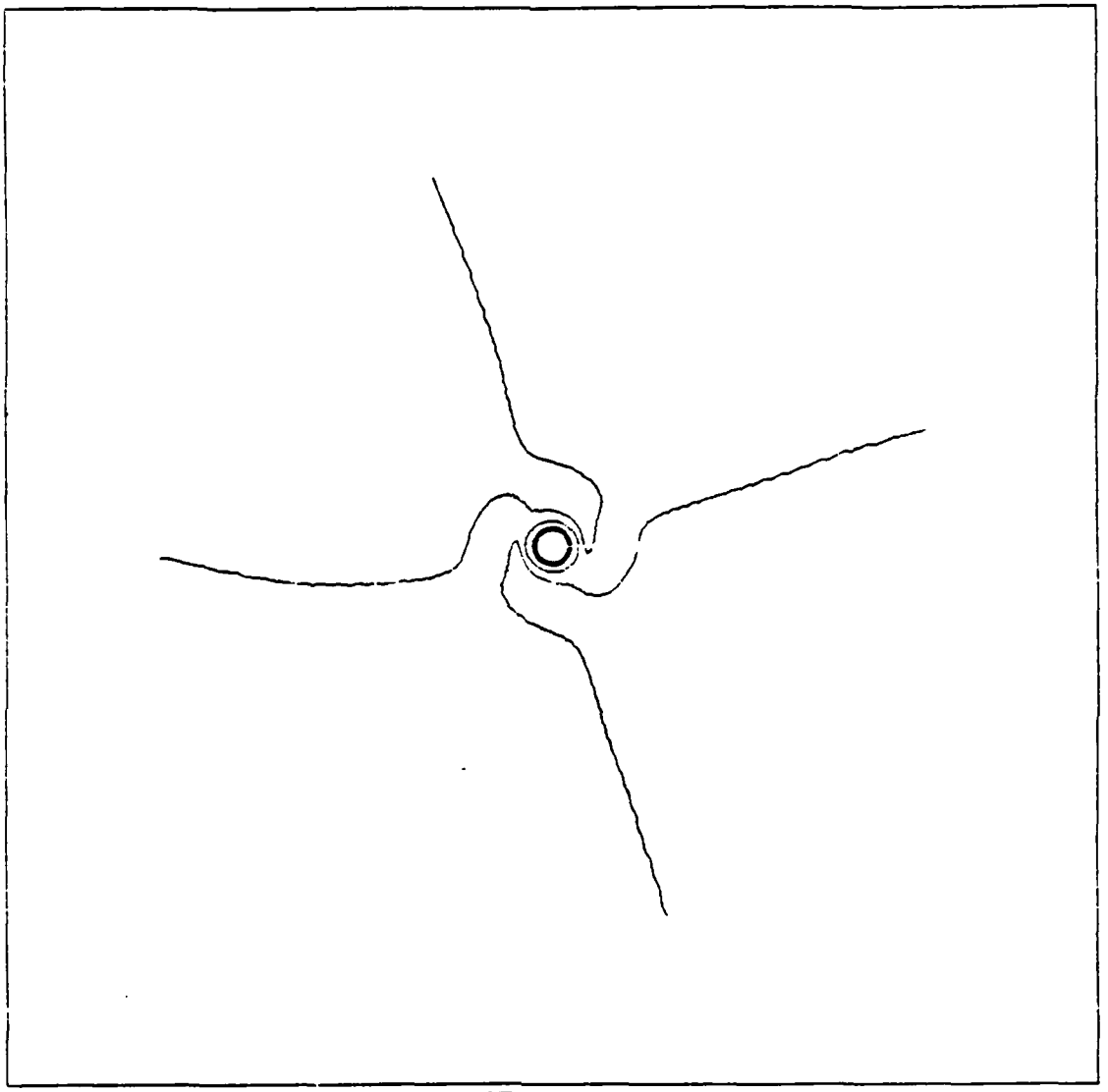

Figure 7i. Circular Cylinder– Pure Rotation

Streamlines

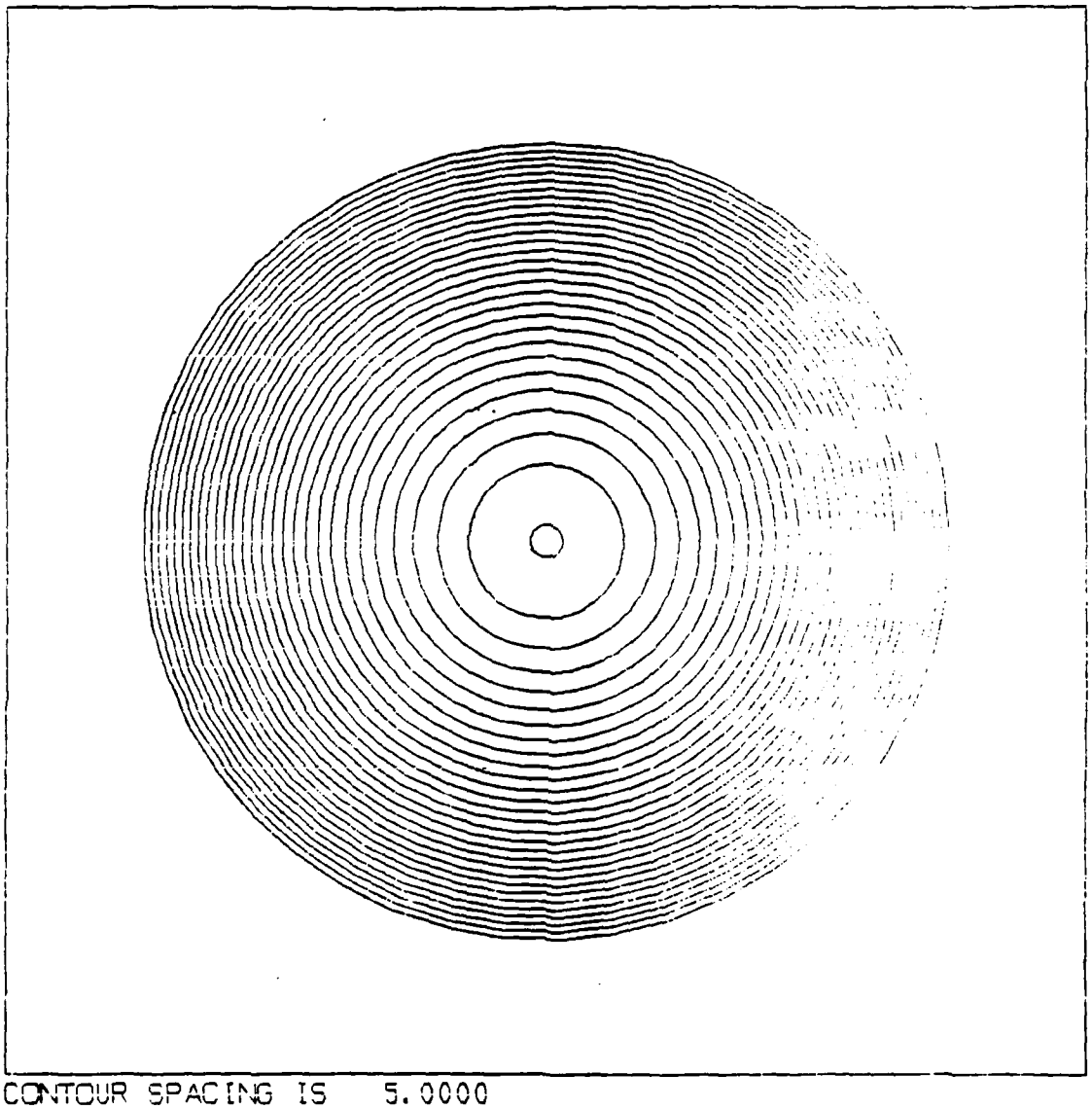

Figure 7h. Circular Cylinder– Pure Rotation

Body-Axis Velocity Vectors

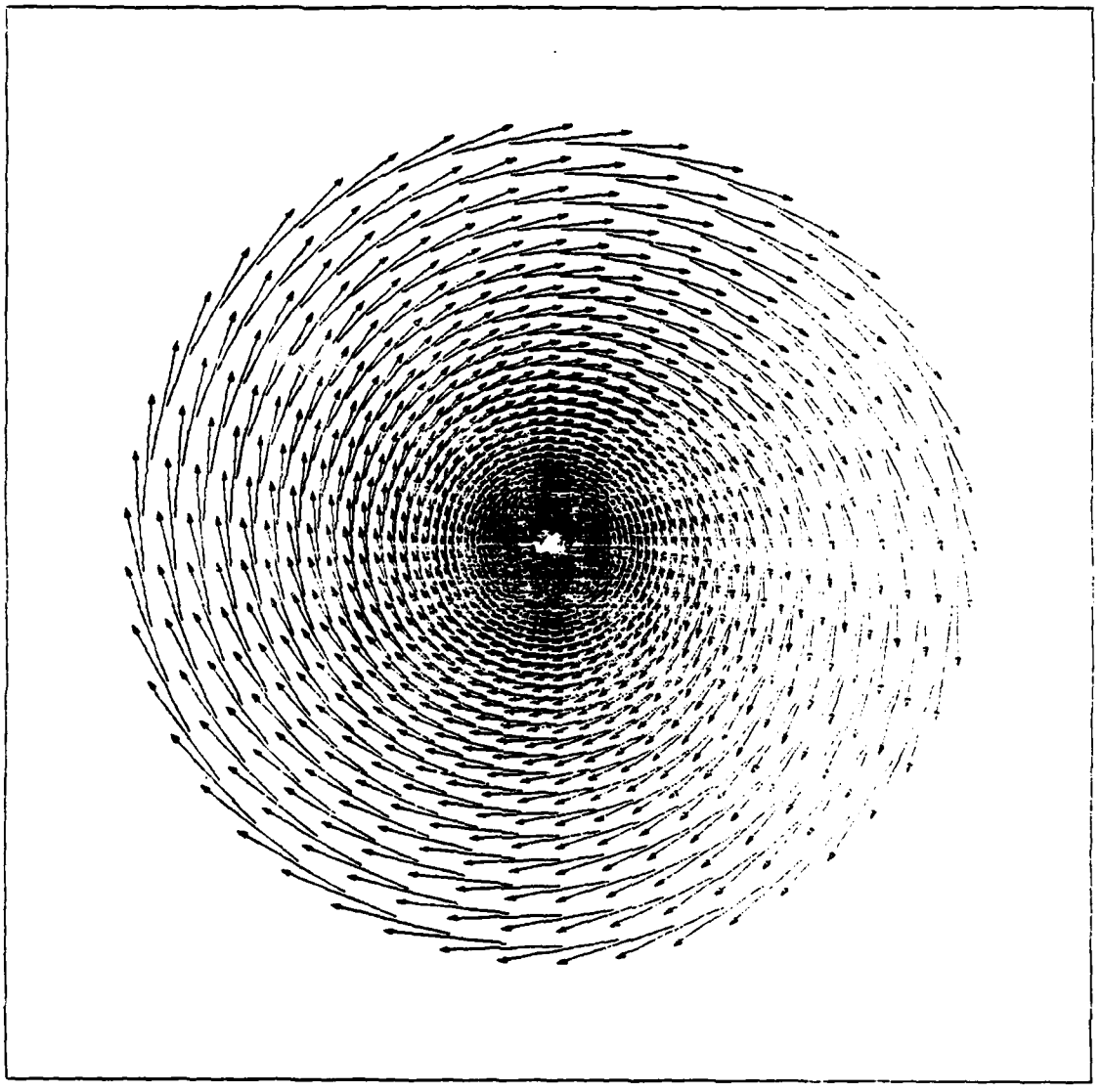

Figure 7g. Circular Cylinder- Pure Rotation

Inertial Velocity Vectors

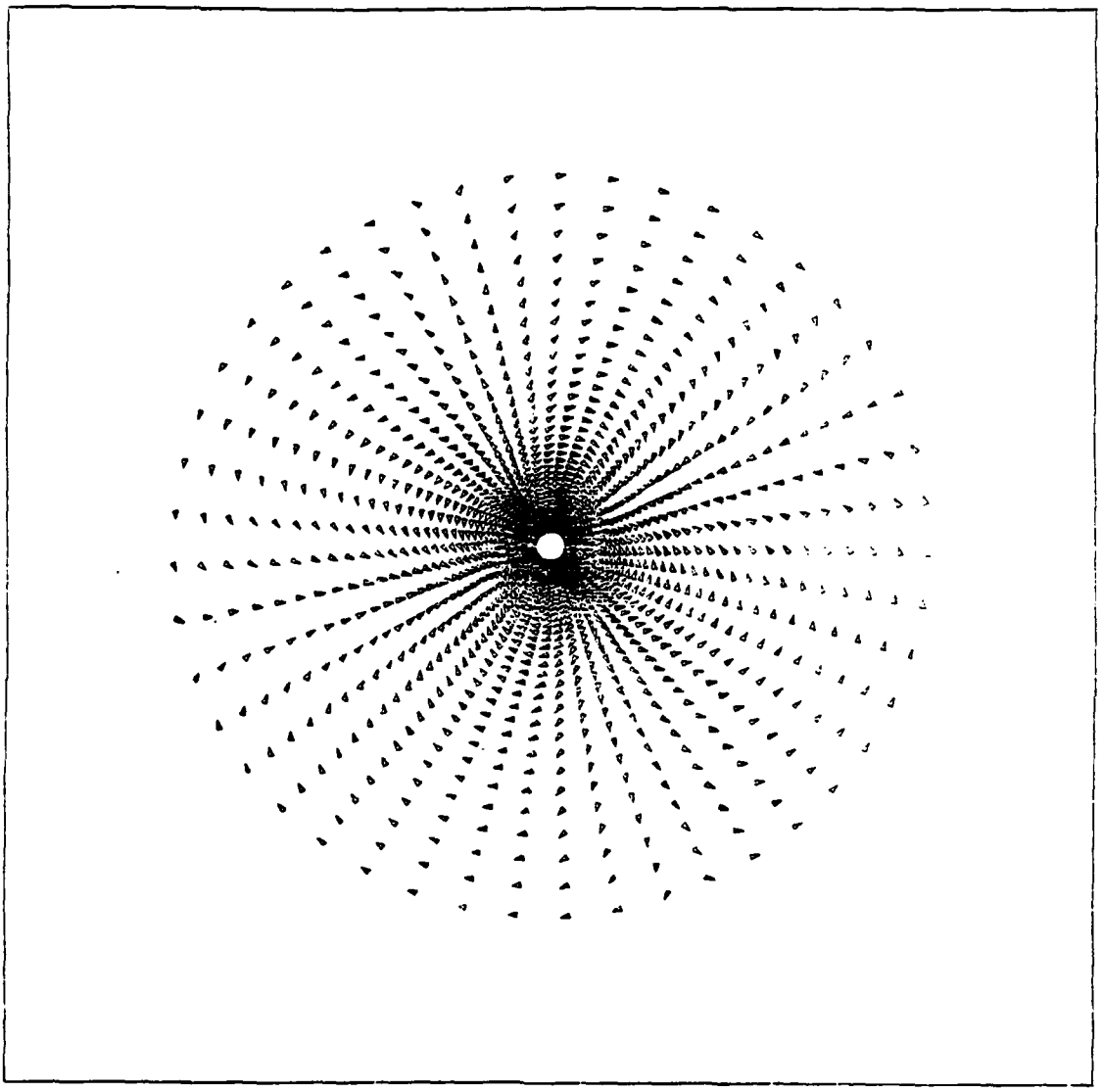

Figure 7f. Circular Cylinder– Pure Rotation

Vorticity Contours

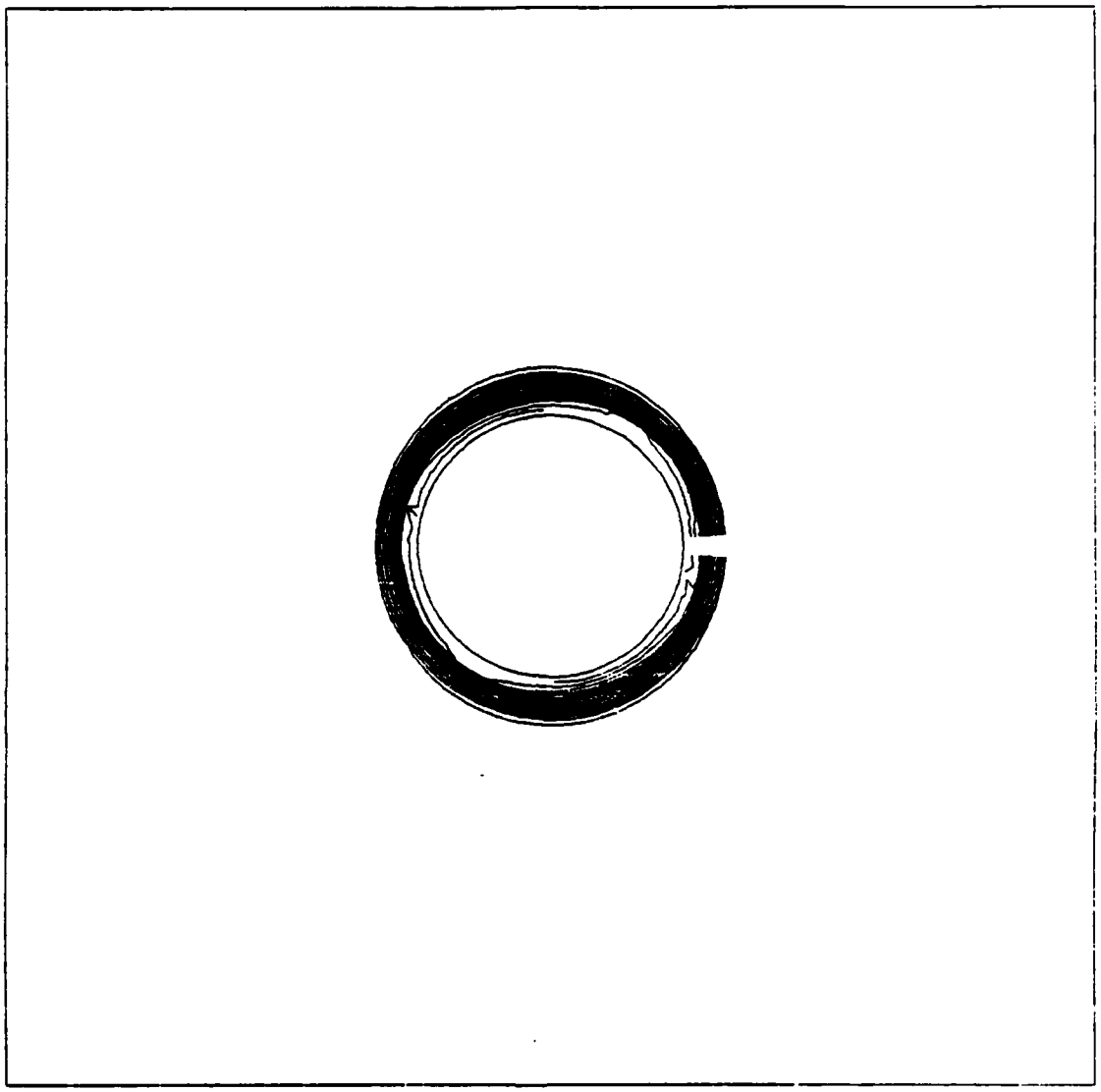

Figure 7e. Circular Cylinder– Pure Rotation

Pressure Isobars

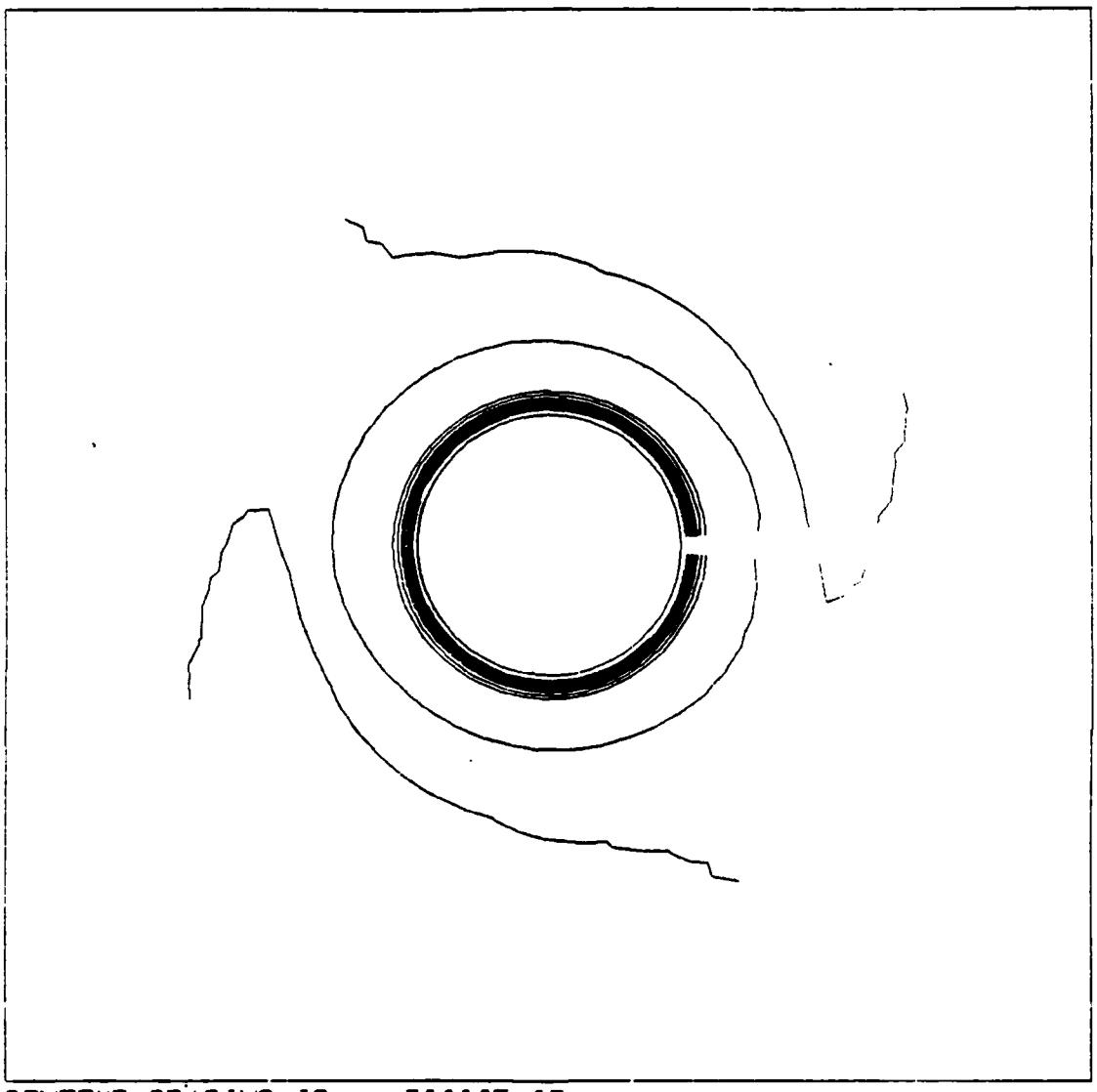

Figure 7d. Circular Cylinder– Pure Rotation

Streamlines

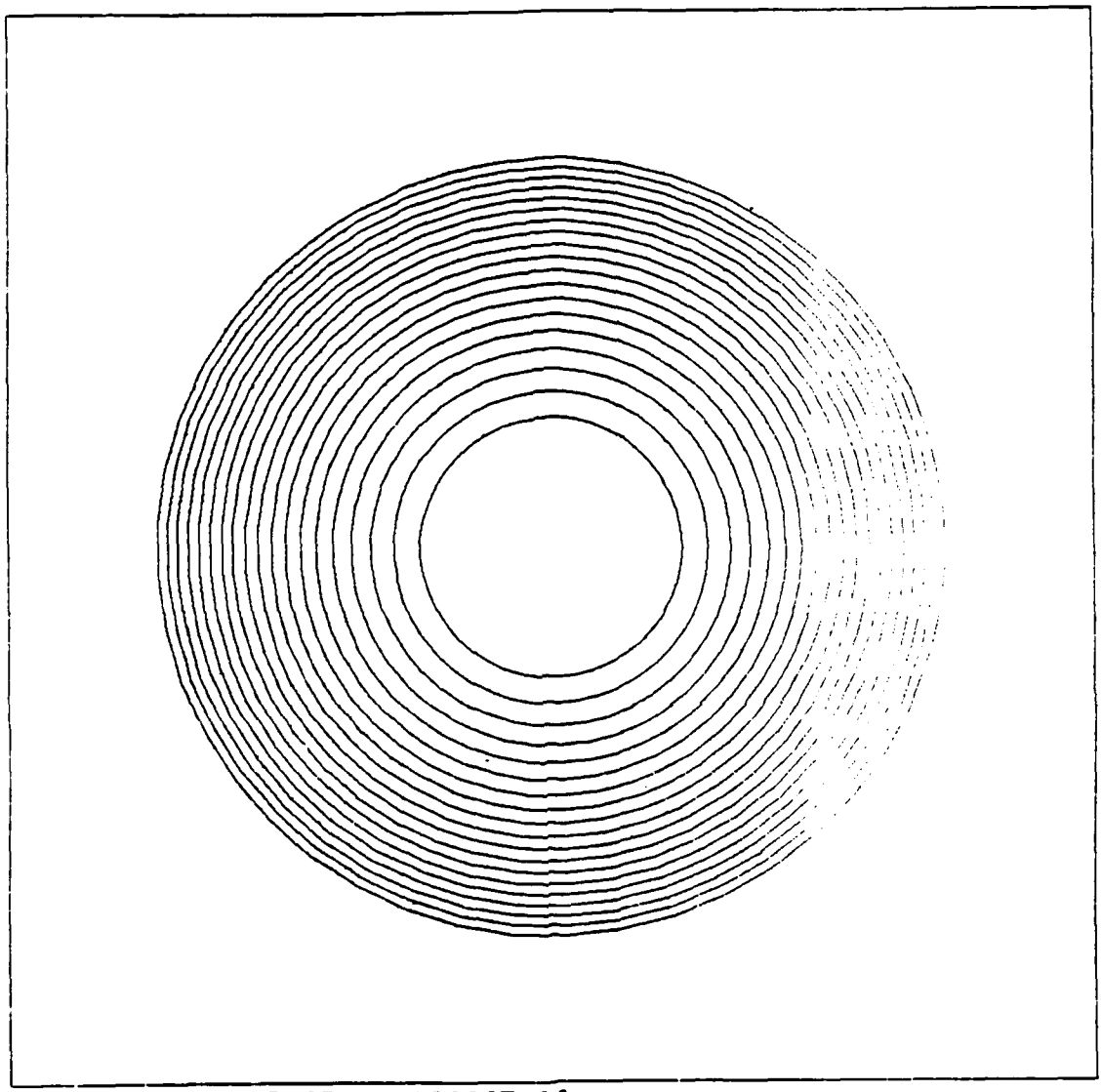

Figure 7c. Circular Cylinder– Pure Rotation

Vorticity Contours

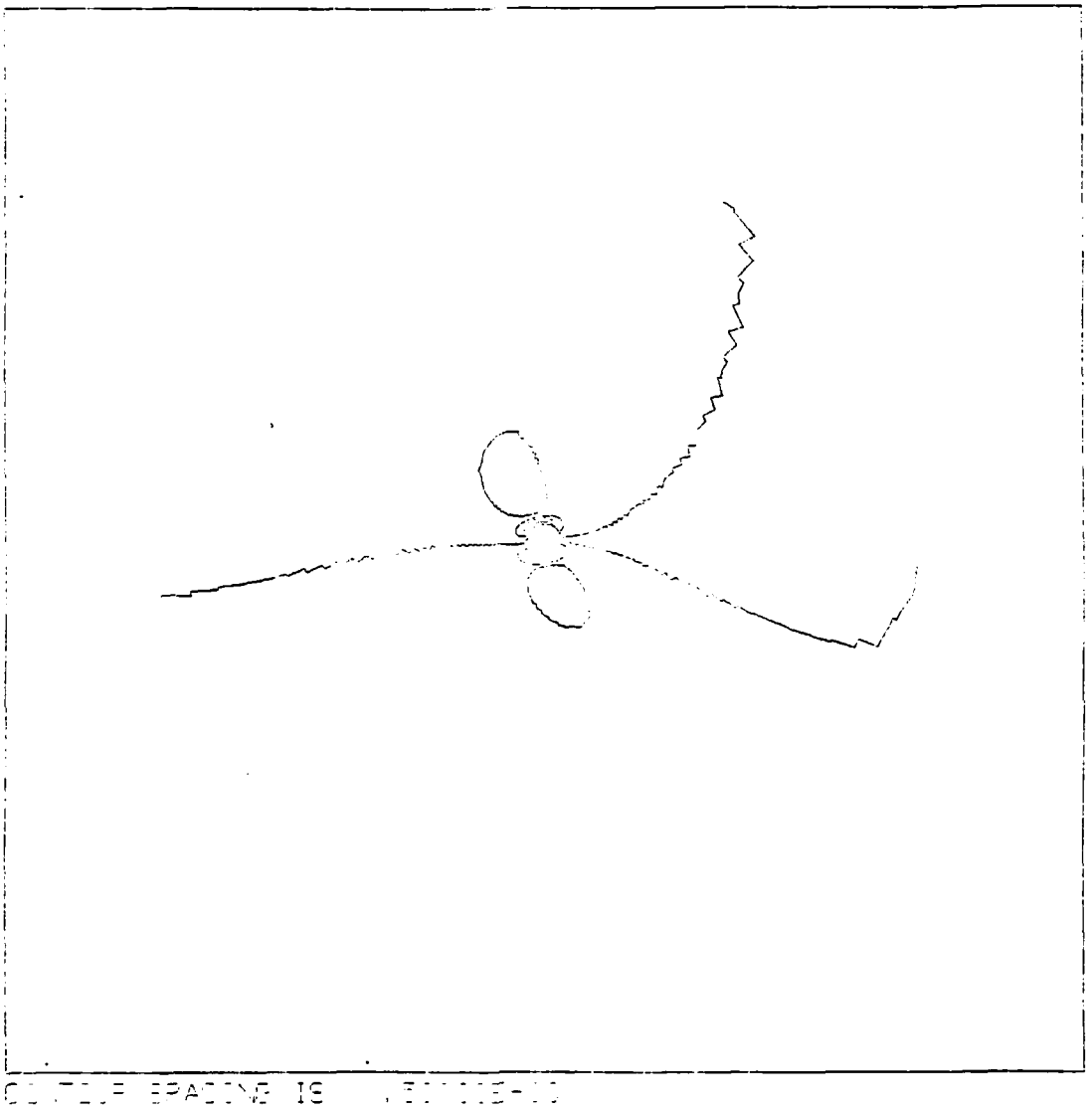

Figure 8g. Circular Cylinder– Pure Translation

VITA

Captain Thomas E. Speer was born on 26 March 1953 in Wichita, Kansas. He graduated from high school in Stanwood, Iowa, in 1971 and attended Iowa State University from which he received the degree of Bachelor of Science in Aerospace Engineering in May 1975. Upon graduation, he received a commission in the USAF through the ROTC program. In August of 1975 he entered active duty and was assigned to the Air Force Armament Laboratory, Aircraft Compatiblity Branch, Eglin AFB, Florida. In 1979 he became a student in the Flight Test Engineer Course, Class 79B, at the Air Force Test Pilot School. Following his graduation in June 1980, he was assigned to the USAF–Canadian Forces Exchange Program. He served as a flight test engineer with the Aerospace Engineering Test Establishment, Flight Dynamics Branch, CFB Cold Lake, Alberta, Canada until entering the School of Engineering, Air Force Institute of Technology, in June of 1983.

Permanent address: Box 381 Star Route
Miramar Beach
Destin
Florida 32541

SECURITY CLASSIFICATION OF THIS PAGE

REPORT DOCUMENTATION PAGE

1a. REPORT SECURITY CLASSIFICATION UNCLASSIFIED	1b. RESTRICTIVE MARKINGS
2a. SECURITY CLASSIFICATION AUTHORITY	3. DISTRIBUTION/AVAILABILITY OF REPORT Approved for public release;
2b. DECLASSIFICATION/DOWNGRADING SCHEDULE	distribution unlimited
4. PERFORMING ORGANIZATION REPORT NUMBER(S) AFIT/GAE/ENY/83D-26	5. MONITORING ORGANIZATION REPORT NUMBER(S)
6a. NAME OF PERFORMING ORGANIZATION School of Engineering	6b. OFFICE SYMBOL (If applicable) AFIT/ENG
7a. NAME OF MONITORING ORGANIZATION	
6c. ADDRESS (City, State and ZIP Code)	7b. ADDRESS (City, State and ZIP Code)
8a. NAME OF FUNDING/SPONSORING ORGANIZATION	8b. OFFICE SYMBOL (If applicable)
9. PROCUREMENT INSTRUMENT IDENTIFICATION NUMBER	
8c. ADDRESS (City, State and ZIP Code)	10. SOURCE OF FUNDING NOS. PROGRAM ELEMENT NO. / PROJECT NO. / TASK NO. / WORK UNIT NO.
11. TITLE (Include Security Classification) See Box 19	
12. PERSONAL AUTHOR(S) Thomas E. Speer, B.S., Capt, USAF	
13a. TYPE OF REPORT MS Thesis	13b. TIME COVERED FROM _____ TO _____
14. DATE OF REPORT (Yr., Mo., Day) 1983 December	15. PAGE COUNT 82
16. SUPPLEMENTARY NOTATION	

17. COSATI CODES		
FIELD	GROUP	SUB. GR.
20	04	
12	01	

18. SUBJECT TERMS (Continue on reverse if necessary and identify by block number)
Aerodynamics, Airfoils, Difference Equations, Navier Stokes Equations,

19. ABSTRACT (Continue on reverse if necessary and identify by block number)

Title: UNSTEADY NAVIER-STOKES CALCULATIONS IN AN ACCELERATED REFERENCE FRAME

Thesis Chairman: James H. Hodge, Major, USAF

Approved for public release: IAW AFR 190-17.

Lynn E. Wolaver 31 Dec 83
Dean for Research and Professional Development
Air Force Institute of Technology (AIC)
Wright-Patterson AFB OH 45433

20. DISTRIBUTION/AVAILABILITY OF ABSTRACT UNCLASSIFIED/UNLIMITED ☒ SAME AS RPT. ☐ DTIC USERS ☐	21. ABSTRACT SECURITY CLASSIFICATION UNCLASSIFIED
22a. NAME OF RESPONSIBLE INDIVIDUAL James H. Hodge, Major, USAF	22b. TELEPHONE NUMBER (Include Area Code) 513-255-3333
22c. OFFICE SYMBOL AFIT/ENG	

DD FORM 1473, 83 APR EDITION OF 1 JAN 73 IS OBSOLETE.

SECURITY CLASSIFICATION OF THIS PAGE

The purpose of this project was to develop a numerical method capable of calculating the laminar flow about a two dimensional accelerating body using the incompressible Navier-Stokes equations. This problem arises in the calculation of the dynamic stall of an airfoil and in the calculation of pitching and heaving stability derivatives for an isolated airfoil. It is also a first step toward solving the three dimensional flow about a complete wing undergoing arbitrary motion at high angles of attack, including departure, spin, and post-stall maneuvers.

The contravariant form of the momentum and continuity equations are derived and a finite difference approximation developed. The contravariant velocity formulation is based on the use of both inertial and body-axis velocities to achieve a form for the momentum equations that has the potential for improved numerical characteristics for rotating coordinate frames.

Numerical calculations to date have not been satisfactory. Test cases presented are Stoke's first problem, a circular cylinder translating at a Reynold's number of 20, and a rotating stationary circular cylinder.

Continuation is included: see 1473

END

FILMED

5-85

DTIC